

10. MINERALOGY AND MINERAL CHEMISTRY OF HYDROTHERMALLY ALTERED SEDIMENT, MIDDLE VALLEY, JUAN DE FUCA RIDGE¹

Matthew I. Leybourne² and Wayne D. Goodfellow²

ABSTRACT

Two hydrothermal upflow zones and a hydrothermal reaction zone were drilled in Middle Valley, a sedimented rift valley at the northern end of the Juan de Fuca Ridge, during Leg 139 of the Ocean Drilling Program. Site 856 (Bent Hill; BH) is a fossil high-temperature hydrothermal system that hosts massive sulfides, Site 858 (Area of Active Venting; AAV) is an active hydrothermal system venting fluids up to 276°C, and Site 857 is a hydrothermal reaction zone south of AAV. Alteration at BH is zoned laterally away from a high-temperature, silicified, brecciated, and veined core that consists of quartz-(Fe)chlorite-muscovite-rutile-chalcopyrite-pyrrhotite (Zone Ia). Surrounding Zone Ia are altered sediments that are zoned away from the core as follows. Zone IIa consists of albite-chlorite-pyrite alteration of moderately indurated and brecciated sediment. Zones IIIa and IVa are characterized by hydrothermal anhydrite and calcite, respectively, in addition to illite and pyrite, and are less intensely indurated than sediments from the inner, higher temperature zones.

Sediments near the center of hydrothermal fluid discharge at AAV are lithified, brecciated, and veined, and consist of the assemblage wairakite-quartz-epidote-sphene-pyrite (Zone Ib). Zone Ib is surrounded by alteration zones that are progressively less altered away from centers of fluid discharge. From the core outward, these are: Zone IIb (quartz-epidote-pyrite); Zone IIIb (albite-chlorite-pyrite); Zone IVb (anhydrite-illite-pyrite); and Zone Vb (calcite/dolomite-illite-pyrite). Sediments intercalated with mafic sills below 460 meters below sea-floor at Site 857 are mineralogically similar to Zones Ib and IIb at AAV, suggesting that the hydrothermal fluid venting at AAV was generated in a hydrothermal reaction zone in the basal parts of the Middle Valley sedimentary sequence.

The mineralogical differences between the core assemblages at the BH and AAV hydrothermal upflow systems are a function of hydrothermal fluid temperature and composition. Fluid inclusions and chlorite chemistry of Zone Ia suggest that the Bent Hill massive sulfide deposit was produced by high-temperature (300°–400°C) fluid. The absence of Ca-bearing hydrothermal phases and the destruction of detrital Ca-minerals indicate that the end-member hydrothermal fluids at BH were probably depleted in Ca relative to AAV fluids.

Vent fluid (184°–276°C) and fluid inclusion (270°–290°C) temperatures clearly show that AAV is a lower-temperature hydrothermal system. The occurrence of wairakite, anorthitic plagioclase, epidote, and sphene that formed at the expense of detrital K-bearing minerals is consistent with fluid Ca contents that are higher than for basalt-equilibrated, end-member hydrothermal fluids. At BH and AAV, the mineral zonation and temperature gradients are controlled by the mixing of entrained seawater with upwelling hydrothermal fluid. The convex-up pattern of mineral zonation about both upflow zones is consistent with fluid inclusion temperatures, pore water compositions, and bulk sediment compositions.

INTRODUCTION

Middle Valley, a sediment-covered rift near the northern end of the Juan de Fuca Ridge, has been the focus of extensive geophysical and geological research over the past decade with the discovery of high heat flow (Davis and Lister, 1977; Davis, Goodfellow, et al., 1987) and associated massive sulfide deposits (Adshead et al., 1986; Davis, Goodfellow, et al., 1987; Goodfellow and Blaise, 1988; Goodfellow and Franklin, in press). Two hydrothermal centers have been investigated intensively: the Area of Active Venting (AAV; Site 858), which has active chimneys venting 184°–276°C fluids (Davis, Mottl, Fisher, et al., 1992), and Bent Hill (BH; Site 856), where sulfide mounds have been mapped and sampled by submersible, dredging, and coring (Fig. 1). Both of these areas, a hydrothermal reaction zone (Site 857), and relatively unaltered hemipelagic and turbiditic sediment near the eastern margin of the valley (Site 855) were cored during Ocean Drilling Program (ODP) Leg 139 in order to better understand hydrothermal processes in sedimented rifts.

The objectives of this study were to document the mineralogy and mineral chemistry in hydrothermal fluid upflow and reaction zones,

to relate mineralogical changes to temperature and distance from fluid upflow zones, and to place physical and chemical constraints on fluid-sediment reaction conditions. Previous work on shallow sediment and sulfide cores that penetrated the mound structures in Middle Valley have documented the near-surface mineralogical and chemical zoning about active and fossil upflow zones (Goodfellow and Blaise, 1988; Goodfellow et al., in press; Goodfellow and Franklin, in press). Deep cores recovered during Leg 139 allow us to examine the third dimension, with an emphasis on the deeper portions of hydrothermal upflow (Sites 856 and 858) and reaction zones (Site 857).

GEOLOGICAL SETTING

Four sites were drilled in Middle Valley during ODP Leg 139 (Fig. 1). Site 856 is known from previous work (Davis, Goodfellow, et al., 1987; Goodfellow and Blaise, 1988; Goodfellow et al., in press; Goodfellow and Franklin, in press) to be an inactive hydrothermal upflow zone with an associated massive sulfide deposit (BH). Site 858 is a vent field with hydrothermal fluids venting from anhydrite chimneys on sediment mounds (Goodfellow et al., in press; Goodfellow and Franklin, in press). The vent field is characterized by heat flow values > 1 Wm⁻² (Davis and Villinger, 1992). Site 857 was drilled to better understand the hydrology and the depth and conditions of hydrothermal fluid reaction whereas Site 855 was drilled to evaluate whether fluid recharge was occurring at the margins of the rift (Davis, Mottl, Fisher, et al., 1992; Davis and Villinger, 1992).

¹ Mottl, M.J., Davis, E.E., Fisher, A.T., and Slack, J.F. (Eds.), 1994. *Proc. ODP, Sci. Results*, 139: College Station, TX (Ocean Drilling Program).

² Mineral Resources Division, Geological Survey of Canada, 601 Booth Street, Ottawa, Ontario, Canada K1A 0E8.

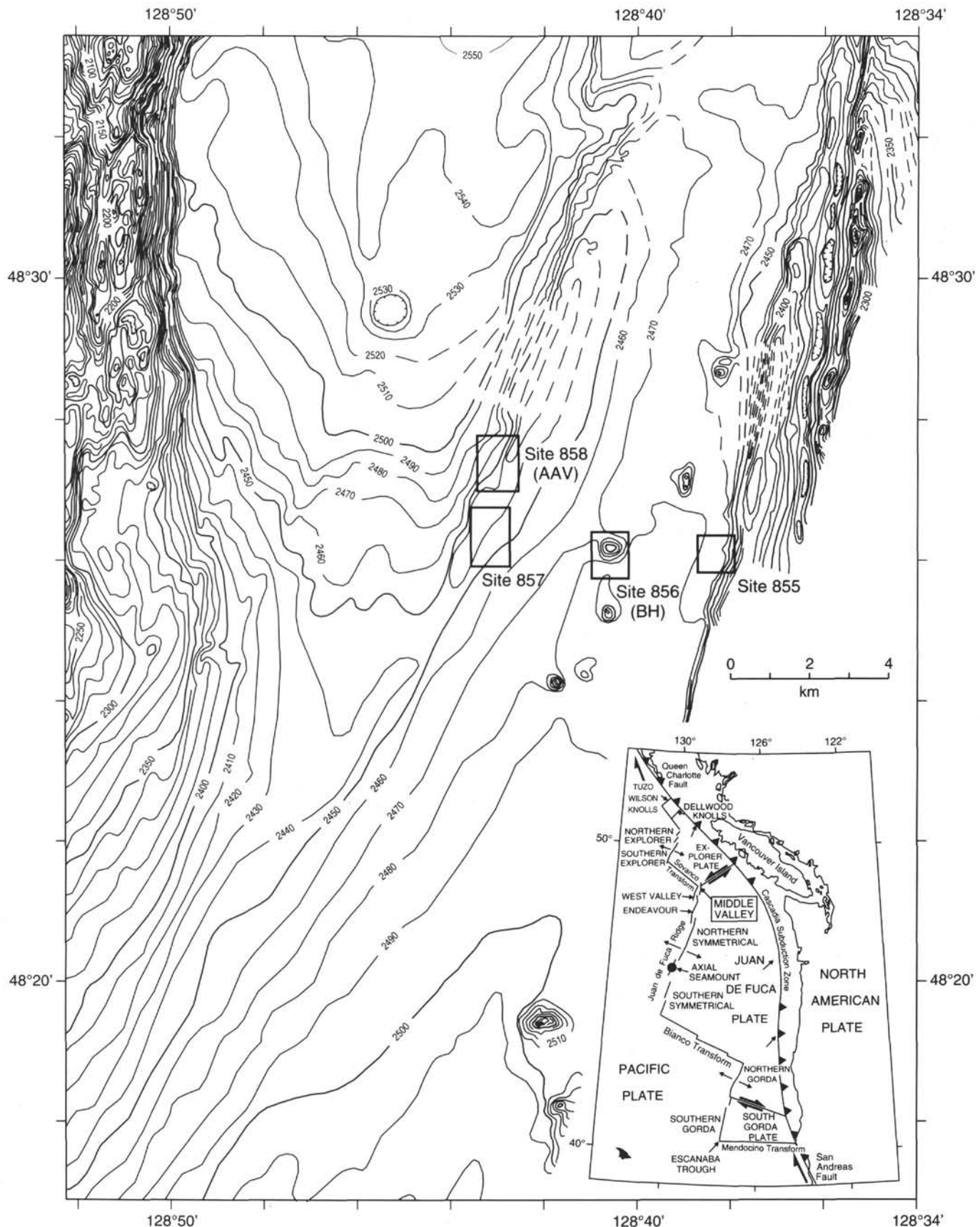


Figure 1. Seabeam bathymetry of Middle Valley showing the Leg 139 site locations (Davis, Currie, Sawyer, 1987; Davis, Mottl, Fisher, et al., 1992). AAV = Area of Active Venting, BH = Bent Hill. Inset map shows the location of Middle Valley at the northern end of the Juan de Fuca Ridge.

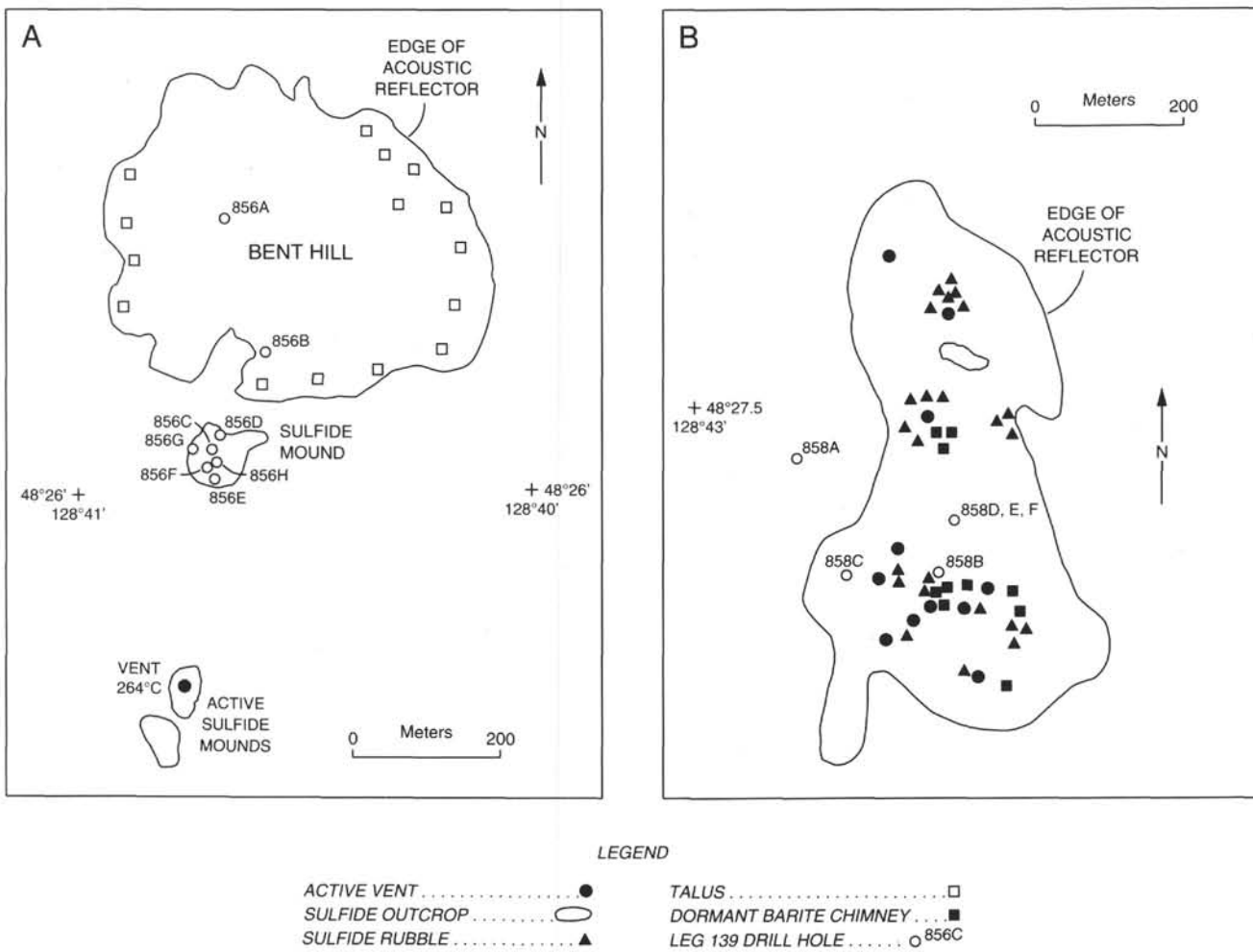


Figure 2. Maps showing the locations of drill holes, active vents and mounds, and sulfide outcrops. A. Site 856. B. Site 858.

Site 856 (Bent Hill)

Bent Hill is a 500-m diameter and 60-m high mound structure located 3 km from the eastern margin of Middle Valley (Fig. 1). A smaller (100-m-wide, 35-m-high) mound of massive sulfide occurs near the southern margin of BH. Further to the south are two small (25-m-high) sulfide mounds, one venting 264°C fluids from anhydrite-sulfide chimneys (Goodfellow and Franklin, in press). Eight holes were drilled at Site 856, and samples from seven of these holes were studied. Holes 856A and 856B are from the top and southern edge of Bent Hill and Holes 856D to 856H were collared near the summit of the sulfide mound at the southern margin of Bent Hill (Fig. 2A).

Hole 856A consists of interbedded hemipelagic and turbiditic sediments (Fig. 3). Sediments in the upper part of Hole 856A are unconsolidated (0–5 meters below seafloor; mbsf) to weakly indurated (5–25 mbsf). Below 25 mbsf, sediments become more indurated and change color with depth. The sediments are dominantly olive-grey to 12 mbsf, olive-grey to blue-green between 12 and 60 mbsf, and medium to dark grey from 60 mbsf to the bottom of the hole. Turbidite sequences are commonly thinly laminated and less indurated than hemipelagic silty clay. A mafic sill was encountered at the base of the hole (112 mbsf) although no thermal effects in the overlying sediment were observed (Davis, Mottl, Fisher, et al., 1992).

Hole 856B intersected 121.7 m of hemipelagic and turbiditic sediment (Fig. 4). The uppermost 17.5 meters of Hole 856B is dominated by relatively unaltered, unconsolidated to weakly indurated medium-grey sediment. Unconsolidated clastic sulfides occur between 18.39 and 24.17 mbsf, and turbiditic sediment with variable

sulfide contents between 24.17 and 26.31 mbsf. The sulfide sediment is interpreted to have formed by the slumping of sulfide debris from the adjacent sulfide mound (Davis, Mottl, Fisher, et al., 1992). Sediments are fractured and brecciated and contain disseminated pyrite between 27 and 77 mbsf. Two types of breccia are recognized: crackle breccia composed of angular, moderately indurated, clast-supported, medium-grey sediment; and matrix-supported channelway breccia with rounded to subrounded clasts of silty clay (Davis, Mottl, Fisher, et al., 1992). The sediments become increasingly indurated and the color changes from light grey to bluish-grey between 77 mbsf and the mafic sill near bottom of the hole. A 5–6-m-thick mafic sill was also intersected at 62 mbsf (Davis, Mottl, Fisher, et al., 1992).

Sulfide minerals from Holes 856D through 856H are predominantly pyrrhotite, pyrite, sphalerite, chalcopyrite, isocubanite, and less commonly marcasite and galena. Secondary magnetite after pyrrhotite is a major phase in Holes 856G and 856H. Only carbonate and silicate minerals interstitial to sulfides, and veined and altered sediment between 25 and 30 mbsf in Hole 856H, are considered here as the detailed sulfide mineralogy is described elsewhere (Duckworth et al., this volume).

Site 858 (Area of Active Venting)

Site 858 is an active vent field 2.4 km northwest of Site 856 and 1.5 km east of a rift-parallel extensional fault (Fig. 1). The vent field is 800 m by 400 m and hosts at least 15 active vent sites with anhydrite chimneys that are discharging fluids with temperatures between 184° and 276°C (Davis, Mottl, Fisher, et al., 1992). Seven holes were

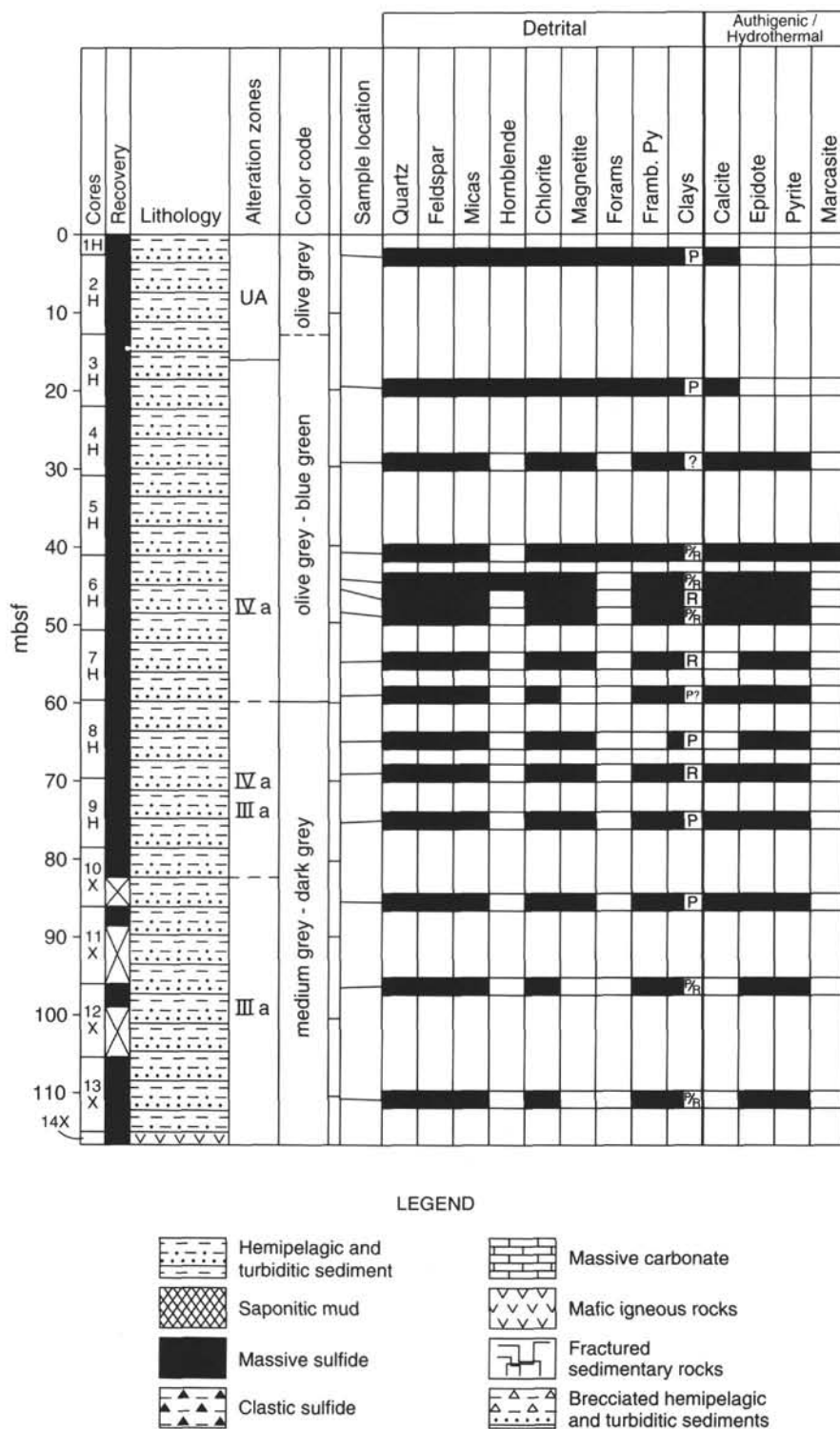


Figure 3. Stratigraphic section of Hole 856A showing the general sedimentology, alteration zones, and detrital, authigenic, and hydrothermal minerals based on thin-section descriptions. UA = unaltered sediment. Letter designates clay recrystallization: P = partial; R = recrystallized. Black = present.

drilled at Site 858 and samples from five holes are described here (Fig. 2B). Holes 858A, 858C, 858D, 858F, and 858B traverse the vent field from the outer western margin to the center of hydrothermal fluid upflow (Fig. 2B). Hole 858B was drilled to a depth of 38.6 mbsf within a few meters of a 276°C hydrothermal vent, whereas Holes 858D and 858F were drilled to a depth of 296.9 mbsf 70 m northeast of Hole 858B.

Hole 858A intersected 339.1 m of hemipelagic and laminated to cross-laminated turbiditic sediments (Fig. 5). Hemipelagic and turbiditic sediments are unconsolidated to weakly indurated near the seafloor (0 to 29 mbsf), but are weakly to moderately indurated between 29 and 71 mbsf, and moderately indurated to lithified between 71 and 339.1 mbsf. An increase in the degree of induration with depth is accompanied by changes in sediment color, from greenish

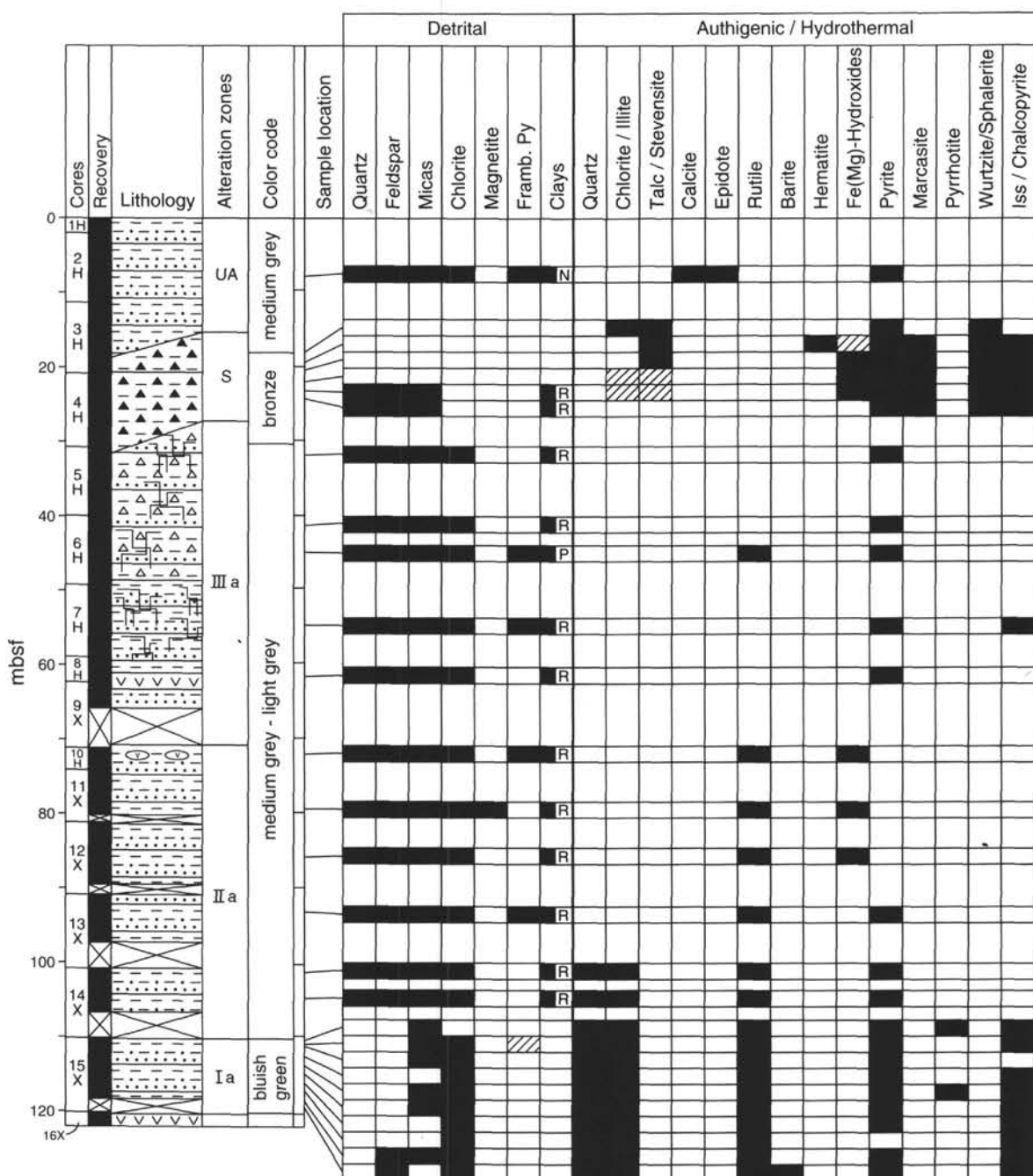


Figure 4. Stratigraphic section of Hole 856B showing the general sedimentology, alteration zones, and detrital, authigenic, and hydrothermal minerals based on thin-section descriptions. UA = unaltered sediment, S = sulfide. Letter designates clay recrystallization: N = non; P = partial; R = recrystallized. Black = present; striped = uncertain identification. Lithology symbols as in Fig. 3.

grey to olive grey between 0 and 20 mbsf, olive grey to medium grey between 20 and 65 mbsf, and medium dark to light grey below 65 mbsf. Hemipelagic sediment is commonly bioturbated between 29 and 256 mbsf.

Hole 858B penetrated 38.6 m of highly altered hemipelagic and turbiditic sediment with a thin zone of massive sulfide and anhydrite between 10.7 and 12.3 mbsf (Fig. 6). The uppermost two meters consists of green saponite mud that is interbedded with hemipelagic silty clay (Davis, Mottl, Fisher, et al., 1992). This saponite mud is similar to hydrothermal sediment recovered near vents by shallow piston and gravity cores (Goodfellow and Blaise, 1988; Goodfellow et al., in press; Turner et al., in press). Between 2 and 10.7 mbsf,

hemipelagic and turbiditic sediments are unconsolidated to weakly indurated and grey to greenish grey. Sediments become indurated with depth and are brecciated below 24 mbsf.

Hole 858C intersected 93.6 m of interbedded hemipelagic and turbiditic sediment (Fig. 7). Sediment induration generally increases with depth except between 5 and 17 mbsf where massive carbonates occur. Sediments range in color from medium to olive grey between 0 and 16 mbsf to light grey below 16 mbsf. Hemipelagic sediment is commonly bioturbated between 49 and 74 mbsf, and brecciated and fractured between 17 and 46 mbsf.

Holes 858D and 858F form a continuous section of interbedded hemipelagic and turbiditic sediment near the core of the hydrothermal

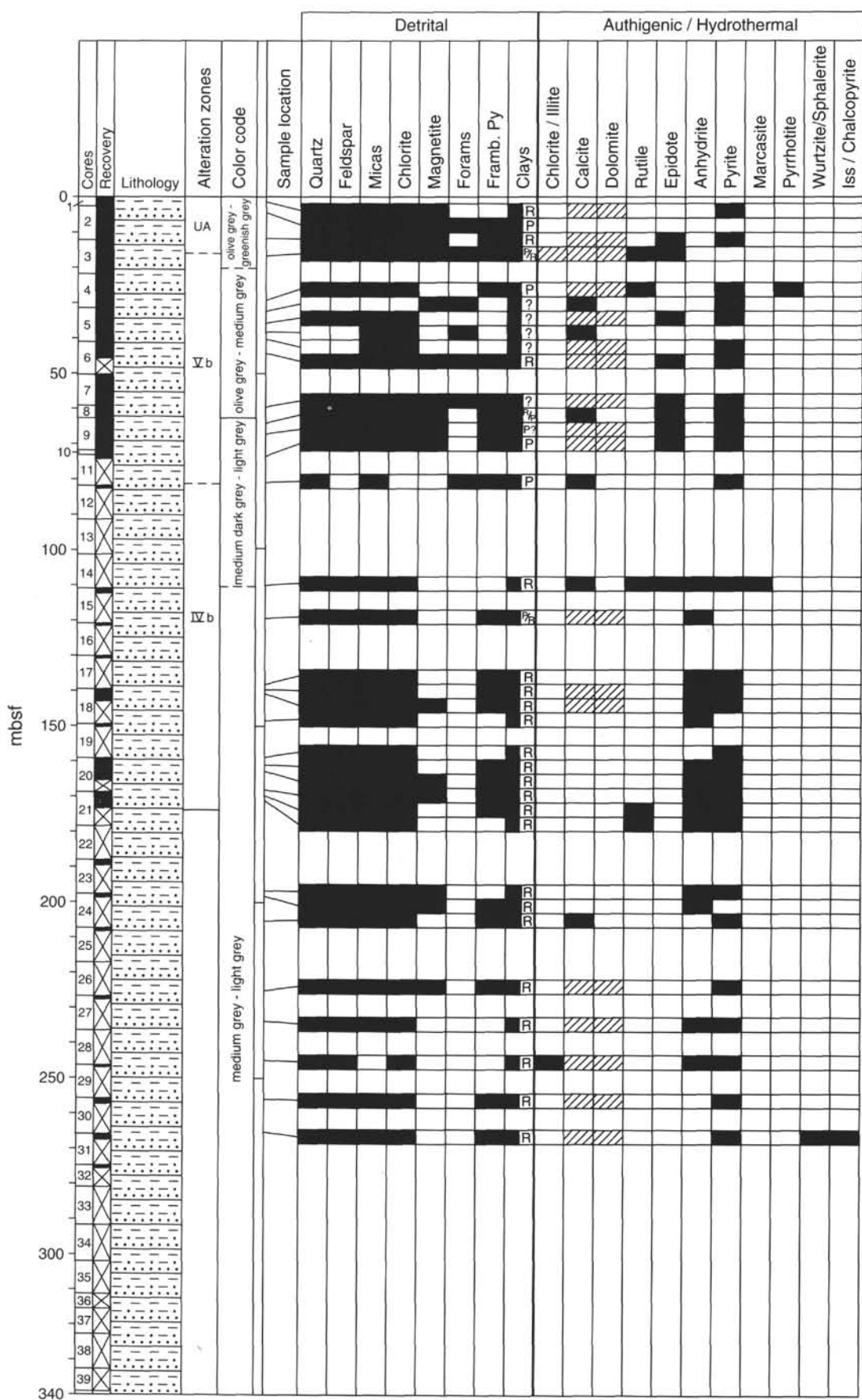


Figure 5. Stratigraphic section of Hole 858A showing the general sedimentology, alteration zones, and detrital, authigenic, and hydrothermal minerals based on thin-section descriptions. UA = unaltered sediment. Letter designates clay recrystallization: N = non; P = partial; R = recrystallized. Black = present; striped = uncertain identification. Lithology symbols as in Fig. 3.

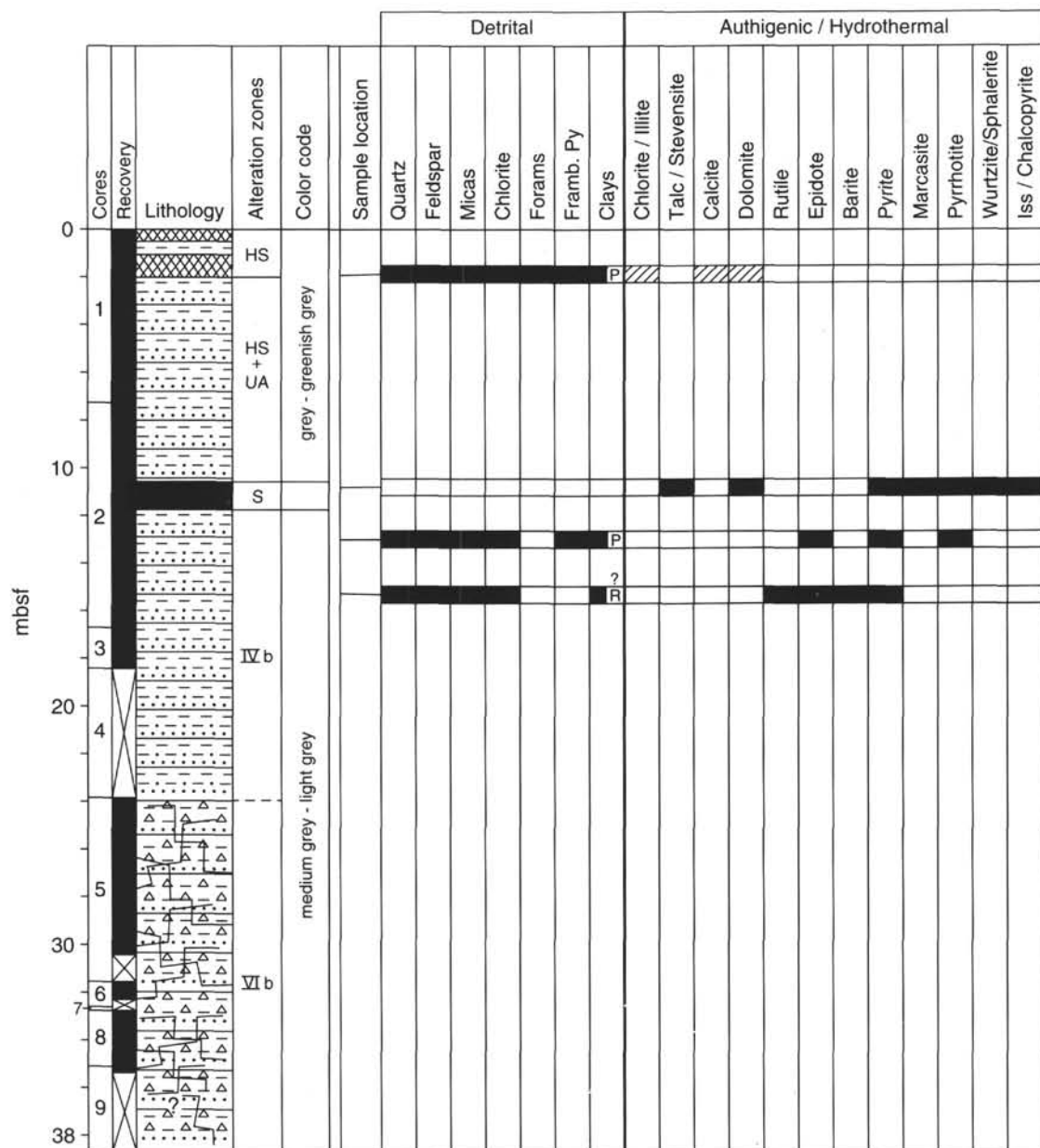


Figure 6. Stratigraphic section of Hole 858B showing the general sedimentology, alteration zones, and detrital, authigenic, and hydrothermal minerals based on thin-section descriptions. UA = unaltered sediment; S = sulfide; HS = hydrothermal sediment. Letter designates clay recrystallization: N = non; P = partial; R = recrystallized. Black = present; striped = uncertain identification. Lithology symbols as in Fig. 3.

upflow zone at Site 858. Holes 858D and 858F intersected 250 m of hydrothermally altered sediment and an additional 46.9 m of underlying mafic flows (Fig. 8). The sediments are unconsolidated to weakly indurated between 0 and 22 mbsf and highly indurated between 22 mbsf and the base of the sedimentary sequence. In the upper part of Holes 858D and 858F (0–14 mbsf), sediments are typically olive grey to greenish grey, whereas the sediments are medium to light grey below 14 mbsf.

Site 857 (Hydrothermal Reaction Zone)

Site 857 is located 1.6 km south of Site 858 and 2.2 km west of Site 856 (Fig. 1) in an area of elevated heat flow (Davis and Villinger, 1992). Holes 857A, 857C, and 857D were collared within 190 m of each other and are treated here as a composite section of the sedimentary sequence to a depth of 936 mbsf. Interbedded hemipelagic and

turbiditic sediments were recovered from the surface to a depth of 480 mbsf (Figs. 9 and 10). Below 480 mbsf, hemipelagic and turbiditic sediments are intercalated with mafic sills (Figs. 10 and 11). Hemipelagic and turbiditic sediments are unconsolidated to weakly indurated and are typically olive grey to greenish grey between 0 and 54 mbsf. Sediments are partly to moderately indurated and olive grey between 54 and 200 mbsf, whereas below 200 mbsf, they are indurated and the sediment color changes from medium dark grey to light grey with depth. Bioturbation is common between 26 and 342 mbsf.

Site 855

Site 855 is in an area of low heat flow near the base of a large fault (115 m throw) at the eastern margin of Middle Valley (Davis, Mottl, Fisher, et al., 1992; Davis and Villinger, 1992) (Fig. 1). Sediment thicknesses near this site are highly variable but generally < 100 m

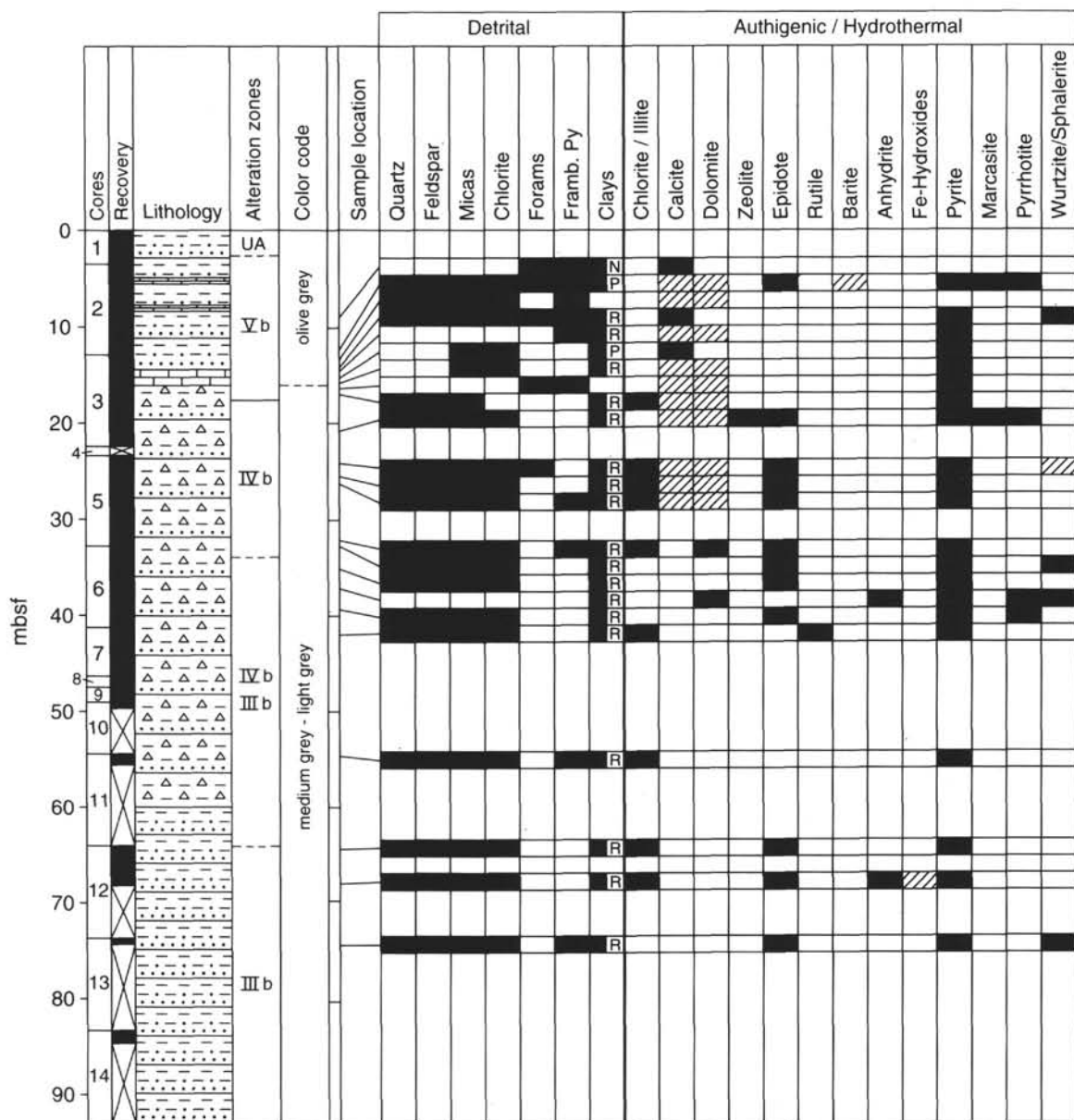


Figure 7. Stratigraphic section of Hole 858C showing the general sedimentology, alteration zones, and detrital, authigenic, and hydrothermal minerals based on thin-section descriptions. UA = unaltered sediment. Letter designates clay recrystallization: N = non; P = partial; R = recrystallized. Black = present; striped = uncertain identification. Lithology symbols as in Fig. 3.

(Davis, Mottl, Fisher, et al., 1992). A total of four holes were drilled at Site 855, at distances between 40 and 125 m from the base of the fault scarp. All three holes sampled at Site 855 are dominated by relatively unaltered, unconsolidated to weakly indurated, interbedded olive grey hemipelagic silty clays and medium to dark grey turbiditic silt and sand. Turbiditic beds display sharp and commonly scoured bases and fine upward into hemipelagic sediment. Hole 855C, the deepest hole (111 m) with the highest (54%) core recovery, penetrated 28 turbidite sequences ranging in thickness from 13 to 131 cm (Davis, Mottl, Fisher, et al., 1992). All holes were terminated in mafic flows and the sediment overlying these flows shows no evidence of thermal metamorphism (Davis, Mottl, Fisher, et al., 1992).

SAMPLING AND ANALYTICAL METHODS

A total of 612 sediment and massive sulfide core samples were collected during Leg 139. Sampling procedures are described in

Davis, Mottl, Fisher, et al. (1992). All samples were described macroscopically and analyzed for major and trace elements (Goodfellow and Peter, this volume); 246 polished thin sections were prepared from selected samples and examined by transmitted- and reflected-light microscopy. Samples of unconsolidated or friable sediment were vacuum-impregnated with epoxy prior to thin-section preparation. X-ray diffraction (XRD) analyses were conducted on 80 powdered bulk sediment samples and interstitial silicate and carbonate minerals drilled from massive sulfides (Holes 856G and 856H). XRD analyses were performed on a Phillips PW1710 X-ray diffractometer at a scanning rate of $6^{\circ}2q$ per minute for the range 3° – $63^{\circ}2q$ using Cu K α radiation at 50 kV and 30 mA.

Silicate, sulfate, carbonate and sulfide minerals in 89 sections were analyzed by a Cameca-Camebax Microbeam electron microprobe utilizing online PAP matrix correction reduction. Due to their fine grain size, clay minerals were analyzed semiquantitatively. Operating conditions used for silicates, carbonates, and sulfates were 15

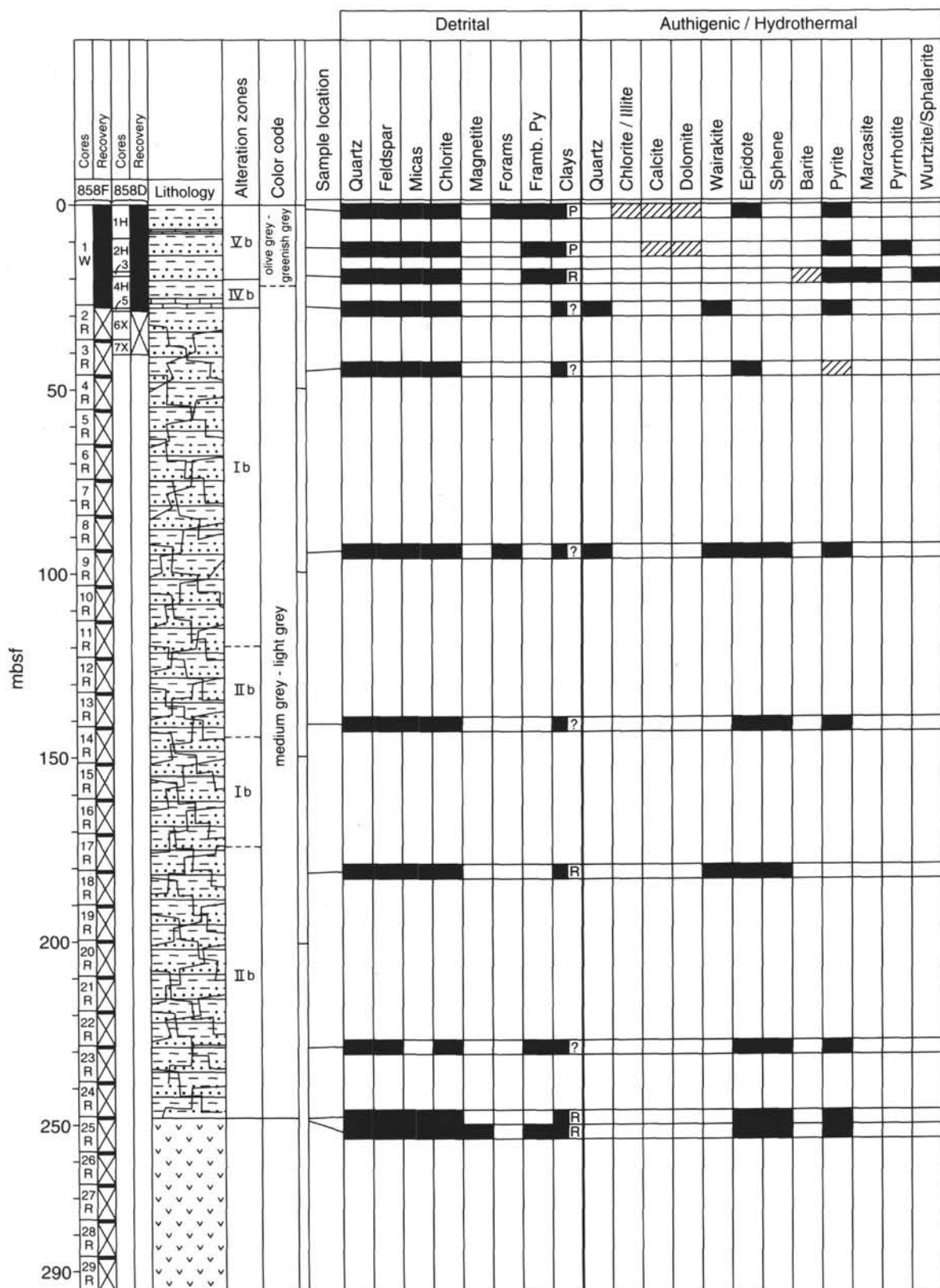


Figure 8. Stratigraphic section of Holes 858D and 858F showing the general sedimentology, alteration zones, and detrital, authigenic, and hydrothermal minerals based on thin-section descriptions. Letter designates clay recrystallization: N = non; P = partial; R = recrystallized. Black = present; striped = uncertain identification. Lithology symbols as in Fig. 3.

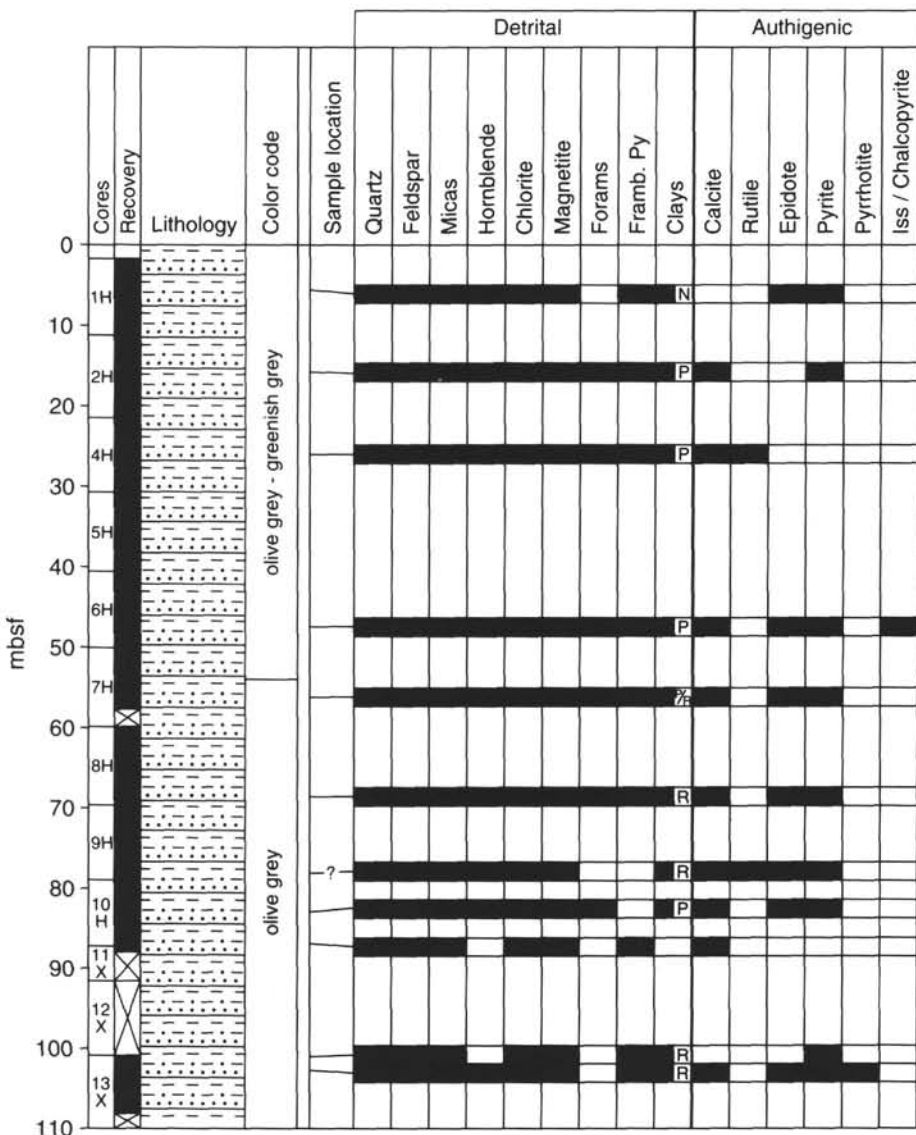


Figure 9. Stratigraphic section of Hole 857A showing the general sedimentology and mineralogy based on thin-section descriptions. Letter designates clay recrystallization: N = non; P = partial; R = recrystallized. Black = present; striped = uncertain identification. Lithology symbols as in Fig. 3.

kV electron acceleration potential and 1–2 µm beam diameter. For feldspars and wairakite, counting times were 40 seconds for all elements and the sample current was 10 nA. Mineral standards used were sodium chloride (Na), potassium bromide (K), quartz (Si), magnetite (Fe), corundum (Al), wollastonite (Ca), and sanidine (Ba). For all other silicates, counting times were 20 seconds at 10 nA sample current for Na, K, Mg, and Fe and 10 seconds at 30 nA for Al, Si, Ca, Ti, Mn, Cr, and Zn. The mineral standards used were labradorite (Na, Al, Si), orthoclase (K), diopside (Mg, Ca), fayalite (Fe), rutile (Ti), rhodochrosite (Mn, Zn), and chromite (Cr). For sulfate and carbonate minerals, 10 seconds counting time was used for all elements at 10 nA (Ca, Mg, Ba, Fe, and Zn) and 30 nA (Sr, Mn, S, and Si) sample current. Mineral standards used were dolomite (Ca, Mg), barite (Ba, S), magnetite (Fe), smithsonite (Zn), strontianite (Sr), rhodochrosite (Mn), and quartz (Si).

Thirty polished thin sections and grain mounts were analyzed using a Cambridge S-200 scanning electron microscope (SEM) fitted with an energy dispersive X-ray (EDS) detection system (Link Analytical AN10 analyzer) to allow semiquantitative determinations of the clay minerals. The SEM was run at 20 kV at working distances of 15 to 30 mm, in both secondary and backscatter modes.

MINERALOGY

Unaltered Sediment

Unaltered sediments were recovered from Site 855, the uppermost 17 m of Holes 856A and 856B, the uppermost 10 m of Hole 858A, and the uppermost 70 m of Hole 857A. Unaltered sediments are unconsolidated to weakly indurated, interbedded, olive-grey hemipelagic silty clays and medium- to dark-grey turbiditic silt and sand. The petrographic and XRD mineralogy of unaltered sediments are consistent with previous studies from Middle Valley and show that hemipelagic sediment consists, in order of decreasing abundance, of quartz, plagioclase, amphibole, mica, chlorite, and epidote with a clay fraction composed of smectite > chlorite > illite > irregular mixed layer clays (Tables 1 and 2; Goodfellow and Blaise, 1988; Al-Aasm and Blaise, 1991; Goodfellow et al., in press; Turner et al., in press). Important minor and trace minerals include calcite, pyrite, and magnetite (Table 1).

Detrital quartz is abundant (up to 40 volume percent [vol%]) and consists of equant, anhedral to subhedral grains devoid of fluid inclusions. Quartz is highly variable in size and ranges from <75 µm in silty clay to >125 µm in turbiditic sandy silt. Detrital feldspar occurs

Table 1. Summary of downhole mineralogy for Hole 855C.

Core, section, interval (cm)	Grain size	Depth (mbsf)	Qz	Fs	Clay	Micas	Ch	Hb	Ep	Mag	M-f	F-py	Carb	Py
139-855C-														
1R-1, 57–61	Silty clay	0.57	xxx	xx	xxxxx	xxx	xx	x		x	xx	x		x
2R-1, 53–57	Silty clay	9.23	xxx	xx	xxxxx	xxx	xx	x		x	xx	x		
3R-1, 45–47	Silty clay	18.15	xxx	xx	xxxxx	xx	xx			x		x	x	x
7R-4, 80–84	Silty clay	61.40	xxxx	xxx	xxxxx	xxxx	xx	xxx		x	xxx	x	xxx	
10R-1, 130–134	Silty clay	86.20	xxx	xx	xxxxx	xx	xx	xx		x		x		x
11R-1, 115–119	Finegrained sand	95.75	xxxx	xxxx	xxxx	x	xx	xxx	xxx	x			x	

Notes: xxxx = dominant (>50%); xxxx = major (11–50%); xxx = minor (3–10%); xx = trace (1–2%); x = rare (<1%); Qz = quartz; Fs = feldspar; Hb = hornblende; Ch = chlorite; Carb = carbonate; Ep = epidote; Mag = magnetite; M-f = microfossils; F-py = frambooidal pyrite; Py = pyrite.

as subequal, subhedral to anhedral, twinned, unaltered grains, although K-feldspar commonly exhibits incipient alteration to chlorite and sericite. The most abundant feldspar is plagioclase (An 1 to An 58) with lesser K-feldspar (Table 3; Fig. 12A). Detrital mica up to 12 µm in length forms up to several vol%. The dominant detrital mica is muscovite, although rare biotite also occurs in some samples. Chlorite occurs as detrital crystals up to 100 µm in length, and also forms a significant component of the clay fraction. Hornblende occurs as equant, subhedral to anhedral grains up to 100 µm in diameter and forms up to 5 vol% (Table 1). Ragged to anhedral detrital Fe-rich, Al-poor epidote (Table 4; Fig. 13) occurs preferentially in coarser-grained turbidites. Frambooidal and anhedral pyrite occur in trace amounts (Table 1) commonly infilling burrows and, less commonly, the centers of foraminifers. Disseminated anhedral to subhedral magnetite occurs in trace amounts throughout Hole 855C (Table 1).

Clay minerals consist of chlorite, illite, and smectite and are typically weakly recrystallized above 10 mbsf. They become increasingly recrystallized and fibrous and display common extinction angles at depths greater than 10 mbsf. In Sample 139-855C-11R-1, 115–119 cm (96 mbsf) in Hole 855C, rare small patches of authigenic clay are present.

Minor calcite (Table 1) occurs as foraminifers and anhedral to subhedral calcite cement in turbiditic sand and silt throughout Hole 855C. Foraminifers are variably infilled with calcite to a depth of 62 mbsf in Hole 855C, below which they are absent.

Hydrothermal Alteration

Site 856 (Bent Hill)

BH (Site 856) has been subdivided on the basis of mineralogy, mineral chemistry, and bulk chemistry (Goodfellow and Peter, this volume) into several alteration zones that increase in temperature toward the center of hydrothermal fluid discharge. These zones are discussed below from the outer margins to the core of fluid upflow, are summarized in Table 5, and are shown in Figure 14. The downhole variation of hydrothermal minerals about the BH massive sulfide mound is given in Figures 3 and 4.

Zone IVa

This zone consists of calcite-illite-pyrite and occurs in Hole 856A between 17 and 86 mbsf (Fig. 3). It is not present in Hole 856B due to mass wasting. Sediments in this zone are weakly to moderately indurated.

Detrital quartz below 45 mbsf in Hole 856A commonly contains abundant fluid inclusions and more irregular boundaries than in unaltered sediment, suggesting partial dissolution and recrystallization. Detrital plagioclase is albited (An ≤ 17) at depths > 44 mbsf in Hole 856A (Table 3; Fig. 12A). K-feldspar below 17 mbsf is partially altered to chlorite and sericite. Pyrite occurs finely disseminated throughout hemipelagic sediment and interstitially within turbiditic silt and sand and is associated with burrows and carbonate concretions, commonly as central accumulations or bands in the concretions. Pyrite also replaces

magnetite, which is present in trace amounts throughout this zone in Hole 856A. Pyrite forms euhedral to anhedral crystals and frambooidal aggregates that range up to 2 vol%. The grain size of pyrite increases with depth (up to 500 µm at 60 mbsf).

Clay minerals are increasingly recrystallized with depth as is evidenced by common extinction in thin section and an increase in grain size. XRD data suggest that the clay fraction consists predominantly of chlorite and illite (Davis, Mottl, Fisher, et al., 1992). In turbiditic silt and sand, clay minerals occur interstitial to detrital quartz and feldspar.

Carbonate occurs mainly as calcite concretions and less commonly as disseminated crystals in the interstices of turbiditic silt and sand. Concretions occur between 17 and 86 mbsf (Table 6) in several forms including laminated (e.g., Sample 139-856A-6H-4, 69–77 cm) and concentrically zoned with a solid core and diffuse margins. Concretions range up to 50 cm in length and differential compaction of sediment around some concretions indicates formation before diagenesis whereas laminated concretions probably formed after sediment diagenesis (Davis, Mottl, Fisher, et al., 1992). Concretions from deeper in the hole (69–76 mbsf; Sample 139-856A-9H-1, 44–47 cm and 139-856A-9H-5, 41–42 cm) consist of irregular patches of anhedral to subhedral calcite up to 0.5 mm in diameter.

Zone IIIa

This zone consists of anhydrite-illite-pyrite and occurs between 60 mbsf and the bottom of Hole 856A (Fig. 3) and between 30 and 70 mbsf in Hole 856B (Fig. 4). Sediments in this zone are moderately indurated to indurated and commonly brecciated.

Detrital quartz commonly hosts two-phase fluid inclusions at depths greater than 55 mbsf in Hole 856B, indicating partial recrystallization. Below 22 mbsf in Hole 856B, K-feldspar is increasingly altered to sericite and chlorite. K-feldspar in Sample 139-856B-6H-4, 124–126 cm ranges in composition between Or 81 and Or 97 (Table 3; Fig. 12A). Detrital plagioclase is replaced by albite (An 8.5). Although anhydrite was not observed in hand samples or thin sections from Holes 856A and 856B, the presence of anhydrite molds and associated elevated SO₄²⁻ contents in pore waters from both holes indicates that anhydrite was present but was dissolved by later fluids (Davis, Mottl, Fisher, et al., 1992). The detection of anhydrite in Core 139-856A-8H by XRD and in Sample 139-856B-3H-6, 34–36 cm by SEM is further evidence of the occurrence of hydrothermal anhydrite (Davis, Mottl, Fisher, et al., 1992). Pyrite in Hole 856B occurs predominantly as isolated crystals and crystal clusters and more rarely as frambooidal pyrite that infills burrows. Shipboard logging noted that pyrite clots and disseminations are more abundant along fluid channelways between breccia clasts between 28 and 66 mbsf (Davis, Mottl, Fisher, et al., 1992). Pyrite is typically subhedral to anhedral and is rarely euhedral. Below 55 mbsf, chalcopyrite and rarely pyrrhotite were observed with pyrite. Magnetite is completely replaced by pyrite below 97 mbsf in Hole 856A (Table 6).

Clay minerals in Hole 856B consist predominantly of illite and Mg-chlorite (Tables 7 and 8; Figs. 15A–C and 16), are recrystallized and increase in grain size with depth. The chlorite and illite clays are amorphous to fine-grained (<10 µm) and fibrous between 55 and 95

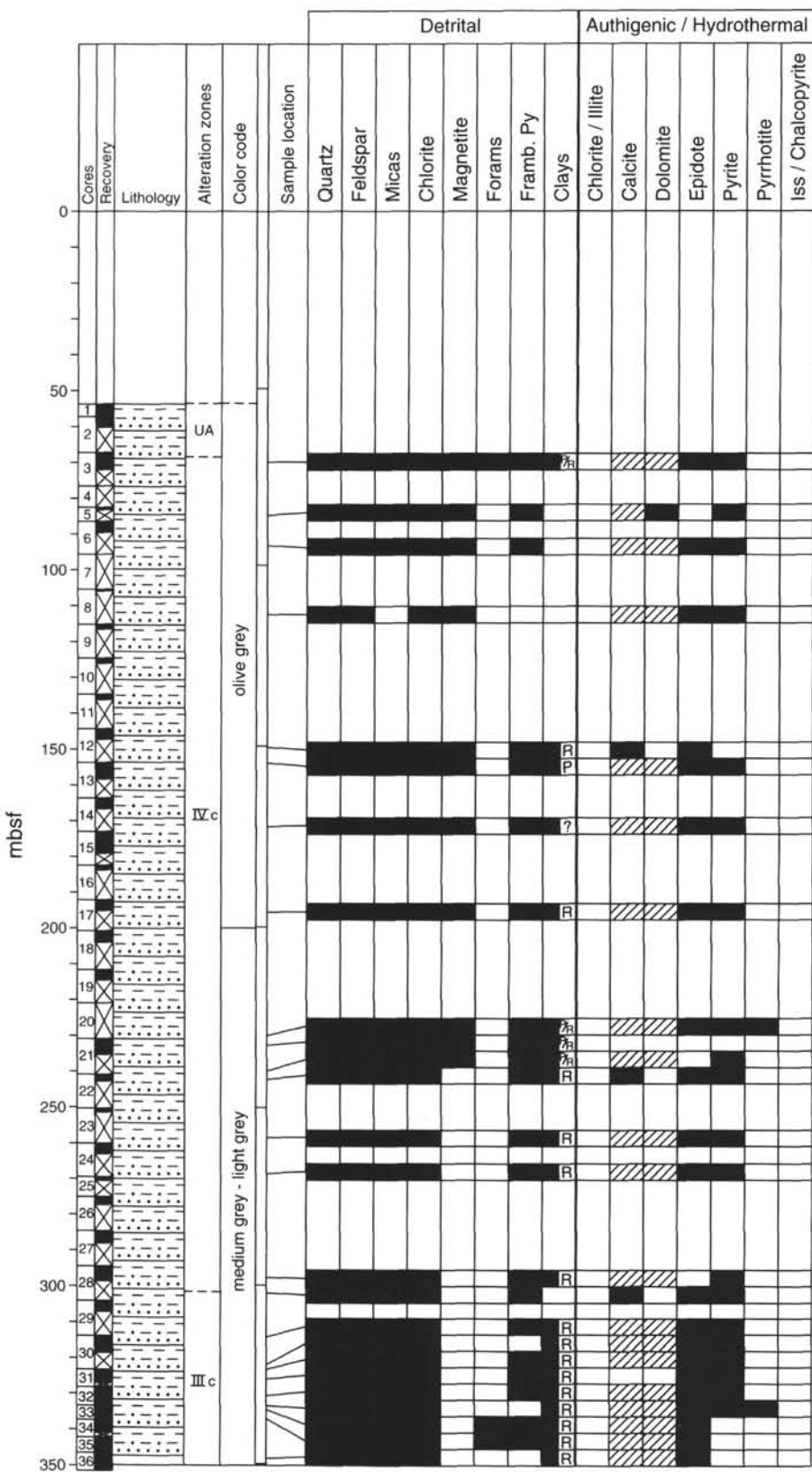


Figure 10. Stratigraphic section of Hole 857C showing the general sedimentology, alteration zones, and detrital, authigenic, and hydrothermal minerals based on thin-section descriptions. UA = unaltered sediment. Letter designates clay recrystallization; N = non; P = partial; R = recrystallized. Black = present; striped = uncertain identification. Lithology symbols as in Fig. 3.

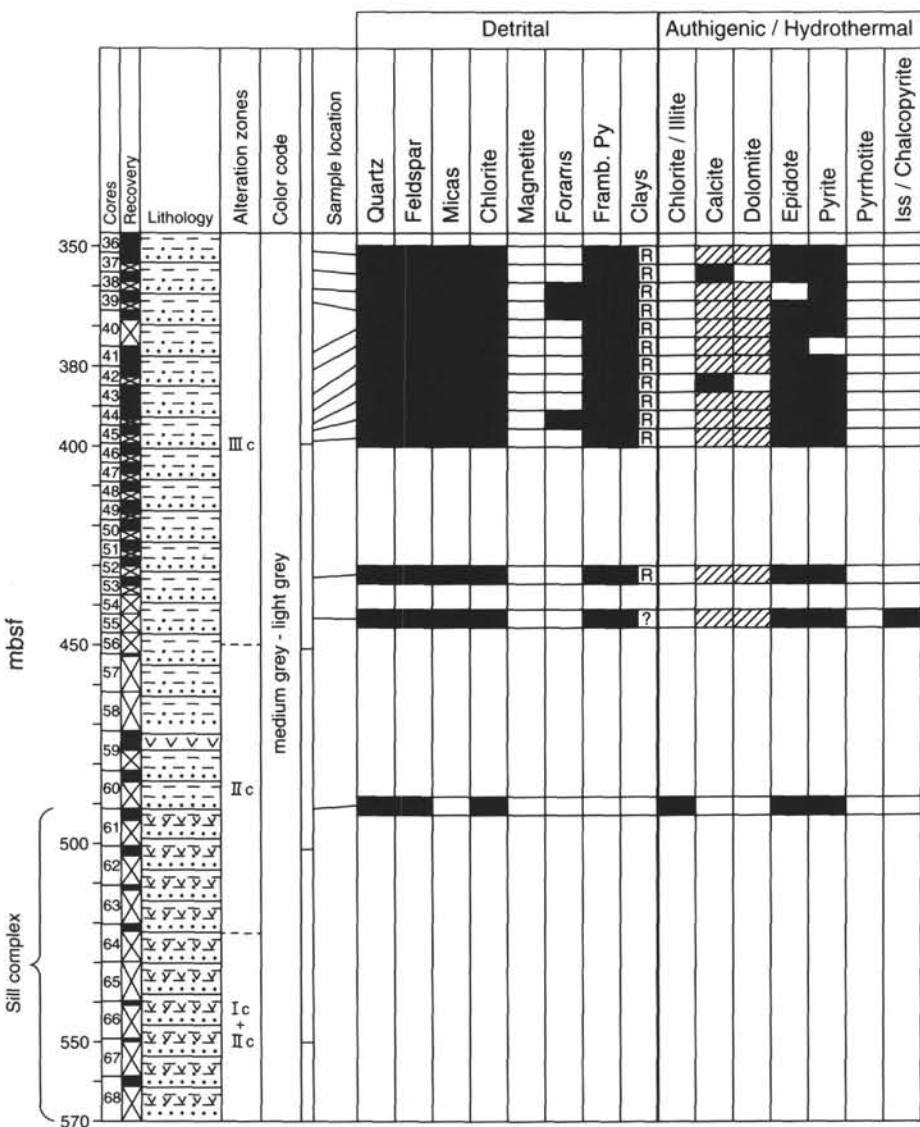


Figure 10 (continued).

mbsf and coarser-grained below 95 mbsf ($10\text{--}25\ \mu\text{m}$; Pl. 1, Figs. 1–6). Clays are more recrystallized in the matrix between breccia clasts.

Zone IIa

This zone, which consists of albite-chlorite-pyrite, occurs between 70 and 110 mbsf in Hole 856B (Fig. 4) and is not present in Hole 856A. Detrital quartz below 75 mbsf has ragged to diffuse boundaries due to overgrowths and recrystallization and is typically anhedral although it rarely exhibits euhedral terminations (Pl. 1, Fig. 1). As in Zone IIIa, plagioclase is altered to albite (Fig. 12A) and K-feldspar is altered to sericite and chlorite. Rutile is an important accessory phase below 72 mbsf in Hole 856B (Table 6; Fig. 4) and commonly occurs in aggregates of 2–5 crystals up to $50\text{--}75\ \mu\text{m}$ in diameter. Rutile's euhedral to anhedral morphology and absence from unaltered sediments indicate that rutile formed authigenically. Pyrite in this zone occurs as anhedral to euhedral isolated crystals and crystal clusters, and is very rarely frambooidal.

Moderately indurated silty clay below 80 mbsf in Hole 856B (Cores 139-856B-12X and -13X) consists of subparallel, aligned, amorphous to fibrous chlorite + illite/muscovite. The clay minerals are up to $25\ \mu\text{m}$ in length and are coarser-grained than in Zone IIIa.

Chlorite and illite/muscovite are more Mg-rich in Zone IIa than Zone Ia (Figs. 15A,B and 16).

Zone Ia-1

This zone occurs in Hole 856B between 110 and 117.5 mbsf (Fig. 4) and is characterized by the high-temperature alteration assemblage quartz-(Fe)chlorite-muscovite-rutile-chalcopyrite-pyrrhotite. Authigenic quartz is typically anhedral to subhedral with ragged boundaries, although quartz separates prepared for isotope analyses commonly exhibit subhedral to euhedral morphologies. Detrital plagioclase and K-feldspar were not observed in this zone and have presumably been destroyed during hydrothermal alteration of sediments to chlorite and illite/muscovite. Pyrite and chalcopyrite form large ($>2\ \text{mm}$) crystal clusters and occur disseminated throughout this zone. Sulfide and sulfate minerals (chalcopyrite-sphalerite-pyrrhotite, chalcopyrite-pyrrhotite, pyrite-chalcopyrite, barite-chalcopyrite, barite, chalcopyrite, and sphalerite) form bedding parallel to high-angle veins in Core 139-856B-15X near the bottom of the hole.

The clay minerals consist of crystalline chlorite and illite/muscovite. Variable Fe and Mg contents in illite/muscovite (Table 8; Fig. 15C) indicate either a muscovite/chlorite mixed layer assemblage or

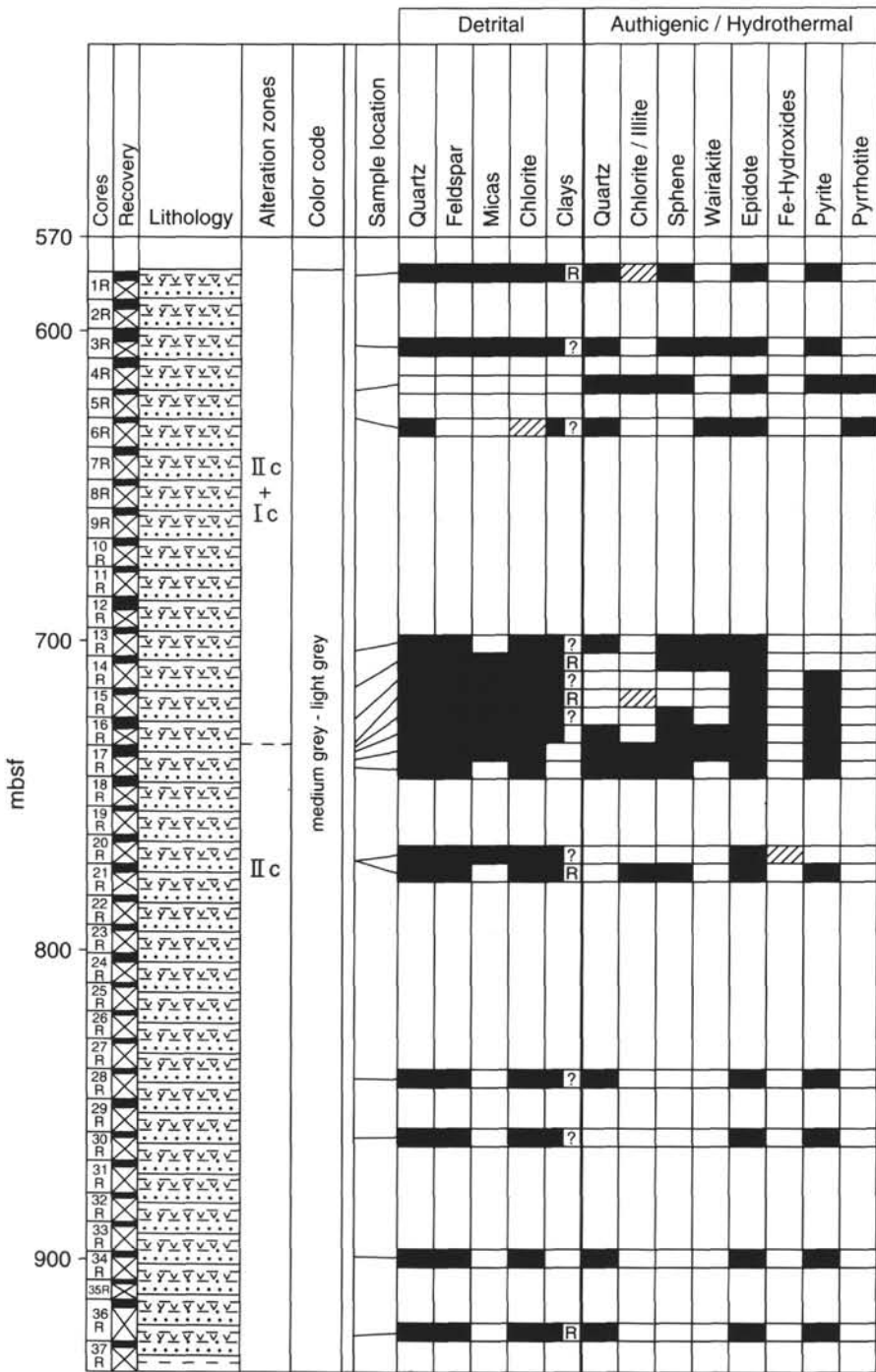


Figure 11. Stratigraphic section of Hole 857D showing the general sedimentology, alteration zones, and detrital, authigenic, and hydrothermal minerals based on thin-section descriptions. Letter designates clay recrystallization: N = non; P = partial; R = recrystallized. Black = present; striped = uncertain identification. Lithology symbols as in Fig. 3.

that the microprobe measured a mixture of muscovite and chlorite. The latter is most likely given the clear separation of chlorite and muscovite in coarse-grained samples in Core 139-856B-15X (Pl. 1, Figs. 1-6). Phyllosilicates from Zones IIIa, IIa, and Ia plotted on a ternary Fe-Al-Mg diagram range in composition from a muscovite end-member (at the Al-apex) to chlorite (Fig. 15A-C). The chlorite in Core 139-856B-15X is typically Fe-rich and generally more Fe-rich than chlorite from Zones IIIa and IIa in Holes 856B and 856A, and core from Sites 857 and 858 (Table 7; Figs. 15 and 16). Chlorite grains in Core 139-856B-15X are rarely zoned from Mg-rich cores to Fe-rich rims (Pl. 1, Fig. 1).

Zone Ia-2

This is a narrow subzone of Zone Ia that immediately overlies the sill at the bottom of Hole 856B (Fig. 4) and is characterized by smectite, chlorite, and albite (this study and Davis, Mottl, Fisher, et al., 1992). This zone contains elevated MgO and CaO and lower SiO₂ contents than Zone Ia-1 (Goodfellow and Peter, this volume).

Albite (< An 9) after detrital plagioclase was detected in samples above the mafic sill (e.g., Sample 139-856B-15X-CC, 20–22 cm; 118.22 mbfs; Table 3; Fig. 12A). Chlorite adjacent to chalcopyrite

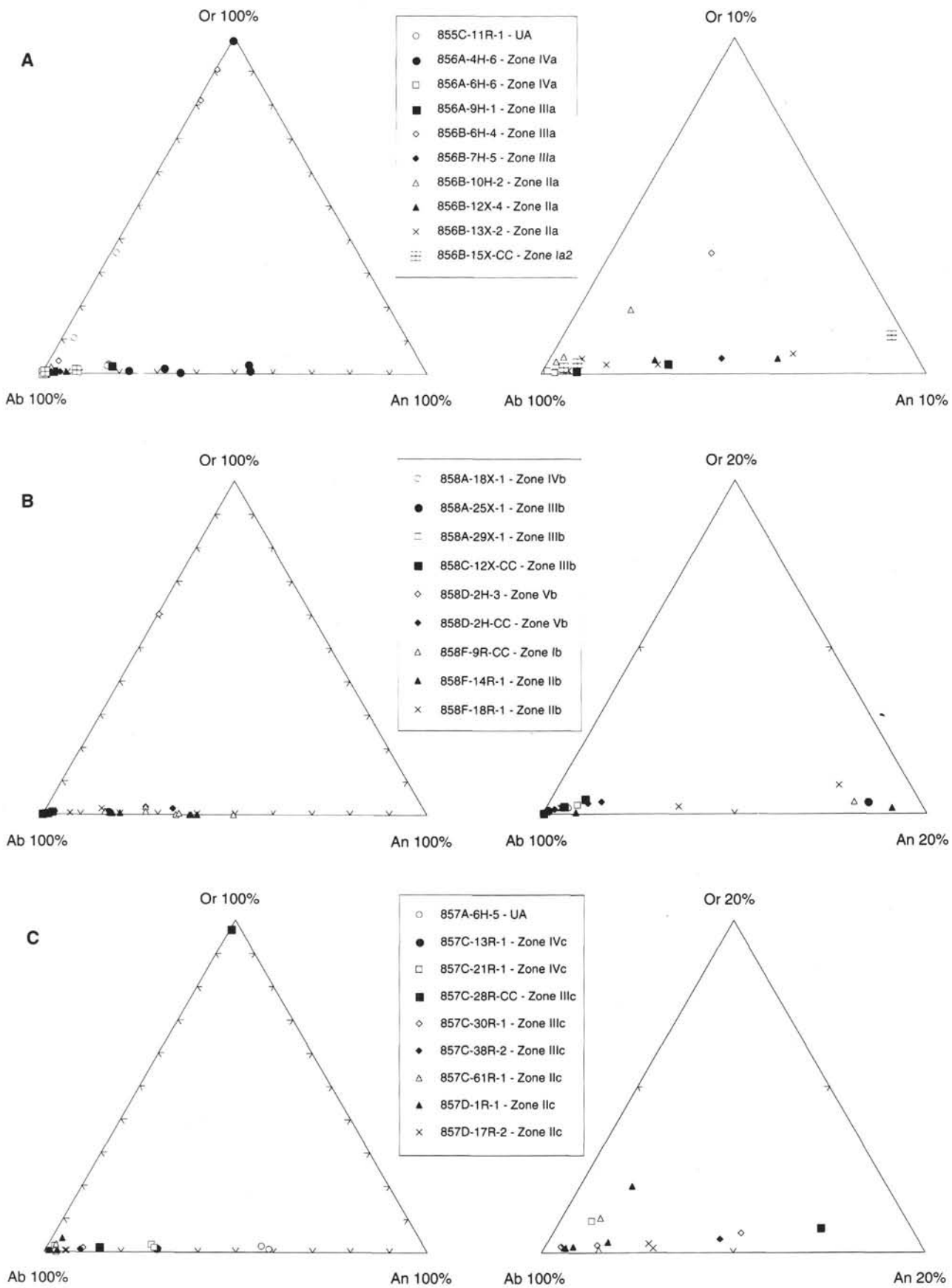


Figure 12. Ternary orthoclase (Or)-albite (Ab)-anorthite (An) diagram for feldspar minerals. A. Sites 855 and 856. B. Site 858. C. Site 857. Data from Table 3.

Table 2. X-ray diffraction mineralogy for Leg 139 bulk samples.^a

Core, section, interval (cm)	Depth (mbsf)	Qz	Pl	Am	Ch	Il	Ca	Sm	Ta	Py	Mr	Se	Do	Si	Gy	An	Wa
139-855C-																	
1R-1, 57–61	0.57	xxxx	xxx		xxx	xx	xxx	x									
2R-1, 53–57	9.23	xxxx	xxxx	x	xxx	x											
3R-1, 45–47	18.15	xxxx	xxx	xx	xxxx	xxx	x	xx									
10R-1, 130–134	86.20	xxxx	xxx	xx	xxxx	xxx	x	xx									
11R-1, 115–119	95.75	xxxx	xxxx	xx	xxx												
139-856B-																	
7H-5, 26–32	55.56	xxxx	xxx		xxx	xx											
13X-2, 63–67	93.23	xxxx	xxxx		xxx	x											
14X-1, 34–36	101.14	xxxx			xxx	xx											
15X-1, 91–93	111.31	xxxx			xxxx	x											
15X-1, 124–126	111.64	xxxx			xxxx	x											
15X-2, 67–69	112.57	xxxx			xxxx	x											
15X-3, 8–10	113.48	xxxx			xxxx	x											
15X-4, 12–14	115.02	xxxx			xxxx	x											
15X-5, 106–108	117.46	xxxx			xxxx	x		xxx									
15X-CC, 20–22	118.22	xxxx	xxx		xxxx												
139-856D-																	
1H-1, 34–37	0.34																
1H-2, 57–59	2.07	xxxx															
1H-3, 16–20	3.16																
1H-5, 66–69	6.66	xxx															
1H-7, 46–48	7.89	xxx															
139-856E-																	
1H-1, 48–50	0.48	xxxx	xx														
1H-1, 73–75	0.73	xxxx	xx		xx												
1H-1, 129–131	1.29																
1H-2, 55–57	2.05																
139-856G-																	
2R-2, 54–56	10.64	xxxx															
6R-3, 132–134	50.62																
7R-4, 35–37	60.45																
139-856H-																	
3R-3, 72–74	25.43																
4R-1, 21–23	26.81																
4R-1, 88–90	27.48																
4R-2, 43–45	28.53																
4R-3, 16–17	29.72																
6R-1, 39–41	37.79																
9R-1, 68–70	53.18																
11R-1, 114–117	62.44																
139-857C-																	
2R-2, 6–10	58.06	xxxx	xx	x	xxx												
3R-3, 110–112	70.60	xxxx	xx	x	xxx	x											
10R-1, 65–67	124.75	xxxx	xx		xxx	x											
13R-3, 52–54	156.62	xxxx	xxxx		xx												
15R-1, 147–149	173.97	xxxx	xx		xx												
17R-2, 61–65	194.01	xxxx	xx		xx												
21R-1, 24–26	230.84	xxxx	xxxx		xxx	xx											
22R-CC, 1–5	242.01	xxx	xx														
28R-2, 119–122	296.49	xxxx															
30R-1, 116–120	314.26	xxxx	xxxx		xxx	x											
38R-2, 50–53	357.80	xxx	xxxx		xxx	x		xxx									
44R-1, 137–140	391.07	xxxx	xxxx		xxx	xx	x										
53R-1, 50–52	433.30	xxx	xxxx		xxxx	x											
139-857D-																	
1R-1, 137–139	582.87	xxxx	xx		xx												
5R-1, 26–28	618.86	xxxx															
14R-1, 22–25																	
17R-2, 10–13	735.50	xxxx	xx		xx												
21R-2, 14–16	773.84	xxxx	xx		xxx												
28R-1, 67–69	839.57	xxxx	xx														
139-858A-																	
1H-2, 5–7	1.55	xxxx	xx		x	x	x										
2H-1, 125–127	3.65	xxxx	xx	x	xxx	xx	xx										
3H-4, 29–33	16.46	xxxx	xx	x	xx	xx	xx										
4H-6, 48–50	29.38	xxxx	xx		xxx	xx	xx	xx									
5H-5, 54–57	37.44	xxxx	xx		xxx	xx	xx	xx									
6H-3, 77–79	44.17	xxxx	xx		xxx	xx	xx	xx									
9X-4, 52–56	67.52	xxxx	xx		xxx	xx	xx	xx									
11X-CC, 10–12	73.57	xxxx	xx		xx	xx	xx	xx									
15X-1, 35–37	110.95	xxxx	xx		xxx	xx	xx	xx									
18X-1, 116–118	140.76	xxxx	xx		xxx	xx	xx	xx									
20X-4, 100–103	164.44	xxxx	xx		xxxx	xx											
21X-3, 57–59	171.98	xxx	xx		xx	xx	xx										
24X-1, 33–35	197.93	xxxx	xxxx		xxxx	xx											
25X-1, 29–32	207.59	xxxx	xx		xxxx	xx											
29X-1, 30–32	246.20	xxxx	xx														

Table 2 (continued).

Core, section, interval (cm)	Depth (mbsf)	Qz	Pl	Am	Ch	Il	Ca	Sm	Ta	Py	Mr	Se	Do	Si	Gy	An	Wa
139-858B-																	
1H-2, 21–23	1.71	x				xx											
1H-2, 50–54	2.00	xxxx	xxx	x	xxx	xx	xx	xxx									
1H-CC, 8–12	6.98	xxxx	xxx		xxx	xx											
2H-6, 69–71	15.39	xxxx	xxx			xxxx	xx										
5H-3, 118–121	28.08	xx				xxxx ^b											
5H-4, 27–29	28.67					xxxx ^b											
139-858F-																	
2R-CC, 7–10	27.87	xxxx				xxx											xxx
9R-CC, 9–11	94.29	xxxx				xx											xxxx
14R-1, 10–12	142.70	xxxx	xxxx			xxx											
18R-1, 14–16	181.44	xxxx	xxx			xxx											
25R-1, 71–73	249.61	xxxx	xxxx			xxxx											xx

Notes: xxxx = major; xxx = minor; xx = trace; x = slight trace; Qz = quartz; Pl = plagioclase feldspar; Am = amphibole; Ch = chlorite; Il = illite; Ca = calcite; Sm = smectite; Ta = talc; Py = pyrite; Mr = marcasite; Se = serpentine; Do = dolomite; Si = siderite; Gy = gypsum; An = anhydrite; Wa = wairakite.

^a Relative mineral abundances were determined from peak heights.

^b Vermiculite, possibly.

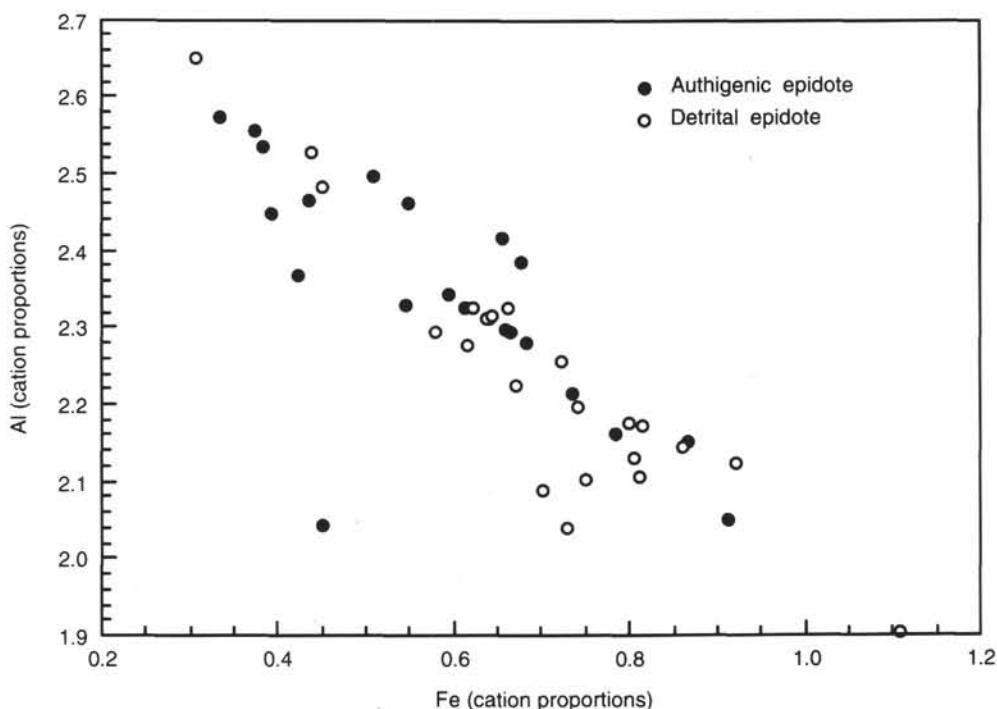


Figure 13. Fe vs. Al (cation proportions) of epidote, showing difference between detrital and authigenic epidote for all sites. Data from Table 4.

veins plots near the Mg-rich end of the chlorite field for Core 139-856B-15X (Sample 139-856B-15X-CC, 20–22 cm; Figs. 15B and 16). Smectite was detected in Sample 139-856B-15X-CC, 20–22 cm immediately above the mafic sill. This sample also contains elevated MgO contents compared to other samples in Core 139-856B-15X, suggesting that the smectite is a hydrothermal saponite. Tabular barite in crystals up to 6 mm in length occur with chalcopyrite in veins below 111 mbsf (e.g., Sample 139-856B-15C-CC, 20–22 cm; Davis, Mottl, Fisher, et al., 1992).

Hydrothermal Minerals in Massive Sulfides

Hydrothermal quartz ranges up to 70 vol% (e.g., Sample 139-856G-2R-2, 54–56 cm) in massive sulfides from Holes 856D through 856H. This quartz consists of euhedral to anhedral crystals up to 400 µm in diameter (typically <100 µm) that commonly display a hexagonal morphology (Pl. 2, Fig. 1), undulose extinction and concentric (growth?) zonation of fluid inclusions (Pl. 2, Figs. 2 and 3). Quartz also cements sulfide clasts.

Talc occurs in Hole 856B as a fine-grained network interstitial to collomorphic and euhedral pyrite (Sample 139-856B-3H-5, 110–113 cm; Pl. 2, Figs. 3–6). Talc displays minor Fe substitution for Mg and low Al contents (Table 9; Fig. 15D,E). The low Al/Mg ratios of clastic sulfide samples in Hole 856B are in agreement with talc that occurs with massive sulfides in shallow cores (Goodfellow and Franklin, in press). Talc is the dominant Mg-silicate in Holes 856D–856H (Tables 2 and 8; Fig. 15D,E; Pl. 2, Figs. 3 and 6) although some samples from Hole 856E also contain hemipelagic components, mostly chlorite, quartz, and feldspar. Authigenic clays occur interstitially to pyrite and barite (Sample 139-856D-1H-2, 43–46 cm) and have locally replaced barite. Below 49 mbsf in Hole 856G, serpentine occurs with talc (Tables 2 and 9).

Hemipelagic sediment occurs interbedded with massive sulfides between 25 and 30 mbsf in Hole 856H (Cores 139-856H-3R and 139-856H-4R) and may represent a hiatus in hydrothermal sedimentation. These sediments are intensely altered and crosscut by an anastomosing network of pyrrhotite–pyrite–sphalerite–chalcopyrite veins. The sediment is altered to chlorite, talc, and smectite (saponite?); this

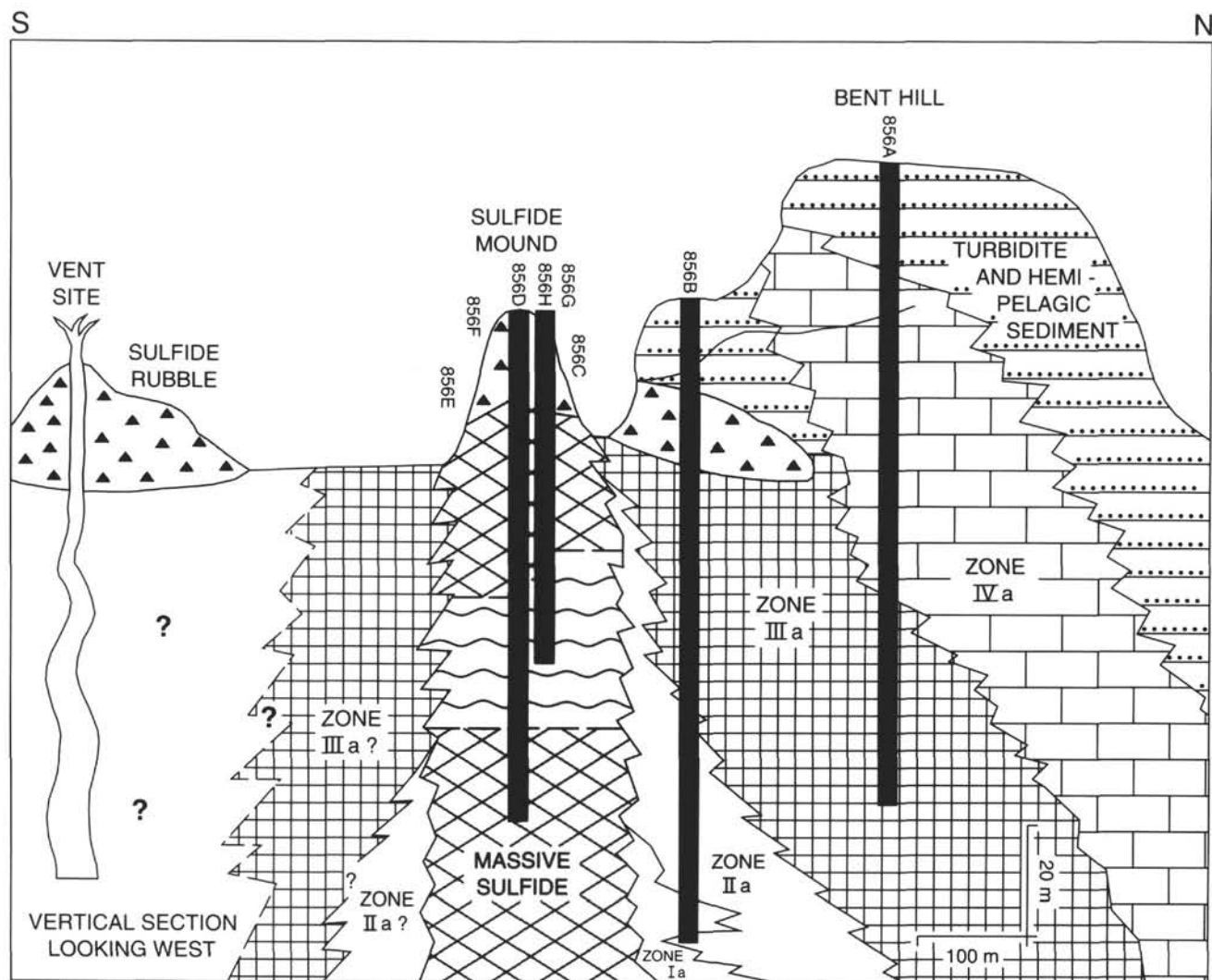


Figure 14. North-south profile of Site 856 (Bent Hill and sulfide mounds) showing the distribution of the alteration zones about the Bent Hill massive sulfide deposit. Zone characteristics are given in the text and in Table 5.

smectite has variable Al contents and plots between chlorite and talc on a Fe-Al-Mg diagram (Table 9; Fig. 15D). Chlorite from Samples 139-856H-3R-3, 72–74 cm and 139-856H-4R-1, 88–90 cm is enriched in MgO compared with most chlorites from Core 139-856B-15X (Fig. 15B; Pl. 3, Fig. 1). Some clay minerals in Sample 139-856H-3R-3, 72–74 cm are FeO-rich and SiO₂- and Al₂O₃-poor (Table 9), plot above the chlorite field in Figure 15, and are compositionally similar to nontronite.

Barite is erratically distributed and forms up to 10–15 vol% (Sample 139-856D-1H-1, 34–37 cm). Its abundance is consistent with bulk contents that range up to 8.8 weight percent (wt%) Ba (Goodfellow and Peter, this volume). Barite forms isolated crystals up to 600 µm in length, rosettes (Pl. 3, Fig. 2), and aggregates of broken, fine-grained crystals. The SrO content of barite ranges up to 3.6 wt% (Table 10).

Dolomite is the dominant carbonate phase in Hole 856G and Hole 856H although calcite, siderite, and magnesite are also present (Pl. 3, Figs. 3 and 4; Table 11; Fig. 17A). Individual dolomite crystals are up to 400 µm in diameter and are coarser grained and less altered near the center of carbonate veins and masses than at the edges. Magnesite typically displays a more elongate, feathery habit than the other carbonate minerals (Pl. 3, Fig. 3). Fe in dolomite commonly shows oscillatory zoning (Pl. 3, Figs. 5 and 6) and dolomite grains are commonly overgrown by later magnetite (Pl. 3, Fig. 5).

Site 858 (Area of Active Venting)

Six different hydrothermal alteration zones (Table 5) are recognized at Site 858; these are distributed laterally and vertically about the center of hydrothermal fluid discharge (Fig. 18). The textural and mineralogical characteristics are discussed below for each zone, from the margins to the core of fluid upflow.

Zone VIb

This zone consists of Mg-smectite (saponite), talc, dolomite, and pyrite between 24 and 38 mbsf in Hole 858B (Fig. 6). Below 24 mbsf, the sediments are brecciated, infilled and/or replaced by Mg-rich clays (saponite or vermiculite), chlorite (Table 2), and anhydrite, and cut by quartz and anhydrite veins. Bulk sediment contains up to 30 wt% MgO (Goodfellow and Peter, this volume). Saponitic muds also occur in the uppermost two meters of Hole 858B (Fig. 6), as has been previously reported for shallow cores from AAV (Goodfellow et al., in press).

Zone Vb

This zone consists of calcite(±dolomite)-illite-pyrite and occurs between 15 and 80 mbsf in Hole 858A (Fig. 5), 2 and 17 mbsf in Hole 858C (Fig. 7), and 0 and 20 mbsf in Hole 858D (Fig. 8). Carbonate

Table 3. Electron microprobe data for detrital and authigenic feldspar in unaltered and hydrothermally altered hemipelagic and turbiditic sediment, Leg 139.

Site:	855C				856A				856A				856A				856B			
Core, section:	11R-1				4H-6				6H-6				9H-1				6H-4			
Interval (cm):	115–119				55–59				90–94				44–47				124–126			
Zone:	UA				IVa				IVa				IIIa				IIIa			
SiO ₂	64.28	66.09	67.01	64.17	60.80	65.58	59.51	55.28	63.60	54.14	67.63	67.43	68.00	66.36	62.81	62.93	63.29	66.42	65.56	
Al ₂ O ₃	22.69	19.56	20.52	22.34	24.63	17.72	25.62	28.63	23.69	27.60	20.05	19.56	20.16	19.74	22.11	17.70	18.72	20.91	19.20	
FeO	0.21	0.12	0.16	0.30	0.10	0.05	0.05	0.63	0.12	0.88	0.12	0.09	0.17	0.17	0.13	0.22	0.17	0.19	0.08	
CaO	3.25	0.28	0.62	3.18	6.31	0.04	7.16	10.68	4.36	10.43	0.03	0.06	0.62	0.17	3.45	0.00	0.06	0.54	0.18	
Na ₂ O	9.16	6.72	9.31	9.20	7.52	0.08	7.06	5.00	8.53	5.01	11.63	10.75	10.56	10.54	8.91	0.33	1.05	10.64	2.10	
K ₂ O	0.44	5.87	1.70	0.36	0.25	16.73	0.08	0.18	0.19	0.49	0.02	0.01	0.05	0.01	0.35	16.04	15.90	0.62	14.46	
BaO	0.00	0.18	0.62	0.25	0.11	0.00	0.00	0.09	0.00	0.00	0.24	0.00	0.00	0.00	0.00	0.42	1.17	0.00	0.79	
Total	100.02	98.82	99.95	99.79	99.71	100.19	99.48	100.67	100.48	98.54	99.71	97.90	99.56	96.99	97.76	97.63	100.37	99.31	102.37	
Si	11.332	11.915	11.817	11.362	10.840	12.108	10.643	9.930	11.166	9.947	11.877	11.986	11.908	11.918	11.330	11.982	11.808	11.726	11.859	
Al	4.717	4.157	4.265	4.662	5.177	3.856	5.401	6.062	4.904	5.979	4.150	4.099	4.162	4.180	4.703	3.974	4.118	4.352	4.095	
Fe	0.030	0.018	0.023	0.044	0.014	0.007	0.007	0.094	0.018	0.135	0.018	0.013	0.025	0.026	0.020	0.035	0.027	0.028	0.013	
Ca	0.614	0.054	0.117	0.602	1.206	0.007	1.371	2.056	0.820	2.054	0.005	0.012	0.117	0.033	0.666	0.000	0.012	0.101	0.035	
Na	3.132	2.351	3.185	3.158	2.599	0.029	2.449	1.740	2.903	1.783	3.961	3.704	3.585	3.669	3.117	0.121	0.381	3.643	0.735	
K	0.098	1.350	0.383	0.081	0.056	3.942	0.018	0.040	0.042	0.115	0.004	0.002	0.011	0.003	0.080	3.896	3.785	0.139	3.336	
Ba	0.000	0.013	0.043	0.017	0.007	0.000	0.000	0.007	0.000	0.000	0.016	0.000	0.000	0.000	0.000	0.031	0.086	0.000	0.056	
An	15.98	1.44	3.18	15.68	31.24	0.17	35.72	53.59	21.78	51.97	0.12	0.32	3.15	0.88	17.25	0.00	0.29	2.61	0.85	
Ab	81.47	62.61	86.42	82.21	67.31	0.72	63.80	45.36	77.10	45.13	99.79	99.63	96.56	99.04	80.68	3.02	9.13	93.81	17.90	
Or	2.55	35.95	10.40	2.11	1.45	99.11	0.48	1.05	1.12	2.91	0.10	0.04	0.28	0.09	2.07	96.98	90.59	3.58	81.26	

Site:	856B				856B				856B				856B				856B				857A		857C	
Core, section:	7H-5				10H-2				12X-4				13X-2				15X-CC				6H-5		13R-1	
Interval (cm):	26–32				54–58				29–33				63–69				20–22				89–93		6–8	
Zone:	IIIa				IIa				IIa				IIa				Ia2				UA		IVc	
SiO ₂	66.71	68.14	67.63	67.58	67.86	66.25	66.95	66.05	64.21	66.60	68.04	67.61	67.20	66.93	66.61	52.62	53.28	61.85						
Al ₂ O ₃	20.55	18.64	19.61	19.50	20.16	20.52	20.19	20.00	19.88	19.62	19.93	20.04	20.88	19.78	19.33	28.48	28.76	24.64						
FeO	0.15	0.10	0.10	0.09	0.19	0.12	0.10	0.17	0.18	0.17	0.16	0.13	0.21	0.12	0.18	0.48	0.84	0.07						
CaO	0.92	0.07	0.04	0.13	0.29	1.24	0.58	0.61	1.24	0.13	0.17	0.33	1.80	0.10	0.16	10.98	11.70	6.32						
Na ₂ O	10.89	10.88	11.60	11.61	11.38	10.89	11.33	11.24	10.23	11.32	11.28	11.33	10.50	11.56	11.42	4.60	4.58	8.34						
K ₂ O	0.08	0.09	0.07	0.02	0.34	0.08	0.08	0.05	0.10	0.02	0.08	0.05	0.20	0.04	0.06	0.29	0.15	0.13						
BaO	0.04	0.00	0.11	0.00	0.00	0.25	0.00	0.10	0.11	0.00	0.09	0.00	nd	0.08	0.00	0.02	0.20	nd						
Total	99.34	97.90	99.16	98.92	100.22	99.35	99.21	98.21	95.95	97.85	99.75	99.48	100.78	98.60	97.76	97.71	99.61	101.36						
Si	11.762	12.114	11.930	11.940	11.860	11.717	11.815	11.793	11.737	11.895	11.920	11.880	11.704	11.878	11.919	9.766	9.728	10.858						
Al	4.271	3.906	4.078	4.061	4.154	4.280	4.200	4.210	4.283	4.131	4.116	4.151	4.288	4.139	4.077	6.232	6.190	5.100						
Fe	0.022	0.014	0.015	0.013	0.028	0.018	0.015	0.026	0.027	0.025	0.024	0.018	0.030	0.017	0.027	0.075	0.128	0.011						
Ca	0.174	0.013	0.008	0.025	0.055	0.235	0.110	0.116	0.242	0.025	0.032	0.061	0.335	0.019	0.031	2.183	2.288	1.188						
Na	3.721	3.749	3.968	3.978	3.855	3.734	3.876	3.890	3.625	3.921	3.831	3.860	3.546	3.976	3.963	1.655	1.620	2.840						
K	0.018	0.020	0.015	0.004	0.076	0.018	0.017	0.010	0.024	0.004	0.018	0.011	0.044	0.008	0.013	0.070	0.035	0.029						
Ba	0.003	0.000	0.008	0.000	0.000	0.017	0.000	0.007	0.008	0.000	0.006	0.000	0.000	0.005	0.000	0.001	0.014	0.000						
An	4.45	0.35	0.20	0.61	1.38	5.90	2.75	2.89	6.22	0.64	0.83	1.56	8.53	0.48	0.78	55.87	58.02	29.29						
Ab	95.09	99.13	99.43	99.29	96.71	93.64	96.83	96.86	93.18	99.25	98.70	98.17	90.33	99.31	98.90	42.35	41.08	70.00						
Or	0.47	0.52	0.37	0.10	1.91	0.46	0.42	0.26	0.61	0.11	0.47	0.27	1.13	0.20	0.32	1.78	0.90	0.71						

Table 3 (continued).

Site:	857C 21R-1			857C 28R-CC			857C 30R-1 116–120			857C 38R-2 50–53			857C 61R-1 129–131			857D 1R-1 137–139			857D 17R-2 53–55			858A 18X-1 116–118		
Core, section:																								
Interval (cm):	24–26			IIIc			IIIc			IIIc			IIc			IIc			IIc			IIa		
Zone:	IVc																							
SiO ₂	62.13	70.80	61.90	65.72	64.96	68.24	70.37	67.20	66.55	69.26	69.09	66.38	68.19	67.48	67.28	67.20	65.94	64.92	69.15					
Al ₂ O ₃	23.88	20.28	24.37	21.67	18.38	19.95	20.22	21.47	21.63	19.72	20.24	21.35	20.67	19.94	19.72	19.54	20.10	20.10	18.28					
FeO	0.30	0.24	0.20	0.02	0.13	0.14	0.19	0.21	0.68	0.19	0.11	0.22	0.06	0.05	0.04	0.08	0.18	0.13	0.20					
CaO	5.48	0.35	5.97	2.90	0.03	0.58	0.18	2.16	1.86	0.45	0.64	0.56	0.65	0.31	0.23	0.22	1.19	1.13	0.25					
Na ₂ O	8.09	11.46	8.34	9.84	0.30	11.57	11.79	10.78	10.44	11.52	11.60	10.73	11.04	11.27	11.44	11.43	10.94	11.05	11.71					
K ₂ O	0.41	0.35	0.22	0.26	16.54	0.09	0.06	0.22	0.14	0.39	0.03	0.70	0.11	0.06	0.05	0.05	0.05	0.10	0.06					
BaO	nd	nd	nd	nd	nd	nd	nd	nd	nd	nd	nd	nd	nd	nd	nd	nd	nd	nd	nd					
Total	100.29	103.47	100.99	100.41	100.33	100.57	102.81	102.03	101.30	101.53	101.71	100.01	100.72	99.17	98.76	98.51	98.40	97.42	99.64					
Si	11.002	11.964	10.903	11.517	11.988	11.882	11.958	11.596	11.566	11.951	11.886	11.660	11.830	11.892	11.905	11.923	11.757	11.705	12.129					
Al	4.985	4.040	5.060	4.478	3.998	4.096	4.051	4.367	4.432	4.012	4.105	4.422	4.227	4.143	4.113	4.086	4.224	4.272	3.779					
Fe	0.045	0.034	0.029	0.003	0.020	0.021	0.027	0.030	0.099	0.028	0.016	0.032	0.008	0.007	0.007	0.011	0.026	0.020	0.029					
Ca	1.040	0.063	1.126	0.545	0.006	0.108	0.033	0.398	0.346	0.082	0.117	0.106	0.121	0.058	0.044	0.042	0.228	0.218	0.047					
Na	2.776	3.754	2.849	3.345	0.108	3.908	3.884	3.606	3.517	3.855	3.870	3.654	3.714	3.851	3.925	3.933	3.782	3.863	3.983					
K	0.092	0.074	0.050	0.058	3.893	0.020	0.013	0.048	0.031	0.085	0.007	0.157	0.025	0.013	0.012	0.011	0.012	0.023	0.013					
Ba	0.000	0.000	0.000	0.000	0.000	0.000	0.000	0.000	0.000	0.000	0.000	0.000	0.000	0.000	0.000	0.000	0.000	0.000	0.000					
An	26.62	1.61	27.97	13.80	0.15	2.68	0.84	9.83	8.90	2.05	2.93	2.71	3.14	1.47	1.10	1.05	5.66	5.31	1.15					
Ab	71.04	96.48	70.79	84.73	2.69	96.83	98.82	88.98	90.31	95.83	96.88	93.29	96.23	98.20	98.59	98.68	94.03	94.12	98.53					
Or	2.35	1.91	1.24	1.47	97.16	0.49	0.34	1.19	0.79	2.12	0.19	4.00	0.64	0.33	0.31	0.27	0.31	0.57	0.32					
Site:	858A 25X-1			858A 29X-1			858C 5H-CC			858D 12X-CC			858D 2H-3 2H-CC			858F 9R-CC								
Core, section:																								
Interval (cm):	29–33			30–32			7–10			8–10			34–36			10–12			9–11					
Zone:	IIIb			IIIb			IIIc			IIIc			Vb			Vb			lb					
SiO ₂	69.19	65.44	69.65	63.85	69.46	68.76	69.72	65.67	67.75	68.58	67.32	57.71	62.03	62.35	59.57	64.19	59.88	55.94	60.45					
Al ₂ O ₃	19.30	22.41	19.85	18.47	19.58	20.24	19.67	19.30	19.78	19.71	20.55	24.75	24.54	24.37	24.00	22.67	26.04	27.58	25.72					
FeO	0.05	0.18	0.09	0.10	0.08	0.06	0.04	0.13	0.11	0.08	0.13	0.18	0.12	0.09	0.07	0.22	0.07	0.07	0.04					
CaO	0.05	3.53	0.32	0.00	0.03	0.39	0.19	0.06	0.43	0.11	0.59	6.79	5.34	5.34	5.44	3.37	7.31	10.22	7.40					
Na ₂ O	11.59	9.72	11.42	0.16	11.88	11.70	11.69	4.81	11.03	11.81	11.43	7.44	8.36	8.30	8.38	9.76	7.64	5.75	7.43					
K ₂ O	0.04	0.13	0.10	15.54	0.00	0.17	0.08	11.12	0.10	0.05	0.12	0.29	0.40	0.40	0.15	0.13	0.04	0.02	0.09					
BaO	nd	nd	nd	nd	nd	nd	nd	0.63	0.00	0.01	0.00	0.00	0.11	0.05	0.00	0.01	0.00	nd	nd					
Total	100.21	101.41	101.43	98.13	101.02	101.31	101.38	101.72	99.20	100.34	100.14	97.16	100.90	100.90	97.62	100.34	100.98	99.58	101.14					
Si	12.042	11.384	11.986	11.982	12.005	11.879	12.005	11.830	11.926	11.948	11.779	10.613	10.926	10.968	10.849	11.299	10.579	10.099	10.651					
Al	3.961	4.596	4.026	4.086	3.990	4.123	3.993	4.098	4.104	4.048	4.240	5.365	5.096	5.053	5.154	4.703	5.423	5.871	5.343					
Fe	0.007	0.025	0.014	0.016	0.011	0.008	0.006	0.020	0.017	0.012	0.019	0.028	0.018	0.013	0.011	0.032	0.011	0.010	0.005					
Ca	0.009	0.658	0.060	0.000	0.005	0.071	0.034	0.011	0.081	0.020	0.111	1.337	1.008	1.006	1.062	0.635	1.384	1.977	1.398					
Na	3.910	3.279	3.809	0.059	3.979	3.920	3.903	1.681	3.766	3.989	3.876	2.652	2.855	2.831	2.960	3.332	2.618	2.012	2.540					
K	0.008	0.030	0.021	3.720	0.000	0.037	0.017	2.554	0.023	0.010	0.027	0.068	0.089	0.090	0.035	0.029	0.008	0.004	0.020					
Ba	0.000	0.000	0.000	0.000	0.000	0.000	0.000	0.045	0.000	0.001	0.000	0.008	0.003	0.000	0.000	0.000	0.000	0.000	0.000					
An	0.23	16.59	1.53	0.00	0.12	1.77	0.86	0.27	2.09	0.49	2.76	32.95	25.51	25.62	26.18	15.89	34.51	49.52	35.32					
Ab	99.56	82.67	97.93	1.56	99.88	97.31	98.70	39.58	97.32	99.25	96.55	65.38	72.24	72.09	72.97	83.39	65.29	50.39	64.17					
Or	0.20	0.74	0.54	98.44	0.00	0.92	0.43	60.15	0.59	0.26	0.68	1.67	2.25	2.30	0.85	0.72	0.21	0.10	0.51					

Table 3 (continued).

Site: Core, section: Interval (cm): Zone:	858F 14R-I 10–12 IIB	858F 14R-I 10–12 IIB			858F 18R-I 14–16 IIB			
		SiO ₂	Al ₂ O ₃	FeO	CaO	Na ₂ O	K ₂ O	BaO
SiO ₂	58.49	69.38	64.05	64.76	64.76	58.97	67.49	68.44
Al ₂ O ₃	27.06	19.75	23.11	23.13	25.91	27.08	21.46	19.94
FeO	0.17	0.13	0.05	0.06	0.27	0.26	0.13	0.05
CaO	8.60	8.35	4.16	4.21	8.30	7.97	1.44	0.16
Na ₂ O	7.70	11.50	9.33	10.54	6.82	7.00	10.71	11.61
K ₂ O	0.02	0.02	0.10	0.07	0.04	0.04	0.08	0.07
BaO	nd	nd	nd	nd	0.05	0.00	0.03	0.00
Total	102.03	101.13	100.80	102.77	97.67	101.31	101.34	100.27
Si	10.304	11.980	11.227	11.187	10.343	10.403	11.672	11.920
Al	5.619	4.021	4.775	4.711	5.612	5.632	4.375	4.096
Fe	0.024	0.018	0.009	0.010	0.041	0.038	0.019	0.007
Ca	1.623	0.064	0.781	0.778	1.633	1.507	0.267	0.030
Na	2.629	3.849	3.170	3.531	2.428	2.396	3.591	3.923
K	0.004	0.005	0.022	0.014	0.009	0.008	0.017	0.015
Ba	0.000	0.000	0.000	0.000	0.003	0.000	0.002	0.000
An	38.12	1.64	19.66	18.00	40.13	38.54	6.89	0.75
Ab	61.77	98.23	79.78	81.67	59.65	61.26	92.67	98.88
Or	0.10	0.13	0.56	0.33	0.22	0.20	0.44	0.37

Note: Based on 32 (O); nd = not determined.

also occurs disseminated in sediments from 225 to 270 mbsf in Hole 858A.

Detrital quartz crystals host two-phase fluid inclusions below depths of 35.7 mbsf in Hole 858A, 33 mbsf in Hole 858C and 27 mbsf in Hole 858D and indicate that quartz has been partially recrystallized and overgrown below these depths. Detrital K-feldspar is variably altered to sericite and chlorite below 16 mbsf in Hole 858A, 21 mbsf in Hole 858C, and 2 mbsf in Hole 858D. The degree of K-feldspar alteration increases to depths of 246 mbsf in Hole 858A and 33 mbsf in Hole 858C, below which it is commonly completely replaced by sericite and chlorite. Detrital plagioclase is altered to albite at depths >25 mbsf in Hole 858A and >21 mbsf in Hole 858C (Table 3; Fig. 12B). Epidote was observed in the uppermost 100 meters in Hole 858A and throughout Holes 858B and 858C. Epidote forms up to 1–2 vol% and ranges up to 75 µm in diameter (Table 12). An anhedral morphology and its concentration in silt and sand laminae indicate a detrital origin. Pyrite occurs finely disseminated throughout hemipelagic silty clay as frambooids, euhedral to anhedral crystals, and crystal aggregates. Euhedral to subhedral pyrite occurs interstitially within turbiditic silt and sand and infills burrows and carbonate concretions. In Hole 858A, pyrite contents are generally <1 vol% but range to 8 vol% in Holes 858C and 858D. Frambooidal pyrite decreases in abundance with increasing depth. Marcasite alteration of pyrite is generally rare (e.g., Sample 139-858A-5H-4, 27–30 cm hosts pyrite with marcasite cores). Pyrrhotite only rarely occurs as disseminated crystals up to 300 µm in diameter and as small cores surrounded by pyrite. Sphalerite crystals up to 100 µm occur locally disseminated in hemipelagic sediment in Hole 858D (Table 12; Fig. 8).

Clay minerals in Holes 858A, 858C, and 858D are variably recrystallized and altered to chlorite and illite, with common extinction angles. The clay minerals are composed of Si-Al-Mg-Fe-K ± Na and Ca, and plot as an array subparallel to the Al-Mg join on a Fe-Al-Mg ternary diagram (Table 8; Fig. 15F,G). The clays vary little in Fe-content but show a large range in Mg-content (Fig. 15G). In Holes 858A and 858C, a general increase in the Mg content of clay minerals with depth is reflected in the bulk chemical compositions (Goodfellow and Peter, this volume).

Carbonate occurs as cement, concretions, and in veins in all holes at this site, and forms massive carbonate breccia in Hole 858C (Goodfellow and Peter, this volume). Carbonate cement is concentrated in silt and sand laminae, and carbonate concretions occur most commonly in turbidites. Carbonate concretions occur above 101 mbsf in Hole 858A (Fig. 5), 40 mbsf in Hole 858C (Fig. 7), and 30 mbsf in Hole 858D (Fig. 8; Table 12). Calcite crystals are also disseminated in hemipelagic sediment above 147 and below 207 mbsf in Hole 858A, above 9 mbsf in Hole 858B, and above 40 mbsf in Hole 858C. A massive carbonate breccia cemented by calcite composed of crystals up to 1 mm in diameter occurs at 15 mbsf in Hole 858C. Calcite is the predominant carbonate phase, although between 33 and 38 mbsf in Hole 858C and between 12 and 14.5 mbsf in Hole 858D, dolomite occurs with calcite (Table 11; Fig. 17B; Davis, Mottl, Fisher, et al., 1992).

Zone IVb

Zone IVb consists of hydrothermal clay, pyrite, and anhydrite. It occurs between 70 and 175 mbsf in Hole 858A (Fig. 5), between 11.5 and 24 mbsf in Hole 858B (Fig. 6), between 17 and 68.5 mbsf in Hole 858C (Fig. 7), and between 20 and 28 mbsf in Hole 858D (Fig. 8). Anhydrite occurs as disseminated crystals and crystal aggregates, veins, and concretions between 62.5 mbsf and 256 mbsf in Hole 858A, 11 and 38 mbsf in Hole 858B, 37 and 68 mbsf in Hole 858C, and 2 and 28 mbsf in Hole 858D (Davis, Mottl, Fisher, et al., 1992; Table 12; Pl. 4, Figs. 1 and 2). In Hole 858F, veins and vugs of anhydrite occur between 110 and 170 mbsf and anhydrite concretions and vugs occur between 170 and 200 mbsf (Davis, Mottl, Fisher, et al., 1992). Disseminated anhydrite laths comprise 1–2 vol% and

Table 4. Electron microprobe data for epidote in unaltered and hydrothermally altered hemipelagic and turbiditic sediment, Leg 139.

Site:	855C				856A				856A				856A				857A				
Core, section:	11R-1				4H-6				6H-3				6H-6				9H-1				6H-5
Interval (cm):	115–119				55–59				103–107				90–94				44–47				89–93
Zone:	UA				IVa				det				IVa				IIIa				UA
Type:	det				det				det				det				det				det
SiO ₂	37.34	38.32	37.87	36.20	38.17	38.44	37.80	37.75	39.99	38.30	38.08	38.00	38.72	36.98	37.87	36.46	37.41	37.35	38.68		
TiO ₂	0.03	0.09	0.22	0.07	0.12	0.20	0.09	0.08	0.12	0.04	0.10	0.08	0.26	0.12	0.01	0.21	0.12	0.05	0.05	0.08	
Al ₂ O ₃	22.29	20.63	24.64	19.05	24.25	23.75	22.17	23.13	22.29	27.17	24.68	24.99	29.04	22.71	23.09	22.39	21.27	22.46	24.30		
Fe ₂ O ₃	13.21	11.56	10.63	17.33	12.15	11.21	13.39	13.56	12.45	7.39	10.74	11.11	5.28	13.08	12.21	15.18	11.16	14.13	10.27		
MnO	0.06	0.17	0.25	0.09	0.16	0.09	0.10	0.31	0.13	0.22	0.25	0.21	0.27	0.17	0.17	0.44	0.07	0.91	0.07		
MgO	0.00	0.18	0.06	0.00	0.05	0.05	0.00	0.00	0.28	0.00	0.05	0.07	0.10	0.05	0.01	0.00	0.00	0.01	0.02		
CaO	23.31	21.80	23.30	20.82	23.47	23.26	23.31	23.16	21.91	23.43	23.13	23.46	23.97	22.85	23.03	22.69	23.19	21.94	23.61		
Na ₂ O	0.00	0.11	0.06	0.01	0.01	0.12	0.00	0.00	0.05	0.06	0.02	0.02	0.00	0.00	0.00	0.02	0.03	0.01	0.03		
K ₂ O	0.04	0.02	0.01	0.02	0.01	0.02	0.01	0.00	0.01	0.05	0.04	0.02	0.02	0.03	0.02	0.05	0.00	0.01	0.01		
Cr ₂ O ₃	0.01	0.04	0.00	0.08	0.03	0.39	0.04	0.00	0.00	0.00	0.00	0.00	0.11	0.00	0.02	0.03	0.00	0.00	0.00		
ZnO	0.00	0.00	0.00	0.03	0.05	0.00	0.06	0.02	0.11	0.03	0.00	0.00	0.03	0.07	0.00	0.14	0.04	0.00	0.02		
Total	96.29	92.93	97.03	93.69	98.47	97.53	96.95	98.00	97.34	96.68	97.09	97.95	97.79	96.05	96.41	97.61	93.30	96.85	97.07		
Si	3.028	3.212	3.016	3.072	3.011	3.055	3.048	3.009	3.202	3.022	3.032	2.999	2.998	3.004	3.056	2.936	3.119	3.024	3.077		
Ti	0.002	0.005	0.013	0.004	0.007	0.012	0.005	0.004	0.007	0.003	0.006	0.004	0.015	0.007	0.001	0.013	0.007	0.003	0.005		
Al	2.130	2.039	2.313	1.906	2.255	2.225	2.107	2.173	2.104	2.527	2.317	2.326	2.651	2.175	2.196	2.126	2.091	2.143	2.279		
Fe	0.806	0.729	0.637	1.107	0.721	0.671	0.812	0.813	0.750	0.439	0.643	0.660	0.307	0.800	0.741	0.920	0.700	0.861	0.615		
Mn	0.004	0.012	0.017	0.007	0.011	0.006	0.007	0.021	0.009	0.015	0.017	0.014	0.018	0.012	0.011	0.030	0.005	0.062	0.005		
Mg	0.000	0.022	0.007	0.000	0.005	0.006	0.000	0.000	0.034	0.000	0.005	0.008	0.011	0.006	0.001	0.000	0.000	0.001	0.002		
Ca	2.025	1.958	1.988	1.894	1.983	1.981	2.014	1.978	1.879	1.980	1.973	1.984	1.989	1.989	1.991	1.957	2.071	1.903	2.013		
Na	0.000	0.018	0.010	0.001	0.001	0.018	0.000	0.000	0.007	0.008	0.002	0.003	0.000	0.000	0.000	0.003	0.004	0.002	0.004		
K	0.004	0.002	0.001	0.002	0.001	0.002	0.001	0.000	0.001	0.005	0.004	0.002	0.002	0.003	0.002	0.005	0.000	0.001	0.001		
Cr	0.001	0.003	0.000	0.006	0.002	0.025	0.002	0.000	0.000	0.000	0.000	0.000	0.007	0.000	0.001	0.002	0.000	0.000	0.000		
Zn	0.000	0.000	0.000	0.002	0.003	0.000	0.003	0.001	0.006	0.002	0.000	0.000	0.002	0.004	0.000	0.008	0.003	0.000	0.001		

Table 4 (continued).

Site:	857C				857D															
Core, section:	30R-1				5R-1				6R-1				17R-2				21R-2			
Interval (cm):	116–120				26–28				20–22				53–55				14–16			
Zone:	IIIC				IIC				Ic				IIC				Ic			
Type:	det				auth															
SiO ₂	38.77	38.20	37.99	38.18	37.57	37.75	38.11	38.81	38.69	37.60	38.56	37.87	36.70	37.16	38.54	37.25	37.99	37.51		
TiO ₂	0.12	0.07	0.38	0.05	0.16	nd	0.11	0.02	0.01	0.14	0.09	0.09	nd	0.09	0.10	0.16	0.11			
Al ₂ O ₃	27.03	24.40	25.06	27.22	21.55	24.30	26.60	26.66	27.77	21.48	25.76	24.82	25.13	26.47	27.54	24.01	26.30	24.44		
Fe ₂ O ₃	7.66	6.80	9.97	6.43	7.43	10.90	9.30	7.35	5.64	14.98	6.46	10.23	11.18	8.46	6.28	11.24	11.14	10.60		
MnO	0.16	0.15	0.02	0.28	0.23	nd	nd	0.12	0.12	0.51	0.16	0.23	0.40	nd	0.18	0.11	0.37	0.03		
MgO	0.00	0.04	0.07	0.03	0.26	nd	nd	0.02	0.04	0.04	0.03	0.66	0.00	nd	0.11	0.16	0.00	0.02		
CaO	24.04	22.91	23.56	23.94	23.02	23.23	23.70	24.15	24.12	22.50	23.51	22.85	22.56	23.50	23.61	23.00	23.02	23.50		
Na ₂ O	0.03	0.08	0.05	0.04	0.23	0.08	0.00	0.01	0.00	0.00	0.00	0.01	0.00	0.01	0.01	0.06	0.08	0.03	0.01	
K ₂ O	0.04	0.02	0.01	0.01	0.01	0.01	0.00	0.00	0.01	0.01	0.02	0.00	0.00	0.02	0.02	0.00	0.00	0.03	0.00	
Cr ₂ O ₃	0.00	0.03	0.02	0.00	1.16	nd	nd	0.00	0.02	0.01	0.00	0.00	0.02	nd	0.01	0.01	0.07	0.00		
ZnO	0.14	0.16	0.07	0.00	0.08	nd	nd	0.04	0.00	0.04	0.00	0.07	0.00	nd	0.05	0.00	0.00	0.00		
Total	97.98	92.86	97.20	96.19	93.78	96.25	97.70	97.27	96.42	97.19	94.63	96.82	96.08	95.61	96.48	95.95	99.08	96.25		
Si	3.023	3.144	3.013	3.019	3.024	3.030	2.993	3.047	3.043	3.043	3.107	3.011	2.955	2.975	3.035	3.003	2.962	3.011		
Ti	0.007	0.004	0.022	0.003	0.010	0.000	0.000	0.006	0.001	0.001	0.008	0.005	0.006	0.000	0.005	0.006	0.010	0.007		
Al	2.485	2.368	2.343	2.537	2.045	2.300	2.463	2.468	2.575	2.049	2.447	2.327	2.386	2.498	2.556	2.282	2.418	2.313		
Fe	0.449	0.421	0.595	0.383	0.450	0.658	0.549	0.434	0.334	0.912	0.392	0.612	0.678	0.509	0.372	0.682	0.654	0.640		
Mn	0.011	0.010	0.001	0.019	0.015	0.000	0.000	0.008	0.008	0.035	0.011	0.015	0.027	0.000	0.012	0.008	0.024	0.002		
Mg	0.000	0.005	0.009	0.004	0.031	0.000	0.000	0.003	0.005	0.004	0.003	0.0								

Table 4 (continued).

Site:	858A	858C	858F	858E
Core, section:	29X-1	5H-CC 7-10	9R-CC 9-11	23R-CC 3-5
Interval (cm):	30-32	IVb	Ib	Ib
Type:	IIIb	det	auth	auth
SiO ₂	37.81	37.16	37.71	37.63
TiO ₂	0.06	0.30	0.26	0.24
Al ₂ O ₃	22.93	23.90	22.89	24.44
Fe ₂ O ₃	13.01	10.85	12.21	14.43
MnO	0.17	0.56	0.28	0.25
MgO	0.01	0.00	0.01	0.13
CaO	23.45	22.34	23.08	22.68
Na ₂ O	0.01	0.02	0.00	0.03
K ₂ O	0.00	0.04	0.03	0.00
Ce ₂ O ₃	0.00	0.02	0.08	0.00
ZnO	0.00	0.06	0.15	0.02
Total	97.44	95.24	97.23	98.30
			95.08	98.00
				96.68
Si	3.026	3.025	3.021	3.005
Ti	0.004	0.018	0.012	0.016
Al	2.163	2.293	2.215	2.150
Fe	0.783	0.665	0.736	0.865
Mn	0.012	0.038	0.019	0.017
Mg	0.001	0.000	0.001	0.004
Ca	2.011	1.948	1.980	1.937
Na	0.001	0.003	0.001	0.005
K	0.000	0.004	0.003	0.000
Zn	0.000	0.004	0.009	0.001

Notes: FeO recast as Fe₂O₃. Formula proportions based on 8 cations. nd = not determined; det = detrital; auth = authigenic; UA = unaltered.

range up to 4 mm in length. In Hole 858C, anhydrite crystals are corroded and broken at 68 mbsf, suggesting reaction with hydrothermal fluids. Barite is rare and was observed only in Hole 858B (Sample 139-858B-2H-6, 69–71 cm), where it forms rosettes composed of crystals up to 200 µm.

Zone IIIb

This zone consists of albite-chlorite-pyrite and occurs between 175 and 320 mbsf in Hole 858A (Fig. 5), and between 33 and 92 mbsf in Hole 858C (Fig. 7). Anhydrite veins cut this zone locally. The alteration mineralogy is similar to the previous two zones (i.e., overgrowth and recrystallization of quartz, albitization of plagioclase, alteration of detrital K-feldspar to sericite and chlorite, and recrystallization of clays to chlorite and illite) except that carbonate and anhydrite are generally absent. Chlorite (Fe/Fe + Mg = 0.35–0.59; Table 7) is more dominant than in previous zones and illite more subordinate based on XRD (Table 2) and lower K₂O contents (Goodfellow and Peter, this volume).

Zone IIb

This zone only occurs in Hole 858F between 120 and 142 mbsf and between 173 and 249 mbsf (Fig. 8) and is characterized by lithified, brecciated, fractured, and veined hemipelagic and turbiditic sediments. These sediments are altered to quartz-epidote-chlorite and crosscut locally by anhydrite-pyrite-chalcopyrite veins.

The clay fraction is dominated by chlorite (Tables 2 and 7) and Fe-Mg-Al silicates (Table 8). Authigenic Fe-Mg chlorite also occurs interstitial to vein wairakite (Sample 139-858F-2R-CC, 7–10 cm and 139-858F-18R-1, 14–16 cm). The alteration of detrital micas to chlorite in Hole 858F is consistent with low K₂O contents of bulk sediments (Goodfellow and Peter, this volume). Epidote is a common phase in Hole 858F and forms up to 20 vol% (Table 12). This epidote consists of granular masses and subhedral to anhedral crystals that are disseminated in both hemipelagic silty clay and turbiditic sediment. The authigenic epidote is generally more Al-rich and Fe-poor than detrital epidote (Table 4; Fig. 13). Authigenic sphene occurs as subhedral to anhedral crystals and xenoblastic aggregates.

Zone Ib

This zone represents the core of hydrothermal fluid upflow at AAV and consists of fractured, veined, and brecciated lithified hemipelagic and turbiditic sediment. These sediments have been altered to the mineral assemblage quartz-wairakite-epidote-pyrite ± sphene ± plagioclase between 28 and 120 mbsf and between 142 and 173 mbsf.

Quartz and wairakite infill euhedral anhydrite(?) molds (Sample 139-858F-2R-CC, 7–10 cm) and voids and form veins in Holes 858C, 858D, and 858F. Wairakite locally replaces the matrix of sediments in Holes 858C and 858F. Veins are wairakite-quartz, wairakite-quartz-epidote, and wairakite-sphalerite. Elongate euhedral crystals of hydrothermal quartz with single and double terminations occur with wairakite in veins in Hole 858F. Wairakite crystals are commonly twinned, equant, subhedral to anhedral, range to up to 2 mm in diameter, and host abundant fluid inclusions (Peter et al., this volume). Matrix wairakite forms up to 35 vol% of the sediment (Sample 139-858F-9R-CC, 9–11 cm) and is typically anhedral due partly to the corrosion of crystal surfaces by hydrothermal fluids. Minor Na substitutes for Ca in wairakite (Ca/Ca + Na ratios range from 0.871 to 0.967; Table 13). K-feldspar was not observed in Hole 858F. Plagioclase compositions in Holes 858D and 858F are highly variable, with the most albite-rich plagioclase occurring above 20 mbsf in Hole 858D and below 180 mbsf in Hole 858F. Plagioclase feldspar at 18.9 mbsf in Hole 858D contains up to An 33. The anorthite content increases downhole, reaching a maximum of An 49.2 at 95 mbsf (Sample 139-858F-9R-CC, 9–11 cm; Table 3; Fig. 12B). The plagioclase in this sample is commonly embayed and displays albite twinning (Pl. 4, Fig. 3). The anorthite content of hydrothermal plagioclase decreases

Table 5. Summary of alteration zones for Sites 856, 858, and 857.

Alteration zones	Hole	Depth (mbsf)	Alteration mineralogy	Comments
<i>Site 856 (Bent Hill)</i>				
IVa (Ca-II-Py)	856A	17–86	Qz - fluid inclusions and irregular boundaries; Plag - altered to albite; K-spar altered to Ser + Ch; clays altered to Ch + II; Ca concretions + cement; Py replaces frambooidal Py; Mag - partly altered to Py	Not present in Hole 856B due to mass wasting.
IIIa (An-II-Py)	856A	60–112	Clay mineral grain size greater than in Zone IVa; An - molds and SO_4^{2-} in pore water; rare Cp + Po	Anhydrite largely removed by retrograde reaction. Sediments fractured and brecciated in Hole 856B.
IIa (Ab-Ch-Ms-Py)	856B	30–70	Qz - ragged/diffuse boundaries, rare euhedral terminations; Plag - altered to albite; clay minerals coarse grained Ch + Ms; Ru a common accessory	Increasing induration with depth.
Ia1 (Qz-Ch-Ms-Ru-Cp-Po)	856B	70–110	Qz - anhedral to hexagonal, abundant fluid inclusions; Fs - all removed below 110 mbsf; Ch - Fe-rich; Ch + Ms coarse grained (to 25 μm); Cp ± Py ± Po veins	Indurated and silicified hemipelagic and turbiditic sediments. Coarse grained compared to previous zones.
Ia2 (Qz-Ch-Sm-Fs)	856B	110–117.5	Minor Fs; Sm - identified by XRD; Ch - Mg-rich near Cp veins; Ba - associated with veins	Narrow subzone adjacent to mafic sill at the base of Hole 856B.
Massive sulfide	856B	117.5–118	Silicates - Ta, Ser, Ch, Sa(Ver?); Carbonates - Do, Ca, Ma	Clastic sulfide zone in 856B shed from adjacent sulfide mound. Ch and Sa(Ver?) only present in veined sediment in Hole 856H.
<i>Site 858 (Area of Active Venting)</i>				
VIb (Sa-Ta-Py)	858B	18.4–23.2	Sa (Ch + Ver?) and Ta zone - bulk sediments up to 30 wt% MgO	Below 24 mbsf, sediment is brecciated, cut by Qz + An veins.
Vb (Ca-II-Py)	858A	24–38	Qz - partially overgrown and recrystallized, minor fluid inclusions; K-feld - partly altered to Ser + Ch; Plag - partly to completely altered to albite; clays variably recrystallized to II + Ch; Ca - cement and concretions; Do - narrow bands in Holes 858C and 858D; Py - recrystallized frambooidal and alteration of Mag, rare Mr, Po, Sp	Sediment weakly to moderately indurated, olive grey to medium grey, commonly bioturbated. Hole 858C brecciated below 17 mbsf.
IVb (An-II-Py)	858A	39–45	An - nodules, lath crystals in sediment and crosscutting veins	Sediment moderately indurated, medium grey, locally bioturbated. Fractured and brecciated in Hole 858C.
IIIb (Ab-Ch-II-Py)	858A	45–52	Qz - overgrown and recrystallized; Plag - altered to albite; clays recrystallized to Ch ± II; Ca a minor component of Hole 858A between 225 and 270 mbsf	Moderately indurated to indurated sediment.
IIb (Qz-Ep-Ch)	858F	52–58	Ep - hydrothermal epidote up to 20 vol%; clays recrystallized to Ch; Sn - common authigenic accessory	Sediments indurated and brecciated. This zone overlaps with Zone Ib.
Ib (Qz-Wa-Ep-Py-Sp)	858F	58–65	Wa - vein phase, rarely as matrix replacement after Fs?; Qz - common vein phase; rare hydrothermal plagioclase; An - veins and vugs (retrograde phase?); Py ± Sp in veins	Sediments indurated and brecciated.
<i>Site 857 (Reaction Zone)</i>				
IVc (Ca-II-Py)	857C	65–70	Clays - recrystallized to II + Ch (\pm Sm?); Ca - concretions and cement (Do occurs from 85–105 mbsf); Py - disseminated; Po ± Py ± Sp veins; Mt - altered to Py	Weakly to moderately indurated hemipelagic and turbiditic sediments. Commonly bioturbated.
IIIc (Ab-Ch-Py)	857C	70–85	Qz - overgrown, partially recrystallized; Plag - altered to albite; K-spar - variably altered to Ser + Ch	Moderately indurated.
IIc (Qz-Ch-Ep-Py)	857C/D	85–93	Ep - up to 30 vol%; Detrital micas rare to absent below 600 mbsf; Sn - common authigenic accessory	Hemipelagic and turbiditic sediments indurated, interbedded with mafic sills.
Ic (Qz-Wa-Ep)	857C/D (veins)	93–105	Qz - commonly euhedral; Wa - common fluid inclusions	Veins crosscutting sediments and mafic sills.

Note: Qz = quartz; Fs = feldspar; Plag = plagioclase; Ab = albite; K-spar = K-feldspar; Wa = wairakite; Ep = epidote; Ca = calcite; Do = dolomite; Ma = magnesite; Ch = chlorite; II = illite; Sm = smectite; Ms = muscovite; Ser = sericite; Sn = sphene; Py = pyrite; Sp = sphalerite; Mr = marcasite; Po = pyrrhotite; Ta = talc; Sa = saponite; Ver = vermiculite; An = anhydrite; Mag = magnetite; Ru = rutile.

Table 6. Summary of downhole mineralogy for Holes 856A and 856B.

Core, section, interval (cm)	Grain size	Depth (mbsf)	Detrital									Hydrothermal/Authigenic															
			Qz	Fs	Clay	Micas	Ch	Hb	Ep	Mag	M-f	F-py	Qz	Ch-Ms	Mg-sil	Carb	Ru	Ba	An	Py	Mr	Po	Cp	Sp	Hem/op		
139-856A-																											
2H-1, 45–47	Silty clay	3.15	xxx	xxx	xxxxx	xxx	xx	x		x	x	x					x										
3H-5, 117–121	Silty clay	19.37	xxx	xxx	xxxxx	xxx	xx	x		x	x	x					x										
4H-6, 55–59	Sandy silt	29.75	xxxx	xxxx	xxxx	xxx	xx		xx	x	x					xxxx		x									
5H-8, 71–75	Sandy silt + silty clay	41.29	xxxx	xxxx	xxxx	xxx	xx		xx	x	x	x				xxx		x	x	x							
6H-3, 103–107	Silty clay	44.73	xxxx	xxx	xxxxx	xxx	xxx	xx	xxx	x	x	x				xx		x									
6H-4, 69–77	Sand	45.89	xxxx	xxx	xxx	x	xx		x	x	x	x				xxxxx											
6H-6, 90–94	Sandy silt	49.10	xxxx	xxxx	xxxx	xxx	xx		xx	x	x	x				xxx											
7H-5, 70–74	Silty clay	56.90	xxx	xxx	xxxxx	xx	x		x	x	x	x						x									
8H-1, 8–10	Fine grained silt	59.78	xxx	xxx	xxxx	x			x			x				xxxxx	x										
8H-5, 84–87	Silty clay	66.54	xxx	xxx	xxxxx	xxx	x	xx	xxx	x	x	x				xxxx		x									
9H-1, 44–47	Silty sand	69.64	xxxx	xxxx	xxxx	x	xx		xxx	x	x	x				xxxx		x									
9H-5, 41–42	Silt	75.61	xxxx	xxx	xxxx	x	x		x	x	x	x				xxxxx		x									
11X-1, 70–72	Silt + silty clay	86.90	xxxx	xxx	xxxxx	xx	x		xx	x	x	x				xxxx		x									
12X-2, 20–24	Silty claystone	97.40	xxx	xxx	xxxxx	xxx	xx		x			x						x									
13X-4, 47–51	Silty clay	110.27	xxxx	xxxx	xxxxx	xxx	xx		x			x						x									
139-856B-																											
2H-5, 115–119	Silty clay	8.95	xxx	xxx	xxxxx	xxx	xxx		x		x					x		x									
3H-5, 110–113	Silt to sand	18.40											x	xxxx													
3H-6, 34–36	Sand and silt	19.14											xxx														
3H-7, 28–30	Sand to clay	20.58											xxx														
3H-CC, 28–31	Sand to clay	21.33											xxx?														
4H-1, 145–147	Sand to clay	22.25	xxx	xxx	xxxxx	x							xxx														
4H-3, 35–37	Silty clay with sulfides	24.15	xx	xx	xxxxx	xxx							x														
5H-2, 67–70	Silty clay	32.47	xxx	xxx	xxxxx	xxx	x																				
6H-2, 23–29	Silty clay and silt	41.53	xxxx	xxx	xxxxx	x	x																				
6H-4, 124–128	Silty clay	45.54	xxxx	xxx	xxxxx	xxx	x			x						x		xx									
7H-5, 26–32	Silty clay	55.56	xxx	xxx	xxxxx	xxx	x			x						x		x									
8H-3, 55–57	Silty clay	62.35	xxx	xx	xxxxx	xx	x																				
10H-2, 54–58	Sandy silt	72.84	xxxx	xxxxx	xxxx	x	xx		x		x					x		x									
11X-5, 53–57	Silty clay	79.83	xxx	xxx	xxxxx	x	xx		x							x		xx									
12X-4, 29–33	Silty clay	86.39	xxxx	xxx	xxxxx	xx	xx						x?			x		xxx									
13X-2, 63–67	Siltstone	93.23	xxxx	xxxx	xxxxx	xxx	xx						x			x		xxx									
14X-1, 34–36	Siltstone	101.14	xxx	xx	xxxx	xxx	x									xxxxx		x									
14X-4, 50–53	Siltstone	105.80	xxx?	xxx	xx	x	x		x							xxx	xxxxx	x	x								
15X-1, 91–93	Silt to silty sand	111.31															xxx	xxxxx	x	x	x	x	x	x	x		
15X-1, 124–126	Silt to silty sand	111.64					x	x									xxx	xxxxx	x	x	x	x	x	x	x		
15X-2, 27–29	Silty clay	112.17				xxx	x										xxx	xxxxx	x	x							
15X-2, 67–69	Siltstone to silty sandstone	112.57				xxx											xxx	xxxxx	x	x							
15X-3, 8–10	Silt	113.48				x	x										xxx	xxxxx	x	x	x	x	x	x	x		
15X-4, 12–14	Silty sand	115.02				x	x										xxx	xxxxx	x	x	x	x	x	x	x		
15X-4, 70–72	Silty clay	115.60				x											xxx	xxxxx	x	x	x	x	x	x	x		
15X-5, 106–108	Silt	117.46					xx										xxx	xxxxx	xx								
15X-6, 6–8	Silt	117.96	xx		xx	xx											xxx	xxxxx	x	x	x	x	x	x	x		
15X-CC, 20–22	Silt or silty claystone	118.22	x														xxx	xxxxx	x	x	x	x	x	x	x		

Notes: xxxx = dominant (>50%); xxx = major (11–50%); xx = minor (3–10%); x = trace (1–2%); x = rare (<1%). Qz = quartz; Fs = feldspar; Hb = hornblende; Ch = chlorite; Carb = carbonate; An = anhydrite; Ep = epidote; Mag = magnetite; M-f = microfossils; F-py = frambooidal pyrite; Ba = barite; Ms = muscovite; Py = pyrite; Mr = marcasite; Po = pyrrhotite; Cp = chalcopyrite; Sp = sphalerite; Hem/op = hematite ± Fe-oxides.

^a = anhydrite detected by SEM only.

Table 7. Electron microprobe data for chlorite in unaltered and hydrothermally altered hemipelagic and turbidite sediment, Leg 139.

Site:	856A	856A	856A	856A	856B	856B	856B	856B	856B
Core, section:	4H-6	6H-3	6H-6	9H-1	10H-2	13X-2	14X-4	15X-1	
Interval (cm):	55–59	103–107	90–94	44–47	54–58	63–69	50–53	91–93	
Zone:	IVa	IVa	IVa	IIIa	IIa	IIa	IIa	IIa	Ia1
Si	5.596	5.330	6.328	5.441	6.303	5.240	5.574	5.396	5.994
Al	2.404	2.670	1.672	2.559	1.697	2.760	2.426	2.604	2.006
Σ_{tet}	8.000	8.000	8.000	8.000	8.000	8.000	8.000	8.000	8.000
Al	2.532	2.487	2.002	2.416	2.821	2.766	2.902	3.220	2.607
Ti	0.011	0.014	0.007	0.011	0.024	0.018	0.005	0.011	0.003
Fe	4.844	5.538	5.069	4.446	5.460	4.144	4.609	4.604	3.378
Mn	0.096	0.060	0.050	0.078	0.156	0.033	0.086	0.064	0.076
Mg	4.375	3.924	4.574	5.060	2.835	4.973	4.099	3.735	5.592
Cr	0.001	0.000	0.000	0.000	0.008	0.000	0.005	0.006	0.000
Zn	0.008	0.004	0.000	0.015	0.002	0.013	0.000	0.011	0.010
$\Sigma_{\text{oct.}}$	11.867	12.027	11.701	12.025	11.307	11.948	11.701	11.650	11.673
Ca	0.050	0.033	0.077	0.018	0.038	0.012	0.004	0.017	0.013
Na	0.005	0.024	0.082	0.023	0.110	0.030	0.028	0.020	0.011
K	0.011	0.011	0.019	0.014	0.020	0.009	0.075	0.003	0.005
$\Sigma_{\text{interl.}}$	0.066	0.068	0.178	0.054	0.168	0.051	0.107	0.040	0.029
Fe/(Fe + Mg)	0.53	0.59	0.53	0.47	0.66	0.45	0.53	0.55	0.38
Site:	856B	856B	856B	856B	856B	856B	856B	856B	856B
Core, section:	15X-2	15X-3	15X-4	15X-5	15X-1	15X-2	15X-2	15X-2	
Interval (cm):	67–69	8–10	70–72	106–108	124–126	27–29	27–29	27–29	
Zone:	Ia1	Ia1	Ia1	Ia1	Ia1	Ia1	Ia1	Ia1	Ia1
Si	5.649	5.477	6.215	5.630	6.202	5.405	5.674	5.784	5.189
Al	2.351	2.523	1.785	2.370	1.798	2.595	2.326	2.216	2.811
Σ_{tet}	8.000	8.000	8.000	8.000	8.000	8.000	8.000	8.000	8.000
Al	3.327	3.908	4.196	3.106	3.558	2.478	3.074	3.296	3.238
Ti	0.011	0.010	0.009	0.014	0.000	0.014	0.027	0.022	0.004
Fe	5.044	5.909	4.784	6.738	4.192	2.562	3.642	4.823	7.331
Mn	0.052	0.079	0.045	0.020	0.026	0.087	0.051	0.056	0.107
Mg	3.000	1.340	1.713	1.684	3.150	6.865	4.746	3.199	1.072
Cr	0.003	0.007	0.000	0.003	0.013	0.004	0.015	0.017	0.004
Zn	0.000	0.025	0.000	0.021	0.020	0.000	0.004	0.000	0.012
$\Sigma_{\text{oct.}}$	11.436	11.279	10.748	11.586	10.959	12.010	11.558	11.412	11.768
Ca	0.019	0.013	0.019	0.011	0.056	0.009	0.017	0.015	0.010
Na	0.031	0.000	0.028	0.026	0.088	0.025	0.029	0.003	0.000
K	0.057	0.004	0.009	0.013	0.109	0.021	0.004	0.001	0.009
$\Sigma_{\text{interl.}}$	0.107	0.017	0.056	0.050	0.253	0.055	0.051	0.020	0.014
Fe/(Fe + Mg)	0.63	0.82	0.74	0.80	0.57	0.27	0.43	0.60	0.87

Table 7 (continued).

Site:	856B				856H				856H				857C				857C			
Core, section:	15X-CC				3R-3				4R-1				4R-2				21R-1		28R-CC	
Interval (cm):	20–22				72–74				88–90				43–45				24–26		30R-1	
Zone:	Ia2				MS				MS				MS				IVc		IIIc	
Si	6.115	6.189	6.074	6.281	6.457	6.489	6.422	6.461	6.092	6.379	6.204	6.767	6.510	6.422	6.330					
Al ^{IV}	1.885	1.811	1.926	1.719	1.543	1.511	1.578	1.539	1.908	1.621	1.796	1.233	1.490	1.578	1.670					
Σt_{eff}	8.000	8.000	8.000	8.000	8.000	8.000	8.000	8.000	8.000	8.000	8.000	8.000	8.000	8.000	8.000					
Al ^{VII}	2.339	2.356	2.469	2.473	2.229	2.224	2.728	2.817	2.262	1.912	2.165	2.497	1.886	2.050	2.517					
Ti	0.011	0.005	0.012	0.011	0.009	0.013	0.008	0.005	0.007	0.008	0.008	0.004	0.031	0.232	0.033					
Fe	5.213	5.274	5.298	4.088	4.219	3.738	4.017	4.040	4.141	3.492	3.908	4.369	3.865	4.259	4.058					
Mn	0.035	0.029	0.034	0.030	0.027	0.022	0.043	0.050	0.034	0.032	0.029	0.046	0.043	0.089	0.050					
Mg	4.125	3.995	3.863	4.938	5.051	5.564	4.601	4.359	5.323	6.322	5.653	4.208	5.786	4.659	4.679					
Cr	0.002	0.000	0.000	0.008	0.005	0.009	0.000	0.006	0.002	0.004	0.000	0.005	0.005	0.010	0.005					
Zn	0.000	0.023	0.011	0.000	0.032	0.012	0.000	0.052	0.005	0.027	0.009	0.017	0.000	0.016	0.027					
$\Sigma \text{oct.}$	11.724	11.682	11.686	11.549	11.571	11.581	11.398	11.328	11.776	11.796	11.772	11.145	11.615	11.315	11.370					
Ca	0.019	0.021	0.021	0.036	0.029	0.022	0.017	0.015	0.018	0.022	0.011	0.161	0.105	0.125	0.082					
Na	0.033	0.039	0.011	0.034	0.083	0.044	0.000	0.011	0.042	0.047	0.048	0.104	0.051	0.054	0.129					
K	0.004	0.001	0.007	0.009	0.009	0.002	0.003	0.009	0.001	0.006	0.000	0.007	0.046	0.121	0.049					
$\Sigma \text{interl.}$	0.056	0.060	0.039	0.080	0.121	0.068	0.020	0.035	0.061	0.075	0.059	0.272	0.202	0.300	0.259					
Fe/(Fe + Mg)	1.26	1.32	1.37	0.83	0.84	0.67	0.87	0.93	0.78	0.55	0.69	1.04	0.67	0.91	0.87					
	0.56	0.57	0.58	0.45	0.46	0.40	0.47	0.48	0.44	0.36	0.41	0.51	0.40	0.48	0.46					

Site:	857C				858A				858C				858D				858F				858F	
Core, section:	61R-1				21X-3				25X-1				5H-CC				2H-3				2H-CC	
Interval (cm):	129–131				57–59				29–32				7–10				34–36				10–12	
Zone:	IIc				IVb				IIIb				Vb				Vb				IIb	
Si	6.285	6.394	6.106	6.190	5.772	5.680	5.115	5.147	5.549	5.524	5.599	5.397	5.586	5.651	5.354	5.272	5.497	6.331				
Al ^{IV}	1.715	1.606	1.894	1.810	2.228	2.320	2.885	2.853	2.451	2.476	2.401	2.603	2.414	2.349	2.646	2.728	2.503	1.669				
Σt_{eff}	8.000	8.000	8.000	8.000	8.000	8.000	8.000	8.000	8.000	8.000	8.000	8.000	8.000	8.000	8.000	8.000	8.000	8.000				
Al ^{VII}	2.349	2.333	2.497	3.614	2.868	2.777	0.886	3.122	2.522	2.695	2.623	2.894	2.512	2.428	2.654	2.889	2.959	2.101				
Ti	0.004	0.006	0.032	0.018	0.016	0.007	1.092	0.017	0.004	0.012	0.006	0.007	0.021	0.003	0.008	0.009	0.010	0.285				
Fe	2.521	2.754	3.118	3.685	4.627	5.171	4.757	5.349	4.427	4.890	4.483	5.545	4.431	4.386	4.424	4.131	5.966	3.376				
Mn	0.096	0.080	0.043	0.065	0.061	0.130	0.077	0.078	0.070	0.084	0.040	0.061	0.160	0.076	0.091	0.118	0.063	0.089				
Mg	6.426	6.264	5.874	2.856	4.051	3.631	4.985	3.229	4.889	4.138	4.650	3.234	4.751	5.008	4.733	4.728	2.680	5.472				
Cr	0.004	0.022	0.020	0.000	0.000	0.006	0.009	0.013	0.005	0.000	0.007	0.005	0.001	0.006	0.008	0.002	0.018	0.012				
Zn	0.010	0.044	0.032	0.022	0.019	0.009	0.013	0.009	0.010	0.034	0.043	0.054	0.019	0.016	0.027	0.023	0.035	0.066				
$\Sigma \text{oct.}$	11.410	11.504	11.615	10.260	11.642	11.731	11.820	11.816	11.926	11.852	11.853	11.800	11.896	11.923	11.944	11.900	11.730	11.401				
Ca	0.251	0.082	0.012	0.045	0.018	0.017	0.056	0.010	0.007	0.015	0.024	0.028	0.023	0.017	0.024	0.001	0.013	0.057				
Na	0.030	0.061	0.050	1.441	0.004	0.019	0.040	0.027	0.042	0.019	0.005	0.028	0.019	0.027	0.033	0.015	0.012	0.058				
K	0.000	0.006	0.008	0.109	0.004	0.008	0.015	0.007	0.009	0.005	0.000	0.005	0.000	0.002	0.000	0.001	0.009	0.012				
$\Sigma \text{interl.}$	0.281	0.150	0.070	1.594	0.026	0.044	0.111	0.043	0.058	0.039	0.028	0.061	0.043	0.046	0.058	0.017	0.033	0.126				
Fe/(Fe + Mg)	0.39	0.44	0.53	1.29	1.14	1.42	0.95	1.66	0.91	1.18	0.96	1.71	0.93	0.88	0.93	0.87	2.23	0.62				
	0.28	0.31	0.35	0.56	0.53	0.59	0.49	0.62	0.48	0.54	0.49	0.63	0.48	0.47	0.48	0.47	0.69	0.38				

Notes: Calculated on the basis of 28 (O), 16 (OH); Fe as Fe^{2+} . MS = massive sulfide.

Site 856

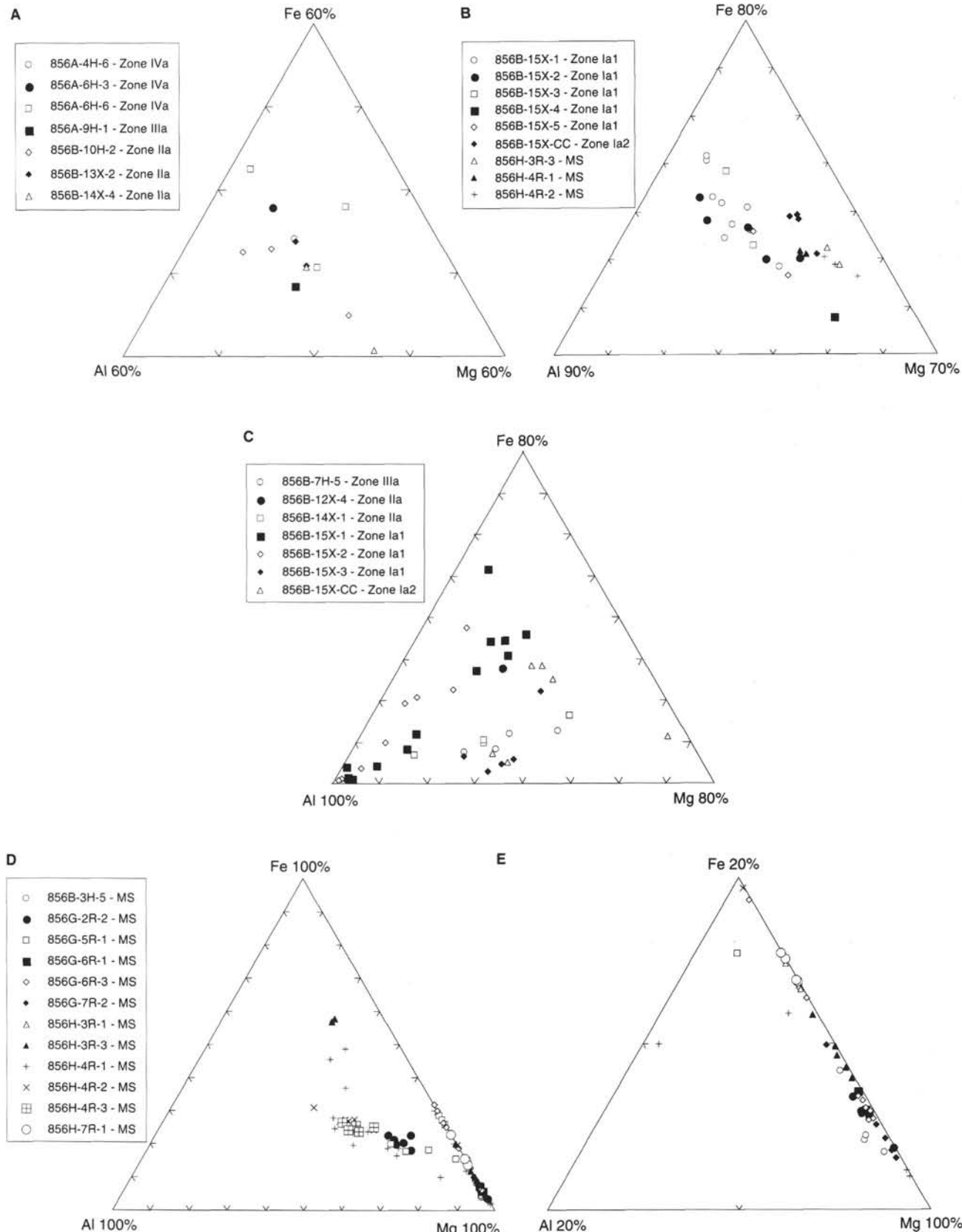


Figure 15. Ternary $\text{Al}_2\text{O}_3\text{-Fe}_2\text{O}_3\text{-MgO}$ diagram of clay and chlorite minerals by site. A. Chlorite from Site 856, alteration Zone IVa through IIa. B. Chlorite from Site 856, alteration Zone Ia and massive sulfides. C. Clay minerals from Site 856. D. Talc and saponite minerals from Site 856. E. Enlargement of field for talc minerals from Site 856. F. Chlorite from Site 858. G. Clay minerals from Site 858. H. Chlorite minerals from Site 857. I. Clay minerals from Site 857. Data from Tables 7 through 9.

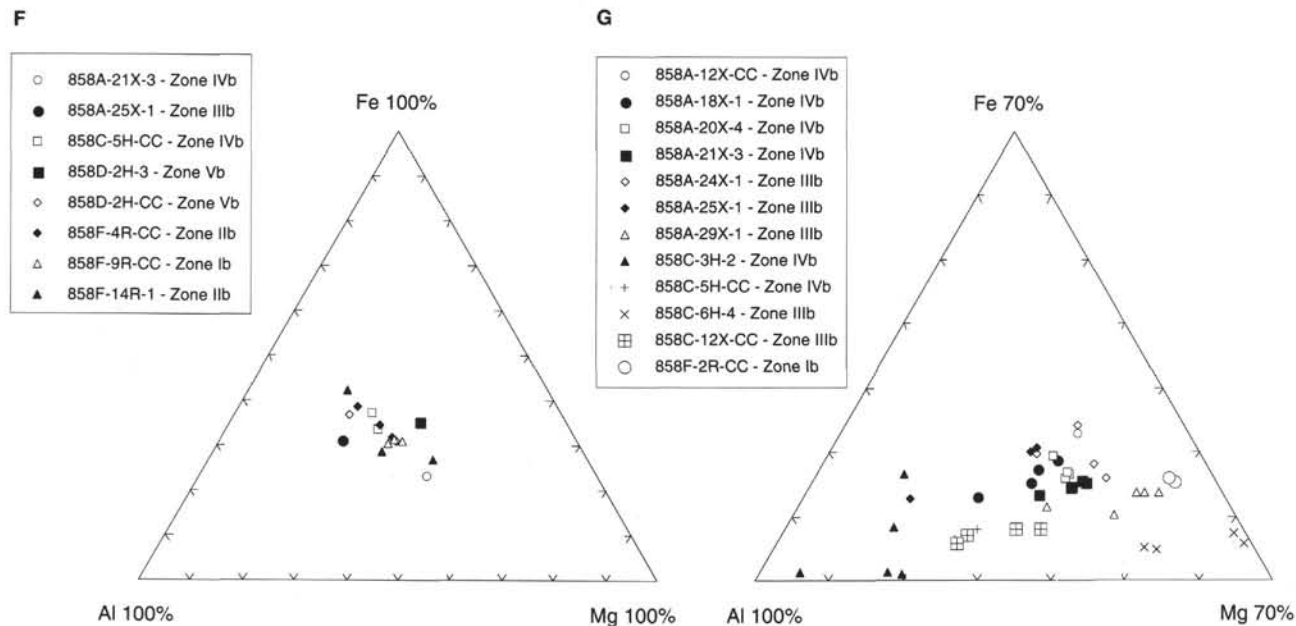
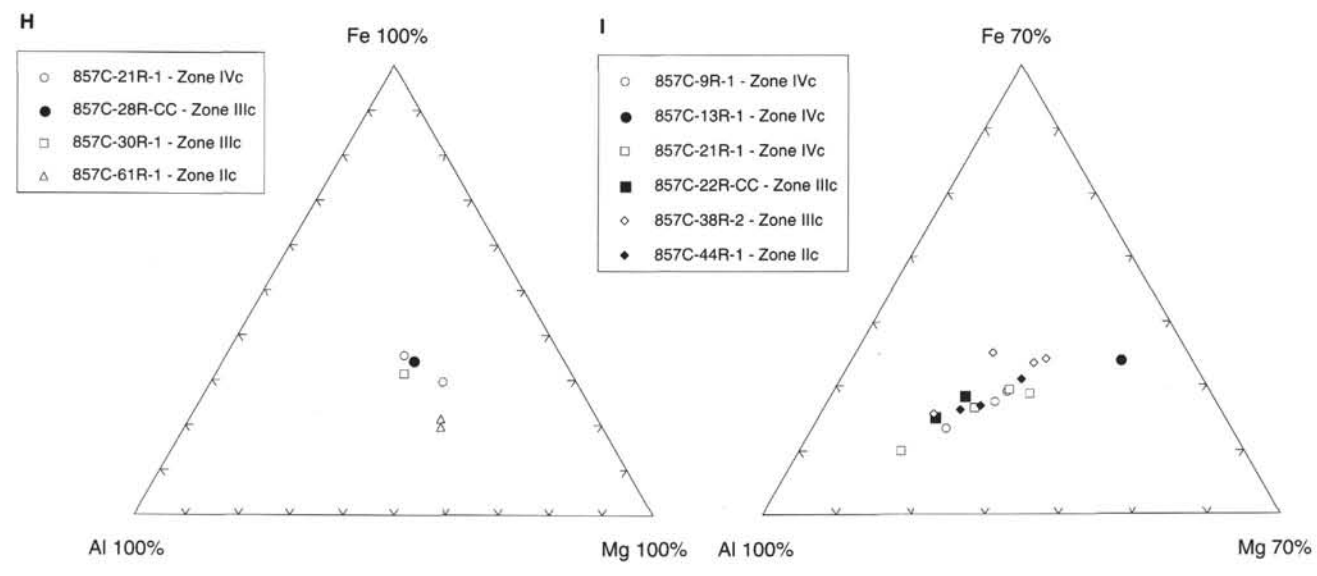
Site 858**Site 857**

Figure 15 (continued).

with depth below 150 mbsf, reaching a maximum of An 15 in Sample 139-858F-18R-1, 14–16 cm. Pyrite occurs as disseminated euhedral to anhedral crystals and more rarely in veins.

Hydrothermal Minerals Associated with Massive Sulfides

The only massive sulfides recovered at AAV during Leg 139 occur between 10.7 to 11.5 mbsf in Hole 858B (Fig. 6; Goodfellow and Peter, this volume). The massive sulfide is composed of pyrite, sphalerite, chalcopyrite, isocubanite, pyrrhotite, and marcasite. Pyritic hemipelagic and turbiditic sediments are cut by anhydrite veins between 11.5 and 24 mbsf. The gangue silicate interstitial to massive sulfide is compositionally similar to talc (Table 9) that has been documented for massive sulfides recovered in shallow cores from AAV (Goodfellow et al., in press; Goodfellow and Franklin, in press). Fine-grained anhedral

to subhedral dolomite (up to 45%; Table 11; Fig. 17B) with abundant fluid inclusions also occurs interstitially to massive sulfide.

Saponite clays are dominant to a depth of 2 mbsf in Hole 858B and have been described in detail from piston cores (Goodfellow et al., in press). Clasts (up to 500 µm) of hydrothermal clays (Sample 139-856B-1H-2, 50–54 cm) are composed primarily of saponite and are similar to saponite observed in hydrothermal sediment near active vents (Goodfellow and Franklin, in press).

Site 857

Four alteration zones have been identified at Site 857; these are summarized in Table 5. The textural and mineralogical characteristics are presented below.

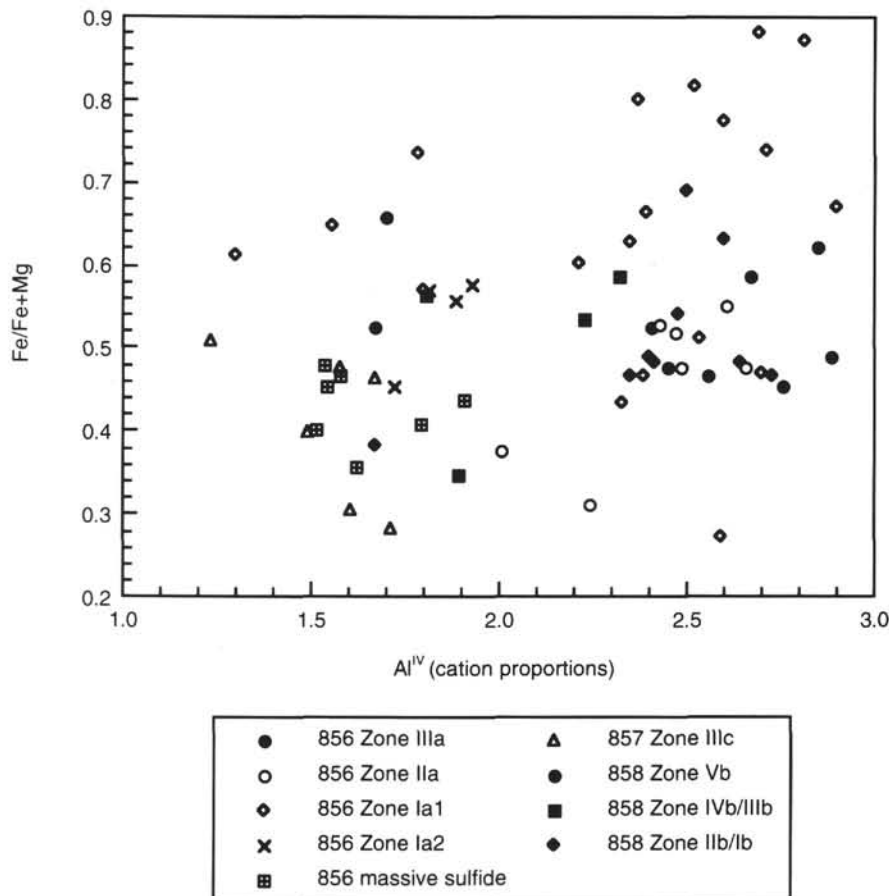


Figure 16. Al^{IV} vs. $\text{Fe}/(\text{Fe} + \text{Mg})$ for chlorite minerals from all sites. Al^{IV} calculated by stoichiometry. Data from Table 7.

Zone IVc

This zone consists of calcite-clay-pyrite and occurs between 70 and 300 mbsf in Holes 857A (Fig. 9) and 857C (Fig. 10). Detrital hornblende was not observed in Hole 857A below 26 mbsf (Table 14), although hornblende was detected by XRD to a depth of 105 mbsf in Hole 857A and to a depth of 82 mbsf in Hole 857C (Davis, Mottl, Fisher, et al., 1992). Epidote is a common accessory mineral in Holes 857A, 857C, and 857D (Table 14). The epidote in Hole 857A and above 450 mbsf in Hole 857C is interpreted to be of detrital origin, whereas epidote below 450 mbsf in Hole 857C and in Hole 857D is of hydrothermal origin. Detrital epidote is a trace component (typically <2 vol%) in unaltered sediment and consists of anhedral to ragged grains that are concentrated in turbiditic sediment. Detrital epidote is also more Fe-rich and Al-poor compared to authigenic epidote (Table 4; Fig. 13).

Disseminated euhedral to anhedral pyrite occurs throughout the entire sedimentary sequence at Site 857 and pyrite commonly infills burrows to a depth of 350 mbsf (Pl. 4, Fig. 4). Framboidal pyrite persists to the bottom of Hole 857C. Magnetite is an accessory phase in Holes 857A and 857C but is altered to pyrite below 241 mbsf.

Clay minerals are partially recrystallized between 15 mbsf and 268 mbsf in Holes 857A and 857C. At depths >268 mbsf, the clays are completely recrystallized and display common extinction and parallel alignment. The clays from Holes 857A and 857C are probably smectite or illite (Si, Al, Mg, Fe, Na, K, Ca and minor Ti; Table 8; Fig. 15H,I). The high Na contents of some clays (Table 8) suggests a Na-montmorillonite.

Carbonate cement and concretions are a minor to major component of the sediments between 53 and 450 mbsf (Table 14). Carbonate is less

common below 300 mbsf. Carbonate concretions may be graded (e.g., Sample 139-857C-9R-1, 8–9 cm) or laminated, and in one sample laminae are offset several mm by microfaults (Sample 139-857C-6R-1, 1–2 cm; Pl. 4, Fig. 5). Calcite is the dominant carbonate mineral, with the exception of a narrow zone near the top of Hole 857C where dolomite occurs (85–105 mbsf) (Table 11; Fig. 17C). Carbonate is visually absent in Hole 857D, consistent with low CO₂ (Goodfellow and Peter, this volume), although dolomite was detected by XRD in Sample 139-857D-5R-1, 26–28 cm.

Zone IIIc

Zone IIIc consists of albite-chlorite-pyrite and occurs between 250 and 450 mbsf in Hole 857C (Fig. 10). Detrital quartz contains abundant fluid inclusions below 330 mbsf and increasingly diffuse boundaries below 395 mbsf in Hole 857C and Hole 857D. Quartz-epidote-carbonate veins and vugs occur at 399 mbsf in Hole 857C. At depths greater than 300 mbsf, detrital plagioclase has been altered to albite (Table 3, Fig. 12C; Pl. 4, Fig. 6) and the anorthite content of plagioclase decreases from An 58 at 48 mbsf to less than An 9 below 314 mbsf (Table 3; Fig. 12C). K-feldspar is partially altered to sericite/chlorite below 47 mbsf. Shipboard logging noted clasts of massive sulfide at 388 mbsf (Davis, Mottl, Fisher, et al., 1992).

Zone IIc

This zone consists of quartz-chlorite-epidote-pyrite ± sphene below 450 mbsf in Holes 857C and 857D (Figs. 10 and 11). Detrital quartz displays ragged and diffuse grain boundaries, with abundant fluid inclusions. Detrital K-feldspar is altered to chlorite and detrital

Table 8. Electron microprobe data for clay minerals in unaltered and hydrothermally altered hemipelagic and turbiditic sediment, Leg 139.

Site:	856B				856B				856B				856B				856B						
Core, section:	7H-5		12X-4		14X-1				15X-1		15X-1												
Interval (cm):	26-32		29-33		34-36				91-93														
Zone:	IIIa		IIIa		IIIa				la1														
Si	6.651	7.712	6.527	6.558	5.680	6.364	8.763	7.830	6.911	7.799	5.062	5.265	6.571	6.593	6.678	5.635	5.668	6.326	6.579	4.172	8.710		
Al ^{IV}	1.349	0.288	1.473	1.442	2.320	1.636	0.000	0.170	1.089	0.201	2.938	2.735	1.429	1.407	1.322	2.365	2.332	1.674	1.421	3.828	0.000		
Σ tet.	8.000	8.000	8.000	8.000	8.000	8.000	8.763	8.000	8.000	8.000	8.000	8.000	8.000	8.000	8.000	8.000	8.000	8.000	8.000	8.000	8.710		
Al ^I	2.463	2.666	1.663	2.246	1.908	2.487	2.432	1.924	2.668	2.288	1.427	1.163	3.587	2.948	3.802	1.681	2.082	3.392	3.747	0.802	2.921		
Ti	0.071	0.060	0.102	0.119	0.013	0.000	0.011	0.003	0.008	0.005	0.074	0.007	0.002	0.011	0.011	0.000	0.006	0.003	0.007	0.007	0.000		
Fe	0.520	0.324	0.854	0.788	2.322	0.637	0.210	0.822	0.634	1.719	3.254	3.408	0.252	0.675	0.076	2.635	2.140	0.532	0.057	5.806	0.119		
Mn	0.017	0.006	0.028	0.010	0.031	0.059	0.084	0.069	0.101	0.050	0.035	0.015	0.000	0.049	0.009	0.014	0.043	0.000	0.001	0.085	0.024		
Mg	1.882	1.028	2.768	2.014	1.868	1.756	0.427	2.061	1.572	0.824	1.774	2.145	0.408	0.673	0.148	1.826	1.322	0.723	0.211	0.774	0.034		
Zn	0.007	0.000	0.029	0.000	0.009	0.012	0.010	0.009	0.002	0.015	0.000	0.000	0.010	0.000	0.003	0.005	0.000	0.000	0.000	0.019	0.000		
Σ oct.	4.960	4.084	5.445	5.176	6.150	4.952	3.175	4.888	4.985	4.900	6.564	6.739	4.249	4.367	4.045	6.160	5.599	4.650	4.022	7.493	3.098		
Ca	0.028	0.127	0.037	0.029	0.011	0.018	0.012	0.016	0.007	0.024	0.038	0.011	0.037	0.030	0.007	0.040	0.037	0.017	0.022	0.002	0.010		
Na	0.135	0.390	0.141	0.063	0.038	0.071	0.030	0.042	0.059	0.024	0.018	0.018	0.155	0.231	0.159	0.058	0.087	0.070	0.162	0.008	0.008		
K	0.632	0.671	0.500	0.471	0.018	1.126	0.087	0.381	0.363	0.012	0.138	0.022	1.108	1.402	1.235	0.197	0.867	0.859	1.396	0.000	0.000		
Σ interl.	0.795	1.188	0.678	0.563	0.067	1.215	0.128	0.439	0.429	0.060	0.195	0.050	1.301	1.662	1.400	0.294	0.991	0.945	1.580	0.010	0.018		
Si/Al	1.75	2.61	2.08	1.78	1.34	1.54	3.60	3.74	1.84	3.13	1.16	1.35	1.31	1.51	1.30	1.39	1.28	1.25	1.27	0.90	2.98		
Site:	856B				856B				856B				856B				856B						
Core, section:	15X-2		15X-2		15X-2				15X-3		15X-CC						20-22						
Interval (cm):	27-29		27-29		67-69				8-10		Ia2												
Zone:	Ia1		Ia1		Ia1				Ia1														
Si	6.728	7.383	6.679	5.984	6.318	5.772	5.153	6.350	5.650	5.866	6.528	5.526	6.264	6.647	6.137	6.375	6.090	6.586	5.765	5.481	5.219	6.694	7.266
Al ^{IV}	1.272	0.617	1.321	2.016	1.682	2.228	2.847	1.650	2.350	2.134	1.472	2.474	1.736	1.353	1.863	1.625	1.910	1.414	2.235	2.519	2.781	1.306	0.734
Σ tet.	8.000	8.000	8.000	8.000	8.000	8.000	8.000	8.000	8.000	8.000	8.000	8.000	8.000	8.000	8.000	8.000	8.000	8.000	8.000	8.000	8.000	8.000	
Al ^{VI}	3.788	3.923	3.715	3.467	3.813	2.569	1.973	3.723	3.112	3.057	3.854	1.481	2.853	3.790	2.460	2.823	2.678	0.419	1.190	1.211	1.201	2.542	2.438
Ti	0.012	0.010	0.009	0.006	0.008	0.013	0.005	0.007	0.008	0.009	0.003	0.042	0.004	0.006	0.011	0.007	0.008	0.001	0.000	0.009	0.012	0.002	0.009
Fe	0.056	0.035	0.043	0.654	0.069	1.709	3.390	0.216	1.407	1.518	0.033	1.946	0.426	0.047	0.414	0.186	0.341	0.860	2.350	2.262	2.578	0.449	0.277
Mn	0.005	0.000	0.004	0.029	0.006	0.050	0.008	0.003	0.011	0.002	0.005	0.011	0.007	0.000	0.008	0.000	0.003	0.007	0.020	0.018	0.040	0.001	0.001
Mg	0.082	0.051	0.138	0.409	0.176	1.095	0.876	0.256	0.430	0.555	0.172	2.870	1.620	0.179	2.592	2.133	2.454	4.939	2.462	3.063	2.529	1.860	1.804
Zn	0.005	0.008	0.002	0.001	0.002	0.008	0.000	0.008	0.019	0.000	0.001	0.008	0.003	0.005	0.001	0.010	0.006	0.009	0.016	0.010	0.017	0.005	0.010
Σ oct.	3.947	4.027	3.912	4.565	4.074	5.445	6.252	4.213	4.988	5.141	4.067	6.358	4.913	4.027	5.486	5.159	5.490	6.237	6.038	6.573	6.377	4.859	4.539
Ca	0.009	0.018	0.020	0.019	0.033	0.035	0.011	0.002	0.006	0.007	0.019	0.080	0.042	0.022	0.073	0.072	0.065	0.216	0.058	0.046	0.044	0.168	0.128
Na	0.122	0.048	0.165	0.099	0.108	0.056	0.039	0.146	0.132	0.064	0.130	0.028	0.085	0.147	0.048	0.056	0.047	0.062	0.819	0.017	0.674	0.600	0.729
K	1.410	0.536	1.552	1.266	1.518	0.613	0.286	1.335	1.095	0.664	1.274	0.005	0.881	1.288	0.215	0.239	0.051	0.024	0.009	0.022	0.026	0.106	0.215
Σ interl.	1.542	0.602	1.737	1.385	1.659	0.704	0.336	1.483	1.234	0.736	1.424	0.114	1.008	1.457	0.336	0.367	0.164	0.302	0.885	0.086	0.744	0.874	1.072
Si/Al	1.33	1.63	1.33	1.09	1.15	1.20	1.07	1.18	1.03	1.13	1.23	1.40	1.36	1.29	1.42	1.43	1.33	3.59	1.68	1.47	1.31	1.74	2.29

Table 8 (continued).

Site:	857C				857C				857C				857C				857C				858A			
Core, section:	9R-1				13R-1				21R-1				22R-CC				38R-2				44R-1		12X-CC	
Interval (cm):	8-9				6-8				24-26				1-5				50-53				137-140		11-12	
Zone:	IVc				IVc				IVc				IIIc				IIIc				IIc		IVb	
Si	6.791	7.003	7.105	6.785	8.102	6.331	6.808	6.522	7.221	7.298	6.721	7.331	7.294	6.204	7.334	6.684	6.314	6.162						
Al ^{IV}	1.209	0.997	0.895	1.215	0.000	1.669	1.192	1.478	0.779	0.702	1.279	0.669	0.706	1.796	0.666	1.316	1.686	1.838						
Σ tet.	8.000	8.000	8.000	8.000	8.102	8.000	8.000	8.000	8.000	8.000	8.000	8.000	8.000	8.000	8.000	8.000	8.000	8.000						
Al ^I	1.882	1.736	2.264	1.243	2.883	1.991	2.127	2.200	2.358	2.434	1.632	1.963	2.575	1.331	2.13	2.470	2.273	1.515						
Ti	0.055	0.090	0.046	0.085	0.051	0.033	0.051	0.067	0.127	0.039	0.275	0.150	0.027	0.113	0.048	0.028	0.067	0.054						
Fe	1.034	0.791	0.609	1.471	0.378	1.269	1.137	0.961	0.673	0.911	1.325	1.166	0.732	1.532	1.070	1.035	0.985	1.719						
Mn	0.013	0.031	0.015	0.020	0.018	0.029	0.019	0.030	0.035	0.008	0.009	0.019	0.023	0.040	0.011	0.011	0.022	0.011						
Mg	1.275	1.032	0.839	2.273	0.515	1.780	1.385	1.199	0.730	0.901	1.404	0.869	0.732	1.643	1.256	1.275	1.141	2.394						
Zn	0.019	0.000	0.019	0.001	0.018	0.000	0.000	0.000	0.019	0.017	0.005	0.000	0.000	0.001	0.000	0.000	0.027	0.010						
Σ oct.	4.278	3.680	3.790	5.093	3.863	5.102	4.720	4.457	3.941	4.310	4.651	4.168	4.089	4.661	4.519	4.818	4.515	5.703						
Ca	0.944	1.311	1.045	0.196	0.173	0.137	0.244	0.173	0.236	0.121	0.425	0.240	0.087	1.028	0.106	0.052	0.105	0.109						
Na	0.422	0.625	0.585	0.973	0.451	0.791	0.697	1.634	1.269	1.027	0.540	1.068	1.464	0.441	0.983	0.117	1.572	0.157						
K	0.345	0.459	0.285	0.238	0.082	0.344	0.337	0.249	0.544	0.301	0.386	0.484	0.237	0.420	0.194	0.921	0.452	0.423						
Σ interl.	1.711	2.395	1.915	1.407	0.707	1.271	1.278	2.056	2.049	1.449	1.351	1.792	1.889	1.284	1.090	2.129	0.688							
Si/Al	2.20	2.56	2.25	2.76	2.81	1.73	2.05	1.77	2.30	2.33	2.31	2.78	2.22	1.98	2.62	1.77	1.59	1.84						
Site:	858A				858A				858A				858A				858A				858A			
Core, section:	18X-1				20X-4				21X-3				24X-1				24X-1				25X-1			
Interval (cm):	116-118				100-103				57-59				IVb				33-35				33-35			
Zone:	IVb				IVb				IVb				IIIb				IIIb				IIIb			
Si	6.070	7.514	6.336	6.760	6.360	7.275	6.626	6.325	5.944	6.693	5.969	6.891	6.221	5.944	6.061	6.592	6.007	6.293	7.831	6.718				
Al ^{IV}	1.930	0.486	1.664	1.240	1.640	0.725	1.374	1.675	2.056	1.307	2.031	1.109	1.779	2.056	1.939	1.408	1.993	1.707	0.169	1.282				
Σ tet.	8.000	8.000	8.000	8.000	8.000	8.000	8.000	8.000	8.000	8.000	8.000	8.000	8.000	8.000	8.000	8.000	8.000	8.000	8.000	8.000	8.000			
Al ^{VII}	1.977	2.460	1.703	2.134	1.873	2.031	1.883	1.840	1.810	1.870	1.682	1.862	2.172	1.429	1.572	1.937	1.525	2.545	2.262	1.969				
Ti	0.040	0.019	0.243	0.074	0.024	0.022	0.059	0.014	0.016	0.036	0.024	0.015	0.016	0.012	0.008	0.006	0.007	0.015	0.007	0.007	0.007			
Fe	1.265	0.610	1.271	0.940	1.365	0.931	1.047	1.211	1.094	0.937	1.213	0.943	0.958	1.238	1.418	1.266	1.899	0.748	0.975	1.229				
Mn	0.023	0.016	0.033	0.016	0.024	0.012	0.015	0.025	0.030	0.018	0.023	0.023	0.017	0.041	0.047	0.027	0.035	0.027	0.015	0.031				
Mg	2.194	1.099	2.119	1.820	2.143	1.920	2.215	2.409	2.737	2.243	2.805	2.292	2.276	3.069	2.842	1.799	2.479	0.858	1.305	1.671				
Zn	0.022	0.000	0.000	0.010	0.020	0.008	0.000	0.014	0.020	0.003	0.017	0.016	0.000	0.010	0.000	0.005	0.004	0.008	0.001	0.001				
Σ oct.	5.523	4.203	5.369	4.994	5.448	4.925	5.219	5.511	5.705	5.107	5.765	5.151	5.438	5.799	5.886	5.040	5.950	4.201	4.565	4.908				
Ca	0.056	0.142	0.063	0.043	0.029	0.036	0.042	0.045	0.043	0.045	0.036	0.111	0.014	0.049	0.071	0.033	0.053	0.134	0.046	0.078				
Na	0.207	1.042	0.268	0.292	0.342	0.361	0.356	0.263	0.121	0.502	0.110	0.100	0.078	0.479	0.322	1.238	0.181	2.232	0.306	0.951				
K	0.477	0.239	0.323	0.578	0.422	0.368	0.463	0.402	0.558	0.543	0.589	0.549	0.594	0.429	0.107	0.075	0.245	0.231	0.357	0.366				
Σ interl.	0.740	1.423	0.654	0.913	0.793	0.765	0.861	0.710	0.722	1.090	0.735	0.760	0.686	0.957	0.500	1.346	0.479	2.597	0.709	1.396				
Si/Al	1.55	2.55	1.88	2.00	1.81	2.64	2.03	1.80	1.54	2.11	1.61	2.32	1.57	1.71	1.73	1.97	1.71	1.48	3.22	2.07				

Table 8 (continued).

Site: Core, section: Interval (cm); Zone:	858A 29X-1			858C 3H-2			858C 5H-CC			858C 6H-4			858C 12X-CC			858F 2R-CC 8-11 Ib						
	30-32	IIIb	IV	10-15	IVb	110-115	IVb	7-10	IVb	43-51	IIIb	8-10	IIb	8-10	IIb	8-11	Ib					
Si	5.133	5.898	5.118	5.026	5.441	7.742	8.790	7.687	7.629	7.806	7.732	6.727	6.251	6.457	6.788	6.452	5.464	6.806	6.512	6.506	7.639	6.555
Al ^{IV}	2.867	2.102	2.882	2.974	2.559	0.258	0.000	0.313	0.371	0.194	0.268	1.273	1.749	1.543	1.212	1.548	2.536	1.194	1.488	0.361	1.445	
Al ^{tot.}	8.000	8.000	8.000	8.000	8.000	8.000	8.000	8.000	8.000	8.000	8.000	8.000	8.000	8.000	8.000	8.000	8.000	8.000	8.000	8.000	8.000	
Ti	0.888	2.187	1.050	0.975	1.471	2.815	2.511	2.544	3.177	3.215	2.674	2.991	1.578	1.546	0.977	0.846	1.848	2.627	2.932	2.944	1.640	1.241
Fe	0.010	0.014	0.008	0.003	0.010	0.031	0.032	0.141	0.123	0.010	0.004	0.009	0.010	0.007	0.005	0.007	0.538	0.006	0.004	0.005	0.004	0.003
Mn	0.034	0.130	0.895	1.313	1.349	0.880	0.333	0.034	0.656	0.053	0.039	0.355	0.393	0.370	0.341	0.111	0.543	0.601	0.499	0.446	0.359	1.188
Mg	4.612	2.624	4.244	4.489	3.746	0.099	0.000	0.004	0.010	0.008	0.004	0.006	0.015	0.017	0.016	0.016	0.024	0.020	0.010	0.010	0.020	0.035
Zn	0.004	0.000	0.000	0.001	0.000	0.027	0.011	0.000	0.008	0.015	0.000	0.017	0.003	0.000	0.010	0.010	0.000	0.008	0.000	0.000	0.029	0.016
Σ oct.	6.859	5.723	6.656	6.860	6.134	3.800	2.734	3.814	4.117	4.114	4.204	4.867	5.683	5.612	5.899	6.050	5.665	5.136	5.030	4.860	5.307	6.071
Si/Al	1.37	1.37	1.30	1.27	1.35	2.52	3.50	2.69	2.15	2.29	2.63	1.58	1.88	2.09	3.10	2.69	1.25	1.78	1.47	1.47	3.82	2.44

Note: Based on 20 (O), 4(OH).

plagioclase to albite (Table 3; Fig. 12C). Authigenic clays are dominated by chlorite (Pl. 5, Fig. 1) and micas are trace to absent below 612 mbsf in Hole 857D (Table 14), consistent with low sediment K₂O contents (Goodfellow et al., this volume). Authigenic epidote is euhedral to anhedral, commonly abundant (up to 30 vol%) and shows no relationship to the grain-size of the host sediment. Spheine is present below 440 mbsf as anhedral crystals and fine-grained xenoblastic aggregates up to 75 µm in diameter, and forms up to 5 vol%. Pyrite is abundant (Table 14) and coarser grained at the bottom of Hole 857C and in Hole 857D. It occurs as disseminated euhedral to anhedral and corroded crystals in concentrations up to 5 vol% (Pl. 5, Figs. 2 and 3). Pyrite also occurs with pyrrhotite, chalcopyrite, and sphalerite in veins crosscutting altered sediment in Hole 857D (Fig. 11). Sphalerite and chalcopyrite occur in veins as anhedral masses up to 15 mm in diameter (Davis, Mottl, Fisher, et al., 1992).

Zone Ic

This zone occurs between 628 and 736 mbsf in Hole 857D and consists of quartz-wairakite-epidote (Fig. 11). Quartz-wairakite-epidote-actinolite veins also occur in mafic sills between 522 and 740 mbsf (Davis, Mottl, Fisher, et al., 1992).

Euhedral quartz (up to 250 µm in diameter) occurs with epidote ± wairakite and sulfides in veins and vugs below 580 mbsf in Hole 857D. Wairakite is present in veins cutting sediments between 628 and 736 mbsf and mafic sills within Hole 857C and 857D (Davis, Mottl, Fisher, et al., 1992). Wairakite crystals up to 2 mm in diameter are typically twinned, equant, and commonly euhedral to subhedral (Pl. 5, Fig. 4). Wairakite approaches Ca end-member compositions (Ca/Ca + Na = 0.942–0.996; Table 13). Euhedral epidote also occurs in quartz ± wairakite veins (Table 14; Pl. 5, Figs. 5 and 6) and is more Al-rich and Fe-poor than detrital epidote (Fig. 13). Pyrite occurs as disseminated euhedral to subhedral crystals and in veins with pyrrhotite, quartz ± epidote ± wairakite.

DISCUSSION

Sites 856 (BH) and 858 (AAV) are hydrothermal upflow zones with distinct mineral assemblages and mineral zonation patterns (Table 5; Figs. 14 and 18). Both upflow systems are characterized by variably altered and indurated hemipelagic and turbiditic sediments. The hydrothermal alteration zones have a convex-upward geometry (Figs. 14 and 18). The BH upflow zone represents a fossil hydrothermal system associated with a massive sulfide deposit that was penetrated to a depth of 94 mbsf in Hole 856H. The hydrothermal upflow zone at AAV (Site 858) is associated with 184°–276°C vents (Davis, Mottl, Fisher, et al., 1992). These temperatures are similar to fluid inclusion trapping temperatures in anhydrite and wairakite (from Zone IIIb and Ib, respectively) from the most intensely altered sediments at AAV (Peter et al., this volume).

Bent Hill (Site 856)

The sediments in Holes 856A and 856B reflect hydrothermal alteration associated with the inactive BH massive sulfide deposit. The core of the hydrothermal discharge conduit (Zone Ia) occurs between 110 and 118 mbsf in Hole 856B adjacent to the BH massive sulfide deposit (Figs. 4 and 14; Table 5). In Zone Ia, hemipelagic and turbiditic sediment are bleached to pale blue grey, silicified, fractured and brecciated, and cut by pyrrhotite-chalcopyrite veins. The original detrital sedimentary mineralogy has been replaced in Zone Ia by a quartz-(Fe)chlorite-muscovite-rutile-chalcopyrite-pyrrhotite assemblage (Pl. 1, Figs. 1–6). The intensity of sediment alteration in Zone Ia is also evident from the sediment chemistry, in which Si and Fe are enriched and Ca and Na are depleted relative to unaltered sediment (Goodfellow and Peter, this volume).

The pyrrhotite-sphalerite(wurtzite)-isocubanite massive sulfide assemblage at BH suggests hydrothermal fluid temperatures >350°C

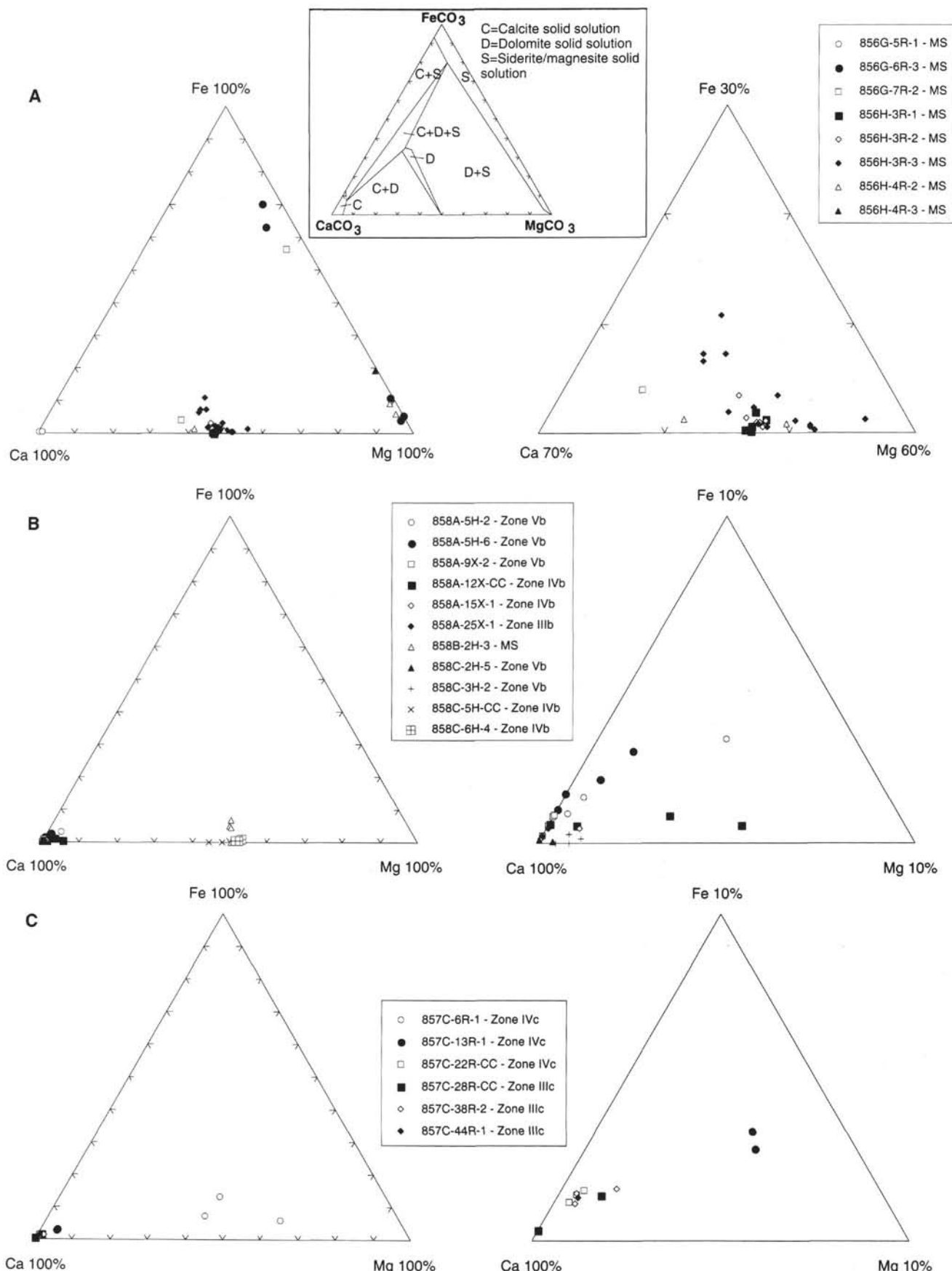


Figure 17. Ternary $\text{CaCO}_3\text{-FeCO}_3\text{-MgCO}_3$ diagram of carbonate minerals. A. Site 856. B. Site 858. C. Site 857. Inset plot with compositional fields after Rosenberg (1967). Data from Table 11.

Table 9. Electron microprobe data for authigenic talc, serpentine, and saponite interstitial to massive sulfide, Leg 139.

Site:	856B				856G				856G															
Core, section:	3H-5				2R-2				5R-1															
Interval (cm):	110–113				54–56				59–61															
Zone:	MS				MS				MS															
Si	8.071	8.440	8.045	7.958	7.964	7.950	7.911	7.955	7.901	7.954	6.021	5.908	6.289	6.084	6.101	6.116								
Al	0.040	0.070	0.066	0.030	0.041	0.040	0.044	0.009	0.021	0.000	1.505	1.476	0.960	1.171	1.412	1.230								
Ti	0.001	0.006	0.002	0.006	0.002	0.002	0.001	0.000	0.000	0.002	0.006	0.004	0.004	0.004	0.004	0.002	0.001	0.002						
Fe	0.197	0.210	0.257	0.503	0.355	0.411	0.356	0.224	0.371	0.376	2.075	1.886	1.993	1.671	1.918	1.878								
Mn	0.007	0.002	0.001	0.001	0.005	0.004	0.007	0.006	0.011	0.010	0.007	0.010	0.011	0.008	0.008	0.005	0.002	0.000						
Mg	5.529	4.734	5.456	5.450	5.619	5.588	5.715	5.823	5.765	5.701	5.571	6.006	5.895	6.309	5.701	5.977	5.834	6.798	7.307	6.105	6.075	6.251	6.780	
Cr	0.000	0.000	0.001	0.000	0.000	0.001	0.002	0.005	0.001	0.002	0.004	0.000	0.005	0.000	0.005	0.000	0.003	0.005	0.006	0.004	0.002	0.001	0.000	
Zn	0.028	0.031	0.054	0.041	0.011	0.011	0.006	0.013	0.011	0.002	0.000	0.004	0.010	0.014	0.001	0.006	0.003	0.000	0.001	0.000	0.000	0.002	0.006	
Ca	0.009	0.008	0.007	0.008	0.005	0.008	0.008	0.001	0.002	0.000	0.023	0.029	0.041	0.019	0.019	0.027	0.027	0.005	0.008	0.021	0.007	0.025	0.009	0.011
Na	0.043	0.039	0.056	0.052	0.020	0.020	0.026	0.004	0.004	0.000	0.024	0.039	0.029	0.080	0.017	0.033	0.034	0.018	0.043	0.063	0.036	0.043	0.071	
K	0.008	0.000	0.006	0.000	0.006	0.006	0.005	0.000	0.002	0.000	0.003	0.005	0.008	0.006	0.005	0.011	0.003	0.004	0.012	0.012	0.019	0.010	0.014	
Fe/(Fe + Mg)	0.03	0.04	0.04	0.08	0.06	0.07	0.06	0.04	0.06	0.06	0.27	0.24	0.25	0.21	0.25	0.24	0.24	0.20	0.16	0.21	0.29	0.27	0.26	
Site:	856G				856G				856G				856G				856G							
Core, section:	6R-1				6R-1				6R-3				6R-3				7R-2							
Interval (cm):	70–72				70–72				17–19				132–134				120–122							
Zone:	MS				MS				MS				MS				MS							
Si	8.057	8.005	7.954	7.961	6.305	5.800	5.692	6.427	6.336	6.509	6.624	6.430	6.224	6.139	6.446	6.785	6.615	6.866	8.008	8.033	6.920	8.042	8.031	
Al	0.016	0.023	0.020	0.013	0.009	0.006	0.007	0.008	0.011	0.010	0.009	0.005	0.035	0.037	0.048	0.023	0.028	0.018	0.017	0.013	0.036	0.015	0.016	
Ti	0.002	0.004	0.001	0.001	0.001	0.000	0.002	0.000	0.000	0.002	0.002	0.004	0.002	0.003	0.001	0.000	0.004	0.002	0.002	0.000	0.003	0.003	0.002	
Fe	0.414	0.356	0.348	0.429	1.737	3.278	3.163	1.232	1.244	2.370	1.105	2.265	0.580	0.654	0.488	0.460	0.568	0.485	0.303	0.252	0.798	0.183	0.209	
Mn	0.005	0.003	0.007	0.005	0.003	0.002	0.004	0.000	0.000	0.006	0.003	0.007	0.002	0.004	0.002	0.002	0.006	0.001	0.006	0.001	0.005	0.004	0.001	
Mg	5.432	5.572	5.670	5.602	7.571	7.040	7.373	7.870	8.026	6.550	7.578	6.797	8.875	8.936	8.512	7.892	8.123	7.728	5.629	5.647	7.212	5.667	5.667	
Cr	0.000	0.000	0.003	0.001	0.003	0.000	0.000	0.000	0.000	0.000	0.000	0.003	0.000	0.000	0.000	0.000	0.000	0.003	0.000	0.000	0.005	0.003	0.004	
Zn	0.000	0.003	0.006	0.008	0.006	0.004	0.000	0.002	0.006	0.008	0.001	0.000	0.000	0.013	0.011	0.006	0.003	0.003	0.004	0.005	0.044	0.022	0.017	
Ca	0.003	0.006	0.011	0.009	0.019	0.024	0.017	0.013	0.015	0.017	0.043	0.040	0.005	0.015	0.008	0.018	0.013	0.015	0.009	0.005	0.005	0.006	0.008	
Na	0.007	0.012	0.028	0.006	0.058	0.079	0.079	0.026	0.038	0.018	0.011	0.024	0.051	0.048	0.021	0.032	0.013	0.001	0.009	0.009	0.009	0.056	0.001	0.002
K	0.001	0.004	0.002	0.000	0.013	0.006	0.003	0.006	0.000	0.006	0.003	0.003	0.015	0.032	0.000	0.006	0.003	0.000	0.000	0.000	0.000	0.007	0.002	0.001
Fe/(Fe + Mg)	0.07	0.06	0.06	0.07	0.19	0.32	0.30	0.14	0.13	0.27	0.13	0.25	0.06	0.07	0.05	0.06	0.07	0.06	0.05	0.04	0.10	0.03	0.04	

Table 9 (continued).

Site:	856H				856H				856H				856H				856H			
Core, section:	3R-1		3R-3		3R-3		3R-3		3R-1		3R-1									
Interval (cm):	60–62		17–19		72–74		72–74		88–90		88–90		21–23		21–23		MS		MS	
Zone:	MS	MS	MS	MS	MS	MS	MS	MS	MS	MS	MS	MS	MS	MS	MS	MS	MS	MS	MS	
Si	6.559	6.673	6.581	6.608	6.588	4.017	4.244	6.757	6.511	6.381	6.450	8.170	5.725	5.081	6.077	5.616	6.056	5.195		
Al	0.004	0.016	0.010	0.007	0.015	1.831	1.587	0.024	0.011	0.013	0.022	0.084	2.512	3.026	2.225	2.587	2.241	2.864		
Ti	0.005	0.000	0.003	0.001	0.003	0.000	0.004	0.000	0.000	0.005	0.005	0.001	0.001	0.011	0.007	0.006	0.005	0.007		
Fe	1.362	1.267	1.158	0.858	1.738	7.329	7.266	0.779	0.760	0.724	1.039	0.658	1.821	2.509	2.006	2.427	2.333	2.815		
Mn	0.007	0.004	0.002	0.000	0.000	0.025	0.000	0.012	0.000	0.000	0.001	0.001	0.010	0.014	0.012	0.013	0.017	0.016		
Mg	7.405	7.272	7.583	7.867	7.003	3.745	3.701	7.621	8.142	8.424	7.780	4.821	4.908	4.723	4.453	4.395	4.122	4.427		
Cr	0.005	0.000	0.003	0.000	0.004	0.012	0.009	0.001	0.000	0.007	0.002	0.003	0.006	0.000	0.000	0.000	0.005	0.000		
Zn	0.046	0.026	0.000	0.000	0.007	0.010	0.006	0.019	0.018	0.015	0.169	0.012	0.000	0.004	0.000	0.000	0.005	0.003		
Ca	0.005	0.046	0.032	0.036	0.032	0.037	0.094	0.006	0.012	0.010	0.054	0.016	0.007	0.007	0.008	0.019	0.013	0.025		
Na	0.063	0.027	0.063	0.019	0.013	0.105	0.080	0.022	0.051	0.046	0.020	0.031	0.044	0.036	0.031	0.043	0.031	0.025		
K	0.004	0.004	0.008	0.000	0.007	0.006	0.007	0.002	0.009	0.006	0.003	0.012	0.003	0.006	0.003	0.002	0.006	0.003		
Fe/(Fe + Mg)	0.16	0.15	0.13	0.10	0.20	0.66	0.66	0.09	0.09	0.09	0.08	0.12	0.12	0.27	0.35	0.31	0.36	0.39		
Site:	856H				856H				856H				856H				856H			
Core, section:	4R-1		135–137		MS		MS		4R-2		6–8		MS		4R-2		6–8		MS	
Interval (cm):	Zone:		MS		MS		MS		MS		MS		MS		MS		MS		MS	
Si	6.374	6.279	6.253	7.093	7.756	7.722	5.711	4.819	5.110	5.044	5.474	5.334	5.285	4.786	5.306	5.067	8.062			
Al	1.452	1.379	1.591	0.678	0.008	0.007	1.822	1.598	2.085	2.191	2.117	2.473	2.326	3.376	2.017	2.664	0.007			
Ti	0.005	0.007	0.003	0.003	0.000	0.001	0.002	0.009	0.005	0.003	0.008	0.006	0.011	0.005	0.004	0.009	0.002			
Fe	1.393	1.603	1.581	0.737	0.151	0.130	2.456	5.334	4.616	3.970	2.326	2.692	2.793	3.292	2.473	2.822	1.125			
Mn	0.011	0.009	0.011	0.015	0.005	0.008	0.010	0.007	0.003	0.017	0.015	0.020	0.021	0.027	0.023	0.021	0.006			
Mg	5.593	5.651	5.349	5.957	6.278	6.375	5.304	4.036	3.497	4.574	5.449	4.818	5.058	3.981	5.783	4.941	4.674			
Cr	0.002	0.000	0.000	0.000	0.002	0.001	0.009	0.004	0.008	0.008	0.002	0.000	0.002	0.008	0.000	0.000	0.002			
Zn	0.000	0.000	0.012	0.000	0.013	0.006	0.000	0.001	0.007	0.002	0.004	0.028	0.013	0.022	0.023	0.033	0.000			
Ca	0.046	0.066	0.051	0.044	0.010	0.007	0.037	0.055	0.065	0.028	0.008	0.003	0.006	0.003	0.004	0.005	0.015			
Na	0.022	0.043	0.182	0.058	0.021	0.022	0.032	0.436	0.292	0.027	0.112	0.095	0.048	0.034	0.093	0.054	0.076			
K	0.015	0.014	0.013	0.017	0.008	0.010	0.010	0.578	0.591	0.006	0.002	0.000	0.003	0.002	0.003	0.004	0.000			
Fe/(Fe + Mg)	0.20	0.22	0.23	0.11	0.02	0.02	0.32	0.57	0.57	0.46	0.30	0.36	0.36	0.45	0.30	0.36	0.19			

Table 9 (continued).

Site:	Core, section:	Interval (cm):	856H			856B		
			4R-3	16-17	MS	7R-I	45-47	MS
Si	5.686	5.346	5.125	5.237	5.091	5.239	7.839	7.617
Al	2.342	2.452	1.997	2.737	2.406	0.002	0.005	0.006
Ti	0.006	0.007	0.006	0.006	0.003	0.006	0.002	0.002
Fe	2.359	2.632	2.649	2.595	2.504	2.428	0.943	1.487
Mn	0.014	0.017	0.019	0.022	0.017	0.019	0.000	0.003
Mg	4.660	4.639	5.369	5.835	5.154	5.413	5.303	5.013
Cr	0.003	0.000	0.001	0.001	0.001	0.004	0.000	0.000
Zn	0.012	0.001	0.000	0.005	0.002	0.004	0.000	0.003
Ca	0.032	0.021	0.016	0.042	0.012	0.018	0.011	0.017
Na	0.028	0.021	0.010	0.028	0.027	0.026	0.104	0.437
K	0.015	0.019	0.004	0.004	0.002	0.002	0.022	0.032
Fe/(Fe + Mg)	0.34	0.36	0.33	0.31	0.33	0.31	0.15	0.23
							0.14	0.14
							0.15	0.15
							0.21	0.22

Notes: Calculated based on 20 (O), 4 (OH). MS = massive sulfide.

(Goodfellow and Franklin, in press). These temperatures generally agree with fluid inclusion trapping temperatures ranging up to 338°C in quartz from Zone Ia (Peter et al., this volume). Calculated temperatures of authigenic chlorite in Zone Ia range from 175°–410°C using the geothermometer of Cathelineau (1988) and are similar to fluid inclusion trapping temperatures in coexisting quartz (181°–338°C; Peter et al., this volume). The Fe contents of the chlorites in Zone Ia generally increase with increasing temperature (based on Al^{IV}) (Fig. 16), indicating a dependence of Fe content on temperature for authigenic chlorite (Cathelineau, 1988). The Fe-rich character of the chlorite in Zone Ia is consistent with formation from a high-temperature, end-member hydrothermal fluid (Mottl et al., 1979; Seewald et al., 1990; Von Damm, 1990). The small amounts of Mg in the chlorites originated either from Mg present in the precursor sediment or from the entrainment of minor amounts of seawater into the center of fluid upflow.

The composition of the high-temperature end-member hydrothermal fluid is further constrained by the formation of authigenic rutile (Zones Ia and IIa) rather than another Ti-bearing mineral such as sphene. The hydrothermal mineralogy (quartz-chlorite-muscovite) in the core of the BH upflow zone is distinctly different from the alteration assemblage (wairakite-epidote-sphene) near the center of fluid upflow at AAV. The absence of epidote or any other Ca-mineral in Zone Ia and low bulk-rock CaO contents (Goodfellow and Peter, this volume) indicates that calcic minerals were destroyed by hydrothermal alteration.

The high-temperature, primary sulfide assemblage at BH is commonly overprinted by a later, lower temperature pyrite-(low-Fe)sphalerite-chalcopyrite-magnetite assemblage that probably formed at temperatures between 210° and 280°C, based on fluid inclusion trapping temperatures in low-Fe sphalerite (Peter et al., this volume). These temperatures overlap vent fluid temperatures of 184°–276°C at AAV and 264°C at BH (Goodfellow and Franklin, in press). The BH massive sulfide formed, therefore, from an earlier high-temperature, metalliferous fluid rather than lower-temperature, metal-poor fluids venting south of BH (Butterfield et al., this volume). Chlorite adjacent to mineralized veins in Zone Ia is commonly more Mg-rich than chlorite removed from the veins (Figs. 15A,B and 16), suggesting that the chalcopyrite + Mg-chlorite vein mineralization was produced by a later, lower-temperature hydrothermal fluid with a greater seawater component than the high-temperature fluid from which the quartz-Fe-chlorite-illite/muscovite assemblage precipitated.

Sediments in hydrothermal alteration zones surrounding the core (Zone Ia) are less intensely altered and brecciated. Unlike Zone Ia, where detrital plagioclase is destroyed, plagioclase in Zone IIa is altered to albite. Furthermore, higher Mg/Mg + Fe ratios for hydrothermal chlorite and illite/muscovite (Fig. 15) in Zone IIa is consistent with lower temperatures and greater interaction of Mg-bearing seawater with the upwelling hydrothermal fluid. Mixing between seawater and hydrothermal fluid is also indicated by the dominance of Mg-carbonates (dolomite, magnesite, and siderite; Fig. 17). High-Mg silicates (talc, serpentine, saponite, and chlorite) are also associated with massive sulfide and sulfide sediment in Holes 856G and 856H and are consistent with rapid mixing between hydrothermal fluid and seawater (Goodfellow et al., in press).

Zones IIIa and IVa in Holes 856A and 856B are characterized by anhydrite and calcite, respectively. The mineralogy of these zones is consistent with precipitation from entrained seawater that mixed with and was heated by outward-flowing hydrothermal fluid. The low sulfate content of end-member hydrothermal fluids (Von Damm, 1990; Lydon et al., 1992; Butterfield et al., this volume) indicates that all the sulfate was derived from entrained seawater, whereas a component of the Ca probably originated from the hydrothermal breakdown of plagioclase, detrital epidote, and biogenic calcite in Zones Ia and IIa (Goodfellow and Peter, in press). Fluid flow in Zones Ia and IIa is largely fracture controlled, whereas in Zones IIIa and IVa, it is focussed along permeable turbidites. As a result, the cross-stratal permeability in Zones IIIa and IVa is relatively low. The common occur-

Table 10. Electron microprobe data for sulfate minerals in hydrothermally altered hemipelagic and turbiditic sediment and interstitial to massive sulfide, Leg 139.

Site:	856D		856E		858A		858A		858A		858A	
Core, section:	1H-1		1H-1		15X-1		18X-1		20X-4		21X-1	
Interval (cm):	34-37		48-50		35-37		116-118		100-103		31-34	
Zone:	MS		MS		IVb		IVb		IVb		IVb	
Type:	Ba		Ba		An		An		An		An	
CaO	0.06	0.04	0.03	0.03	0.04	0.09	0.31	39.58	40.55	40.44	39.51	39.79
MgO	0.00	0.00	0.00	0.00	0.00	0.01	0.00	0.00	0.00	0.00	0.00	0.00
BaO	61.96	61.96	65.06	65.41	64.10	62.72	61.10	0.07	0.03	0.00	0.00	0.27
FeO	0.03	0.06	0.06	0.07	0.03	0.05	0.00	0.00	0.07	0.17	0.05	0.00
ZnO	0.29	0.00	0.02	0.00	0.00	0.00	0.00	0.05	0.00	0.00	0.03	0.00
SrO	3.17	3.03	2.05	1.17	1.91	2.54	3.64	0.18	0.06	0.14	0.11	0.15
MnO	0.06	0.00	0.00	0.00	0.00	0.06	0.00	0.01	0.02	0.03	0.00	0.00
SO ₃	31.90	35.13	34.77	34.57	34.82	34.55	34.63	59.51	60.47	60.92	58.60	60.57
SiO ₂	0.10	0.06	0.09	0.01	0.04	0.05	0.05	0.05	0.00	0.01	0.05	0.00
Total	97.55	100.29	102.06	101.25	100.94	100.05	99.74	99.47	101.13	101.60	98.45	100.90
Site:	858A		858A		858A		858A		858C		858C	
Core, section:	21X-3		24X-1		29X-1		29X-1		6H-4		12X-CC	
Interval (cm):	57-59		33-35		30-32		30-32		43-51a		8-10	
Zone:	IVb		IIIb		IIIb		IIIb		IIIb		IIIb	
Type:	An		An		An		An		An		An	
CaO	38.98	39.21	38.56	39.35	39.69	40.59	39.03	39.14	39.49	39.96	38.91	39.72
MgO	0.00	0.00	0.00	0.00	0.00	0.00	0.00	0.00	0.00	0.00	0.00	0.00
BaO	0.02	0.00	0.00	0.06	0.06	0.00	0.00	0.00	0.00	0.07	0.13	0.07
FeO	0.08	0.09	0.15	0.02	0.00	0.00	0.07	0.03	0.08	0.02	0.05	0.00
ZnO	0.22	0.05	0.00	0.00	0.02	0.09	0.08	0.00	0.21	0.00	0.00	0.02
SrO	0.09	0.18	0.11	0.13	0.00	0.00	0.06	0.08	0.08	0.14	0.18	0.31
MnO	0.00	0.03	0.00	0.00	0.00	0.00	0.02	0.00	0.06	0.00	0.02	0.05
SO ₃	61.10	60.76	60.49	60.92	59.51	59.57	58.04	58.63	58.28	58.15	49.95	58.82
SiO ₂	0.02	0.02	0.02	0.06	0.01	0.01	0.01	0.03	0.05	0.01	0.02	0.02
Total	100.50	100.34	99.33	100.54	99.29	100.26	97.30	97.91	98.25	98.34	89.25	99.00

Note: Ba = barite; An = anhydrite; MS = massive sulfide.

Table 11. Electron microprobe data for carbonate minerals hydrothermally altered hemipelagic and turbiditic sediment and interstitial to massive sulfide, Leg 139.

Site:	856G			856G			856G			856G			856H		
Core, section:	5R-1			6R-3			6R-3			7R-2			3R-1		
Interval (cm):	59–61			17–19			132–134			120–122			60–62		
Zone:	MS			MS			MS			MS			MS		
Type:	Ca	Si	Mg	Si	Do		Si	Do		Si	Do		Si	Do	
CaO	52.25	53.57	2.76	4.13	0.85	0.64	0.10	3.08	39.22	30.69	29.97	29.94	30.89	30.99	30.88
MgO	0.07	0.41	9.15	10.88	46.01	42.39	45.98	14.98	17.10	19.60	19.23	19.92	19.21	19.65	19.60
FeO	0.20	0.26	46.06	42.16	3.74	9.35	4.76	39.91	3.32	0.44	1.44	0.88	0.19	0.14	0.23
MnO	0.04	0.06	0.09	0.05	0.67	0.79	0.37	0.10	0.06	0.07	0.13	0.08	0.02	0.00	0.01
SrO	nd	nd	nd	0.06	0.07	0.00	0.05	0.05	0.00						
BaO	nd	nd	nd	0.07	0.00	0.01	0.08	0.02	0.04						
ZnO	0.00	0.04	0.00	0.02	0.09	0.00	0.00	0.07	0.05	0.05	0.00	0.05	0.00	0.00	0.04
SO ₃	nd	nd	nd	0.01	0.04	0.09	0.25	0.06	0.06						
Total	55.00	56.19	58.49	57.32	53.23	53.45	51.39	58.89	59.87	50.98	50.88	50.97	50.69	50.91	50.86
Ca	99.51	98.60	5.36	7.92	1.25	0.96	0.15	5.59	59.80	52.65	51.81	51.33	53.48	53.04	52.95
Mg	0.19	1.04	24.74	29.01	94.45	88.13	94.37	37.84	36.25	46.77	46.24	47.50	46.26	46.77	46.74
Fe	0.30	0.37	69.90	63.08	4.31	10.91	5.48	56.56	3.95	0.58	1.94	1.18	0.26	0.19	0.31

Site:	856H						856H						856H					
Core, section:	3R-2						3R-3						3R-3					
Interval (cm):	84–87						17–19						17–19					
Zone:	MS						MS						MS					
Type:	Do						Do						Do					
CaO	28.89	30.33	29.54	29.94	29.94	30.11	30.15	28.90	30.15	29.81	30.45	28.69	31.11	30.15	31.03	29.80	26.50	29.76
MgO	18.01	19.59	17.96	19.56	19.90	19.84	18.33	16.68	16.07	19.04	16.23	16.14	19.32	19.61	18.31	19.91	24.35	22.83
FeO	0.93	0.66	2.43	0.75	0.79	0.38	2.50	5.23	5.26	1.76	4.75	7.93	0.20	0.58	1.37	0.43	0.97	0.39
MnO	0.06	0.06	0.37	0.01	0.00	0.07	0.06	0.39	0.19	0.10	0.28	0.23	0.05	0.09	0.04	0.12	0.41	0.27
SrO	0.00	0.07	0.00	0.03	0.04	0.02	0.04	0.04	0.05	0.00	0.05	0.00	0.00	0.05	0.10	0.00	0.04	0.00
BaO	0.02	0.00	0.00	0.03	0.00	0.10	0.01	0.00	0.01	0.00	0.00	0.06	0.00	0.00	0.04	0.08	0.07	0.00
ZnO	0.02	0.06	0.15	0.00	0.26	0.04	0.09	0.05	0.00	0.06	0.03	0.00	0.00	0.00	0.03	0.00	0.10	0.00
SO ₃	0.11	0.00	0.02	0.13	0.02	0.06	0.12	0.01	0.05	0.08	0.03	0.10	0.23	0.11	0.07	0.00	0.02	0.01
Total	48.03	50.77	50.47	50.44	50.94	50.61	51.30	51.31	51.77	50.85	51.81	53.15	50.91	50.59	50.99	50.33	52.49	53.31
Ca	52.85	52.21	52.36	51.86	51.43	51.92	52.34	51.43	53.26	51.70	53.67	50.05	53.51	52.09	53.90	51.53	43.36	48.14
Mg	45.82	46.90	44.28	47.12	47.52	47.57	44.27	41.30	39.49	45.92	39.80	39.16	46.22	47.13	44.24	47.89	55.41	51.36
Fe	1.33	0.89	3.36	1.02	1.05	0.51	3.39	7.27	7.26	2.38	6.53	10.80	0.27	0.78	1.86	0.58	1.23	0.50

Table 11 (continued).

Site:	856H			856H			856H			857C			857C			857C			857C			857C																			
Core, section:	4R-2			4R-2			4R-3			6R-1			13R-1			22R-CC			28R-CC			38R-2			44R-1																
Interval (cm):	6-8			43-45			16-17			1-2			6-8			1-5			IVc			-			50-53																
Zone:	MS			MS			MS			IVc			IVc			Ca			Ca			IIIc			Ca																
Type:	Mg	Do	Do	Mg	Mg	Do	Do	Ca	Ca	Do	Ca	Ca	Do	Ca	Ca	Do	Ca	Ca	Do	Ca	Ca	Do	Ca	Ca	Do	Ca	Ca														
CaO	1.13	34.16	37.70	1.19	0.57	21.72	26.76	16.89	42.67	39.03	45.41	42.50	46.87	48.86	53.43	42.55	44.48	43.46	54.00	50.11	54.00	50.11	54.00	50.11	54.00	50.11															
MgO	45.34	24.28	19.21	43.64	37.85	15.15	15.68	23.94	1.49	1.26	0.20	0.12	0.16	0.43	0.00	0.46	0.14	0.18	0.00	0.21	0.00	0.21	0.00	0.21	0.00	0.21															
FeO	5.16	0.74	1.00	7.731	6.07	8.20	5.00	3.98	1.67	1.82	0.92	0.65	0.88	0.88	0.21	0.89	0.85	0.63	0.21	0.87	0.21	0.87	0.21	0.87	0.21	0.87															
MnO	0.08	0.32	0.12	0.27	0.36	1.29	1.30	1.20	1.17	1.15	0.92	1.03	0.87	0.55	0.21	0.67	0.14	1.90	0.60	0.64	0.00	0.00	0.00	0.00	0.00	0.00															
SrO	nd	nd	nd	nd	nd	0.05	0.01	0.03	0.01	0.00	0.03	0.11	0.04	0.01	0.00	0.02	0.05	0.00	0.00	0.05	0.03	0.10	0.02	0.09	0.00	0.00															
BaO	nd	nd	nd	nd	nd	0.08	0.05	0.11	0.02	0.00	0.00	0.00	0.00	0.01	0.00	0.05	0.00	0.00	0.00	0.00	0.00	0.00	0.00	0.00	0.00	0.00															
ZnO	0.04	0.04	0.05	0.03	0.00	0.00	0.00	0.00	0.04	0.07	0.03	0.11	0.05	0.00	0.00	0.03	0.00	0.00	0.03	0.00	0.00	0.00	0.10	0.08	0.00	0.08															
SO ₃	nd	nd	nd	nd	nd	0.07	0.07	0.06	0.09	0.13	0.02	0.03	0.02	0.08	0.00	0.04	0.03	0.05	0.00	0.03	0.10	0.02	0.09	0.00	0.00	0.08	0.00														
Total	51.83	59.69	58.18	52.97	56.07	46.86	49.31	46.38	48.38	44.58	54.49	48.04	52.15	51.69	54.50	53.20	50.70	47.99	56.71	53.57	54.00	50.11	54.00	50.11	54.00	50.11															
Ca	1.65	49.86	57.83	1.76	0.87	44.15	51.00	31.69	92.66	92.49	97.87	98.42	98.09	97.45	99.69	96.94	98.09	98.31	99.69	98.10	99.69	98.10	99.69	98.10	99.69	98.10	99.69	98.10													
Mg	92.45	49.30	40.98	89.36	80.06	42.84	41.56	62.48	4.50	4.15	0.59	0.40	0.48	1.19	0.00	1.47	0.44	0.57	0.00	0.57	0.00	0.57	0.00	0.57	0.00	0.57	0.00	0.57													
Fe	5.90	0.84	1.19	8.89	19.07	13.01	7.44	5.84	2.84	3.37	1.54	1.18	1.43	1.36	0.31	1.59	1.47	1.12	0.31	1.33	0.31	1.33	0.31	1.33	0.31	1.33	0.31	1.33													
Site:	858A			858A			858A			858A			858A			858A			858A			858B																			
Core, section:	5H-2			5H-6			9X-2			12X-CC			15X-1			25X-1			2H-3			50-52			MS																
Interval (cm):	2-4			40-45			38-42			11-13			35-37			IVb			IIIb			29-32			Do																
Zone:	Vb			Vb			Ca			Vb			Ca			Ca			Ca			Ca			Ca																
Type:	Ca			Ca			Ca			Ca			Ca			Ca			Ca			Ca			Ca																
CaO	40.59	49.88	50.25	50.47	44.84	47.27	49.34	54.88	53.45	52.64	52.83	49.25	50.52	52.53	53.15	51.89	53.10	53.06	53.84	29.17	28.03	54.00	53.84	29.17	28.03	54.00	53.84	29.17	28.03												
MgO	1.06	0.12	0.19	0.00	0.38	0.24	0.00	0.00	0.00	0.00	0.00	1.13	1.98	0.29	0.00	0.33	0.00	0.01	0.002	1.162	0.26	0.00	0.002	1.162	0.26	0.00	0.002	1.162	0.26												
FeO	1.77	0.59	0.92	0.98	1.68	1.21	0.67	0.16	0.37	0.55	0.60	0.55	0.39	0.36	0.41	0.30	0.10	0.32	0.15	0.16	3.77	0.15	0.16	3.77	0.15	0.16	3.77	0.15	0.16	3.77											
MnO	1.31	1.62	2.20	2.45	1.91	2.12	1.48	0.05	0.39	0.79	0.69	0.60	0.49	0.82	0.80	1.58	0.28	0.80	0.27	0.12	0.45	0.27	0.12	0.45	0.27	0.12	0.45	0.27	0.12	0.45											
SrO	0.00	0.00	0.00	0.00	0.00	0.06	0.00	0.00	0.03	0.03	0.00	0.13	0.00	0.03	0.00	0.00	0.00	0.02	0.00	0.05	0.02	0.00	0.05	0.02	0.00	0.05	0.02	0.00	0.05												
BaO	0.07	0.03	0.00	0.00	0.10	0.04	0.04	0.00	0.13	0.00	0.03	0.00	0.00	0.00	0.00	0.16	0.00	0.06	0.03	0.27	0.00	0.06	0.00	0.00	0.27	0.00	0.00	0.00	0.00	0.00											
ZnO	0.06	0.00	0.00	0.00	0.04	0.02	0.00	0.10	0.00	0.12	0.00	0.00	0.00	0.00	0.00	0.00	0.00	0.05	0.24	0.00	0.08	0.06	0.10	0.00	0.05	0.24	0.00	0.08	0.06	0.10	0.00	0.05									
SO ₃	0.04	0.00	0.01	0.04	0.00	0.00	0.04	0.06	0.05	0.10	0.10	0.22	0.16	0.23	0.06	0.07	0.03	0.07	0.03	0.07	0.00	0.05	0.07	0.00	0.05	0.07	0.00	0.05	0.07	0.00	0.05										
Total	50.98	54.07	53.58	53.95	55.05	53.44	53.44	55.66	55.36	55.50	54.64	53.47	54.64	55.10	54.75	54.51	53.59	54.73	54.41	50.83	52.78	54.00	53.84	50.83	52.78	54.00	53.84	50.83	52.78	54.00	53.84										
Ca	93.42	98.77	98.08	98.50	96.07	97.37	98.96	99.78	99.47	99.19	99.12	96.10	94.31	98.72	99.41	98.69	99.86	99.51	99.78	49.68	47.38	99.51	99.78	49.68	47.38	99.51	99.78	49.68	47.38	99.51	99.78	49.68	47.38								
Mg	3.40	0.33	0.51	0.00	1.12	0.69	0.00	0.00	0.00	0.00	0.00	3.06	5.13	0.76	0.00	0.87	0.00	0.02	0.00	50.11	47.64	0.00	0.02	0.00	0.00	0.02	0.00	0.00	0.00	0.02	0.00	0.00	0.02	0.00	0.00	0.02	0.00	0.00			
Fe	3.17	0.90	1.41	1.50	2.81	1.94	1.04	0.22	0.53	0.81	0.88	0.84	0.57	0.53	0.59	0.45	0.14	0.47	0.22	0.21	4.97	0.00	0.47	0.22	0.21	4.97	0.00	0.47	0.22	0.21	4.97	0.00	0.47	0.22	0.21	4.97	0.00	0.47	0.22	0.21	4.97

Table 11 (continued).

Site:	858B				858C				858C				858C			
	2H-3	2H-5	3H-2	10-15	Vb	Vb	110-115	Vb	SH-CC	7-10	Vb	IVb	Do	SH-CC	6H-4	43-51a
Core, section:	50-52	32-34	Vb	Vb	Vb	Vb	Vb	Vb								
Interval (cm):																
Zone:																
Type:																
CaO	27.97	23.47	27.26	53.50	53.55	53.41	47.88	52.67	54.16	53.80	29.66	30.51	32.24	26.49	26.99	28.47
MgO	20.12	17.21	19.79	0.15	0.00	0.00	0.23	0.19	0.33	0.42	19.71	19.02	18.68	21.75	21.35	21.94
FeO	3.76	4.48	3.31	0.02	0.07	0.14	0.17	0.00	0.10	0.15	0.00	0.13	0.54	0.36	0.19	0.19
MnO	0.39	0.29	0.21	0.09	0.08	0.53	0.71	0.50	0.39	0.25	1.14	0.83	1.01	0.60	0.63	0.96
SiO ₂	0.01	0.01	0.04	0.03	0.12	0.03	0.01	0.00	0.02	0.00	0.05	0.01	0.04	0.04	0.03	0.02
BaO	0.00	0.00	0.08	0.01	0.04	0.00	0.00	0.00	0.06	0.06	0.00	0.10	0.15	0.14	0.00	0.05
ZnO	0.13	0.58	0.31	0.11	0.20	0.00	0.00	0.00	0.00	0.00	0.00	0.04	0.13	0.07	0.04	0.01
SO ₃	0.17	0.08	0.36	0.08	0.08	0.03	0.10	0.07	0.04	0.02	0.33	0.35	0.11	0.13	0.13	0.13
Total	52.56	46.34	51.72	53.98	54.13	54.14	50.26	53.42	55.03	54.70	51.14	50.83	52.78	50.95	49.89	52.12
Ca	47.50	46.11	47.52	99.58	99.90	99.80	99.05	99.51	99.16	98.80	51.86	53.56	55.28	46.34	47.37	48.15
Mg	47.52	47.02	47.97	0.39	0.00	0.00	0.67	0.49	0.84	0.06	47.93	46.44	44.55	52.91	52.13	51.61
Fe	4.98	6.87	4.50	0.03	0.10	0.20	0.27	0.00	0.00	0.14	0.21	0.00	0.17	0.74	0.50	0.25

Note: Ca = calcite; Do = dolomite; Mg = magnesite; Si = siderite; MS = massive sulfide; nd = not determined.

rence of carbonate concretions in or near turbiditic sediments indicates that fluid flow occurred along permeable strata in Zone IVa.

Although Zone Ia is adjacent to a mafic sill (of unknown thickness), the high-temperature alteration is not related to the intrusion of the sill. The sediments immediately adjacent to the sill in Zone Ia-2 (e.g., Sample 139-856B-15X-CC, 20–22 cm) are less intensely altered than those in Zone Ia-1 with albite present in Zone Ia-2 but not in Zone Ia-1. The geochemistry of these subzones supports this interpretation (Goodfellow and Peter, this volume). The sediments in Zone Ia-2 are distinct in containing Mg-smectite (Table 2) and having high MgO contents (Goodfellow and Peter, this volume). Thus, sill intrusions postdate the high-temperature alteration in Hole 856B. A sill was also intersected at the base of Hole 856A, but at this site, no high-temperature alteration such as in Zone Ia is observed.

Area of Active Venting (Site 858)

The AAV (Site 858) is an active hydrothermal system with fluid temperatures up to 276°C (Davis, Mottl, Fisher, et al., 1992). The AAV is a lower-temperature hydrothermal system than Bent Hill and is lacking in extensive sulfide mineralization (Goodfellow and Franklin, in press). Temperatures of minerals precipitated near the center of fluid upflow are well constrained by fluid inclusions (Peter et al., this volume) and direct measurements of vent fluids (Goodfellow and Franklin, in press). Hydrothermal minerals at AAV are zoned laterally and vertically about the core of the fluid upflow zone (Fig. 18). Heat flow values (Davis and Villinger, 1992) and pore water compositions (Lydon et al., 1990; Butterfield et al., this volume) are similarly zoned about these hydrothermal vents.

The core of the AAV discharge conduit (Zone Ib) is characterized by highly indurated, brecciated, fractured and veined sediments in Holes 858D and 858F. The hydrothermal mineralogy consists of quartz-wairakite-epidote ± plagioclase-pyrite. Fluid inclusion measurements show that wairakite in Zone Ib formed at temperatures between 250° and 300°C (Peter et al., this volume). These temperatures are consistent with field studies that show wairakite to be stable between 200° and 320°C (Schiffman et al., 1985). Experimental studies (Seyfried et al., 1991) also indicate that AAV feldspar probably formed at temperatures <325°C.

The occurrence of anhydrite veins and concretions in Zones Ib and IIb in Hole 858F suggests that hydrothermal fluid conditions fluctuated temporally and spatially at AAV. The occurrence of high-temperature anhydrite (230° and 311°C; Peter et al., this volume) below 236 mbsf in Hole 858A indicates that seawater was entrained into the core of the upflow zone and rapidly heated by hydrothermal fluid (Lydon et al., 1992). The occurrence of wairakite at 21.3 mbsf in Hole 858C near carbonate concretions that formed between 110° and 250°C (Zone Vb, 15–17 mbsf; Peter et al., this volume) is additional evidence for fluctuating hydrothermal conditions.

The core of the upflow zone at AAV (Zone Ib) is surrounded by quartz-epidote-chlorite (Zone IIb). Although the sediments in this zone are brecciated and fractured, the hydrothermal alteration is more pervasive, with epidote comprising up to 20 vol%. The coarse-grained nature of this epidote suggests temperatures up to 300°C (Schiffman et al., 1985). The chlorite is somewhat more Mg-rich than chlorite from the high-temperature zone at Site 856 (Zone Ia and IIa; Figs. 15B and 16), indicating alteration by a mixed seawater and hydrothermal fluid (Goodfellow and Peter, this volume). Zone IIIb (albite-chlorite-pyrite), IVb (anhydrite-illite-pyrite), and Vb (calcite-illite-pyrite) indicate progressively lower temperatures and intensity of hydrothermal alteration and are consistent with the mixing of entrained seawater with outward migrating hydrothermal fluid (Goodfellow and Peter, this volume). The temperatures of these zones are partly constrained from fluid inclusion temperatures ranging from 230° to 280°C for Zone IIIb and from 112° to 247°C for Zones IVb and Vb (Peter et al., this volume). The temperatures for Zones IVb and Vb are consistent with temperatures estimated from oxygen isotope data (Goodfellow et al., in press).

Table 12. Summary of downhole mineralogy, Leg 139.

Core, section, Interval (cm)	Grain size	Depth (mbsf)	Detrital										Hydrothermal/Authigenic												
			Qz	Fs	Clay	Micas	Ch	Ep	Mag	M-F	F-py		Qz	Ta	Carb	Wa	Ep	Ru	Sn	Ba	An	Py	Mr	Po	Cp
139-858A-																									
1H-2, 5-7	Silty clay	1.55	xxx	xx	xxxxx	xxx	xx		x	xx	x											x			
2H-1, 125-127	Silty clay	3.65	xxx	xx	xxxxx	xx	x		x	xx	x											x			
2H-7, 57-59	Silty clay to silt	11.97	xxxx	xx	xxxxx	xxx	xxx	xxx	x	x	x											x			
3H-4, 29-33	Silty clay	16.46	xxxx	xx	xxxxx	xxx	xx	x	x	x	x											x			
4H-6, 48-50	Silty clay	29.38	xxx	xx	xxxxx	xx	xx		x		x											x			x
5H-2, 2-4	Silty clay to clayey silt	32.42			xxx				x		xxx											x			
5H-4, 27-30	Silt	35.67	xxxx	xx	xxx	xx	xxx	xx														xxxx			xx
5H-6, 40-45	Silty clay	38.80			xxx	x	x															xxxx			
5H-CC, 10-11	Silt				xxxx	x	x															xxxx			x
6H-3, 77-79	Silty clay and silt	44.17	xxxx	xx	xxxxx	xx	xx	x	x	x	x											x			
8H-2, 31-33	Silt to silty clay	60.64	xxxx	xx	xxxxx	x	xxx	x	x	x	x											x			x
9X-2, 38-40	Silt to silty clay	64.38	xxx	x	xxxxx	xxx	xx	x	x	x	x											x			x
9X-4, 52-56	Silty clay	67.52	xxx	xx	xxxxx	xx	x	x	x	x	x											x			x
11X-CC, 10-12	Sandy siltstone	73.57	xxxx	xx	xxxxx	xx	x	xx	x	x	x											x			x
12X-CC, 11-13		81.91	x		xxx	x																xxxx			x
15X-1, 35-37	Sandstone	110.95	xxxx	xx	xxxxx	x	xx	x		x												x	x	x	x
16X-1, 38-40	Claystone	120.68	xxx	xx	xxxxx		?															x		xx	
18X-1, 116-118	Silty claystone	140.76	xxx	xx	xxxxx	xx	x															x	x	x	x
18X-2, 109-111	Silty claystone	142.19	xxx	xx	xxxxx	xxx	xx														x	x	x	x	
18X-3, 14-16	Silty claystone	142.74	xxx	xx	xxxxx	xxx	xx		x		x										x	x	x	x	
19X-1, 28-30	Silty claystone	149.58	xxx	x	xxxxx	xxx	?														x		x		
20X-1, 62-64	Silty claystone	159.62	xxx	?	xxxxx	xxx	?															x			x
20X-3, 39-41	Sandstone	162.32	xxxx	xx	xxxxx	xx	xxx															x	xxx	x	x
20X-4, 100-103	Silty claystone	164.44	xxx	xx	xxxxx	xxx	xx		x		x										x	x	x	x	
21X-1, 117-120	Silty claystone	169.77	xxx	xx	xxxxx	xxx	xx		x		x										x	x	x	x	
21X-2, 31-34	Silty claystone	170.41	xxx	xx	xxxxx	xxx	xx														x	x	x	x	
21X-3, 57-59	Siltstone	171.98	xxxx	x	xxxxx	xxx	xx														x	x	x	x	
24X-1, 33-35	Siltstone	197.93	xxx	xx	xxxxx	xx	?		x		x										x	x	x	x	
24X-1, 72-74	Silty claystone	198.32	xxx	xx	xxxxx	xxx	xx		x		x										x	x	x	x	
25X-1, 29-32	Siltstone	207.59	xxx	xx	xxxxx	xxx	xx					x									x			x	
27X-1, 33-35	Siltstone	226.93	xxxx	xx	xxxxx	xxx	xx					x									x			x	
28X-CC, 4-5	Siltstone	236.24	xxxx	xx	xxxxx	xx	xx														v	x	x	x	
29X-1, 30-32	Sandstone	246.20	xxxx	xx	xxxxx	xx	xx														v-x	x	x	x	
30X-1, 67-70	Silty claystone	256.27	xxxx	xx	xxxxx	xxx	xx					x									x			x	
31X-1, 65-67	Silty claystone	265.95	xxxx	xx	xxxxx	xxx	xx					x									x			x	
139-858B-																									
1H-2, 50-54	Silty clay	2.00	xxx	xx	xxxxx	xxx	xx																		
2H-3, 50-52	Sand	10.70																							
2H-5, 16-18	Silt to silty clay	13.36	xxx	xx	xxxxx	xxx	xx	x													x	x	x	x	
2H-6, 69-71	Silty clay	15.39	xxx	xx	xxxxx	xxx	xx	x													x	x	x	x	
139-858C-																									
2H-5, 32-34	Silty clay	9.82			xxx																				
2H-7, 15-17	Silty clay	12.65	xxx	xx	xxxxx	xxx	?	x		xx											x	x	x	x	
3H-1, 78-81	Siltstone	13.78	xx	x	xxxxx		xx																		
3H-2, 10-15	Silty clay	14.60	xx	x	xxxxx		x																		
3H-2, 54-57	Silt to sand	15.04			xxx																				
3H-2, 110-115	Silt to sand	15.60			xxxxx	x	xxx																		
3H-2, 124-126	Silt to sand	15.74			xxx	x	xx																		
3H-3, 38-41	Silt to silty clay	16.38																							
3H-3, 107-109	Silt	17.07	xxxx	xx	xxxxx	xx																			
3H-6, 86-89	Silt	21.36	xxxx	xx	xxxxx	xxx	x	x													xx	xx	x	x	
5H-1, 122-124	Silty clay	24.72	xxx	xx	xxxxx	xxx	?	xx													x				
5H-3, 5-7	Silty clay	26.55	xxxx	xx	xxxxx	xxx	x	xx													v-xx				
5H-3, 61-63	Silty clay	27.11	xxxx	x	xxxxx	xxx	x	xx													xx				
5H-CC, 7-10	Silt	33.20	xxxxx	xx	xxx	xxx	xx	xx													xx				
6H-1, 80-82	Sandy-siltstone	33.80	xxxxx	xx	xxxxx	xxx	x	xx													x		x	x	
6H-2, 75-77	Silty clay	35.25	xxxx	xx	xxxxx	x	?	x													x		x	x	
6H-4, 43-51	Silty-clay	37.93	x	x	xxx																v	x	x	x	

Table 12 (continued).

Core, section, Interval (cm)	Grain size	Depth (mbsf)	Detrital									Hydrothermal/Authigenic														
			Qz	Fs	Clay	Micas	Ch	Ep	Mag	M-F	F-py	Qz	Ta	Carb	Wa	Ep	Ru	Sn	Ba	An	Py	Mr	Po	Cp	Sp	
6H-5, 76–79	Silty claystone	39.76	xxxx	xxx	xxxxx	xxx	xx	x													x		x			
7H-1, 90–92	Silty clay + sandy silt	42.40	xxx	xxx	xxxxx	xxx	xx									x					x					
11X-1, 33–35	Clayey siltstone	54.83	xxxx	xxx	xxxxx	xx	x					x									x					
12X-1, 42–45	Siltstone	64.20	xxxx	xxx	xxxxx	x	xx	x				x									x					
12X-CC, 8–10	Sand to silt	68.14	xxxx	xxx	xxxxx	xx	xx	xx												xx	x					
13X-1, 25–28	Silty clay	73.95	xxxx	xx	xxxxx	x	xx	x												x		x				
139-858D-																										
1H-1, 115–119	Silty clay	1.15	xxx	xxx	xxxxx	xxx	xx	x				xxx	x				xx				xxx					
2H-3, 34–36	Silty clay	12.64	xxx	xxx	xxxxx	xx	xx					x				x				xx		x				
2H-CC, 10–12	Silty clay	18.92	xxx	xx	xxxxx	xxx	xx													xx	xx		x			
139-858F-																										
2R-CC, 7–10	Siltstone	27.87	xxx	xxx	xxxxx	x	?					v				v					v-x					
4R-CC, 8–10	siltstone to sandstone	46.58	xxxxx	xxx	xxxxx	x	xx									xxxx	xxxx	xx	xx							
9R-CC, 9–11	Sandstone	94.29	xxxx ^a	xxx	xxxx	x	xx													x						
14R-1, 10–12	Siltstone	142.70	xxxx	xxxx	xxxxx	xx	xx													x						
18R-1, 14–16	Siltstone	181.44	xxxx	xxx	xxxxx	x	xx													v	x					
23R-CC, 3–5	Sandstone	229.63	xxxxx	?	xxxx	xx						x					xxxx				x					
25R-1, 9–11	Claystone	248.99	xxx	x	xxxxx	x	xx					x				x				xx		x				
25R-1, 71–73	Claystone	249.61	xxx	x	xxxxx	xx	xx					x				x				xxxx	xxx	xx				

Notes: xxxx = dominant (>50%); xxxx = major (11–50%); xxx = minor (3–10%); xx = trace (1–2%); x = rare (%); v = vein. Qz = quartz; Fs = feldspar; Ch = chlorite; Carb = carbonate; An = anhydrite; Wa = wairakite; Ep = epidote; Mag = magnetite; M-f = microfossils; F-py = frambooidal pyrite; Ba = barite Py = pyrite; Mr = marcasite; Po = pyrrhotite; Cp = chalcopyrite; Sp = sphalerite; Ru = rutile; Sn = sphene.

^a Probably authigenic plagioclase; see text.

Table 13. Electron microprobe data for wairakite in veins and hydrothermally altered turbiditic sediment, Holes 857D and 858F.

Site:	857D				857D				857D				858F				858F				858F				
Core, section:	6R-1		14R-1		22–25		17R-2		53–55		2R-CC		8–11		9R-CC		9–11		lb		18R-1		14–16		
Interval (cm):	20–22																								
Zone:	Ic		lb		lb		lb		lb																
SiO ₂	54.423	55.221	53.514	54.060	53.142	54.650	54.772	52.695	53.596	52.877	55.209	54.950	55.076	55.690	55.795	55.737	55.660	55.234	54.250						
Al ₂ O ₃	22.679	23.450	22.994	22.945	22.497	22.524	22.921	21.683	21.906	22.099	22.358	22.118	22.577	22.103	22.450	22.951	22.582	21.664	22.116						
FeO	0.028	0.004	0.000	0.005	0.076	0.090	0.072	0.000	0.010	0.000	0.027	0.030	0.023	0.014	0.032	0.001	0.076	0.109	0.000						
CaO	12.670	12.822	12.455	12.637	11.685	12.143	12.135	11.668	12.034	11.945	11.803	11.974	12.415	11.865	12.269	11.952	11.750	11.177	11.101						
Na ₂ O	0.027	0.032	0.050	0.065	0.395	0.418	0.373	0.344	0.352	0.272	0.555	0.566	0.231	0.523	0.495	0.538	0.774	0.917	0.821						
K ₂ O	0.014	0.018	0.000	0.017	0.012	0.014	0.011	0.011	0.016	0.006	0.011	0.008	0.002	0.012	0.027	0.030	0.034	0.023	0.011						
Total	89.841	91.547	89.013	89.729	87.807	89.839	90.284	86.401	87.914	87.199	89.963	89.646	90.324	90.207	91.068	91.209	90.876	89.124	88.299						
Ca/Ca + Na	0.996	0.996	0.993	0.991	0.942	0.941	0.947	0.949	0.950	0.960	0.922	0.921	0.967	0.926	0.932	0.925	0.893	0.871	0.882						
Si	32.134	31.994	31.892	31.973	32.077	32.259	32.158	32.308	32.322	32.148	32.482	32.478	32.314	32.657	32.470	32.349	32.447	32.782	32.488						
Al	15.787	16.017	16.155	15.999	16.009	15.675	15.865	15.673	15.575	15.840	15.508	15.412	15.616	15.281	15.403	15.704	15.520	15.158	15.614						
Fe	0.014	0.002	0.000	0.002	0.038	0.044	0.035	0.000	0.005	0.000	0.013	0.015	0.011	0.007	0.016	0.000	0.037	0.054	0.000						
Ca	8.016	7.960	7.953	8.009	7.558	7.680	7.634	7.665	7.776	7.782	7.441	7.583	7.805	7.455	7.651	7.433	7.339	7.108	7.123						
Na	0.031	0.036	0.058	0.075	0.462	0.478	0.425	0.409	0.412	0.321	0.633	0.649	0.263	0.595	0.559	0.605	0.875	1.055	0.953						
K	0.011	0.013	0.000	0.013	0.009	0.011	0.008	0.009	0.012	0.005	0.008	0.006	0.001	0.009	0.020	0.022	0.025	0.017	0.008						

Note: Formula proportions based on 96 (O).

Table 14. Summary of downhole mineralogy for Holes 857A, 857C, and 857D.

Core, section, interval (cm)	Grain size	Depth (mbsf)	Detrital										Hydrothermal/Authigenic							
			Qz	Fs	Clay	Micas	Ch	Hb	Ep	Mag	M-f	F-py	Qz	Ch-II	Carb	Wa	Ep	Sn	Py	Po
139-857A-																				
1H-4, 46–50	Silty clay	6.86	xxxx	xxx	xxxxx	xx	xx	xx	x	x	x	x							x	
2H-3, 125–127	Silty clay	15.65	xxx	xxx	xxxxx	xx	xx	xx	x	x	xxx	xxx		xxxx					x	
4H-4, 25–29	Silty clay	26.65	xxx	xxx	xxxxx	xxx	xx	xx	x	x	x	x		xx					x	
6H-5, 89–93	Silt	47.79	xxxx	xxx	xxxxx	xxx	xx	xxx	xx	x	x	x		xxx					x	x
7H-6, 109–113	Silty clay	56.77	xxxx	xxx	xxxxx	xx	xxx	xx	x	x	x	x		xx					x	
8H-7, 3–7	Silty clay	68.93	xxxx	xxx	xxxxx	xx	xx	x	x	x	x	x		x				x	x	
9H-7, 53–55	Clayey silt		xxxx	xxx	xxxxx	xx	xxx	xx	x	x	x	x		x				x	x	
10H-4, 77–79	Silty sand	84.17	xxxx	xxx	xxxxx	x	xx	x	x	x	x	x		xx				x	x	
11X-CC, 26–28	Silty clay	87.33	xxx	xx	xxxxx	x	xx	x	x	x	x	x		xxxxx						
13X-1, 25–27	Silty clay	101.75	xxxx	xxx	xxxxx	x	xx	x	x	x	x	x								
13X-1, 91–93	Silty clay	102.41	xxxx	xxx	xxxxx	x	xx	x	x	x	x	x		xxx			x	x		
139-857C-																				
3R-3, 110–112	Silty clay	70.60	xxxx	xxx	xxxxx	xxx	xxx		x	x	xx	x		x					x	
6R-1, 1–2	Silty claystone	86.21	xxx	xx		x	x		x	x	x	x		xxxxx						
7R-CC, 1–2	Clayey silt	95.21	xxx	xxx		x	xx	x	x	x	x	x		xxxxx						
9R-1, 8–9	Siltstone	114.58	xxx	x			xx	x	x	x	x	x		xxxxx						
13R-1, 6–8	Siltstone	153.16	xxxx	xxx	xxxxx	x	xxx	x	x	x	x	x		xxxxx						
13R-3, 52–54	Clayey silt	156.62	xxxx	xxx	xxxxx	x	xx	x	xx	x	x	x		xxx			x			
15R-1, 147–149	Silty clay	173.97	xxxx	xxx	xxxxx	xx	xx	x	x	x	x	x		xxxxx			x			
17R-2, 61–65	Sandy/silty clay	194.01	xxx	xx	xxxxx	xx	x	x	x	x	x	x		xx			x			
21R-1, 24–026	Silty claystone	230.84	xxxx	xxx	xxxxx	xxx	xx	x	xx	x	x	x		xx			x	x		
21R-3, 27–29	Silty claystone + siltstone	233.87	xxxx	xxx	xxxxx	xxx	x	x	x	x	x	x								
22R-1, 28–32	Silty claystone	240.58	xxxx	xxx	xxxxx	xx	x	x	x	x	x	x		x						
22R-CC, 1–5	Silty claystone	242.01	xxx	xx	xxxx	xx	x	x	x	x	x	x		xxxxx			x			
24R-1, 31–35	Silty claystone	259.51	xxxx	xxx	xxxxx	xxx	x	x	xxx	x	x	x		xxx			x			
25R-1, 6–8	Silty claystone	268.86	xxxx	xx	xxxxx	xx	x	x	x	x	x	x		xx			x			
28R-2, 119–122	Silty claystone	296.49	xxx	xx	xxxxx	xxx	x	x	x	x	x	x		xx			x			
28R-CC, -	Sandy silt		xxxx	xxx	xxx	xxx	xx	x	x	x	x	x		xxxxx						
30R-1, 116–120	Silty clay + sandy silt	314.26	xxxx	xxx	xxxxx	xx	xx	x	x	x	x	x		xxx						
31R-1, 121–123	Silty claystone	323.91	xxx	xx	xxxxx	xx	xx	x	x	x	x	x		x			x			
31R-2, 15–17	Silty claystone	324.35	xxxx	xxx	xxxxx	xx	x	x	x	x	x	x		xx			x			
32R-1, 34–37	Silty claystone to sandy siltstone	327.94	xxxx	xx	xxxxx	xx	x	x	xx	x	x	x								
33R-1, 56–59	Silty claystone	332.96	xxxx	xxx	xxxxx	xxx	x	x	xxx	x	x	x		xxx			x			
33R-3, 65–68	Silty claystone	336.05	xxxx	xx	xxxxx	xx	x	x	xxx	x	x	x		xx			x			
34R-1, 120–122	Siltstone	337.70	xxxx	xx	xxxxx	xx	xx	x	x	x	x	x		xx						
34R-3, 44–47	Silty claystone	339.94	xxxx	xxx	xxxxx	xx	xx	x	x	x	x	x		xx						
36R-3, 58–61	Silty claystone to siltstone	349.68	xxxx	xx	xxxxx	xx	xx	x	x	x	x	x		xx						
37R-1, 115–119	Silty claystone to siltstone	351.95	xxxx	xxx	xxxxx	xx	x	x	x	x	x	x		xx			x			
38R-2, 50–53	Silty claystone to siltstone	357.80	xxxx	xx	xxxxx	xx	x	x	x	x	x	x		xx						
39R-1, 66–68	Silty claystone to siltstone	361.06	xxxx	xx	xxxxx	xx	x	x	x	x	x	x		xx			x			
39R-3, 62–65	Siltstone	364.02	xxxx	xxx	xxxxx	xx	xx	x	x	x	x	x		xx			x			
41R-2, 122–126	Silty claystone + sandy siltstone	377.62	xxxx	xxx	xxxxx	xx	x	x	x	x	x	x		xx			x			
42R-2, 37–41	Siltstone	381.57	xxxx	xx	xxxxx	xx	xx	x	x	x	x	x		xx						
43R-3, 77–81	Silty claystone	388.47	xxxx	xx	xxxxx	xx	x	x	x	x	x	x		xx						
44R-1, 137–140	Siltstone to silty claystone	391.07	xxxx	xxx	xxxxx	xx	x	x	xx	x	x	x		xx			x			
45R-1, 134–138	Siltstone + silty claystone	395.64	xxxx	xx	xxxxx	xx	xx	x	x	x	x	x		xx			x			
45R-2, 79–81	Silty claystone	396.59	xxxx	xx	xxxxx	xx	x	x	x	x	x	x		xx			x			
46R-1, 71–75	Silty claystone	399.71	xxxx	xx	xxxxx	xx	x	x	x	x	x	x		xx			x			
53R-1, 50–52	Silty claystone	433.30	xxxx	xx	xxxxx	xx	x	x	xx	x	x	x								
55R-1, 24–26	Siltstone	442.24	xxxx	xxx	xxxxx	xx	xx	x	xx	x	x	x		xx			x			
61R-1, 129–131	Sandstone	491.79	xxxx	xxx	xxx		xxxxx		xxx								xx	xxx		
139-857D-																				
1R-1, 137–139	Siltstone	582.87	xxxxx	xxx	xxx	xx					v			xx	xx	x				
4R-2, 75–77	Siltstone	611.15	xxxx	xxx	xxxxx	x				v			x	v-xxx	xxx	v-x				
5R-1, 26–28	Silty claystone	618.86								v-xxxx	xxxxx		v-xxxx	xx	v	v		v		
6R-1, 20–22	Siltstone	628.10	xxxx?		xxxx					v			v	v-xxx					xxx-v	
14R-1, 22–25	Silty claystone		xxxx	xxx	xxxxx	x				v			v	xxx	xxx	x				
15R-1, 74–76	Silty claystone	715.54	xxxx	xxx	xxxxx	x				v			v	xxx	xxx	x				

Table 14 (continued).

Core, section, interval (cm)	Grain size	Depth (mbsf)	Detrital												Hydrothermal/Authigenic						
			Qz	Fs	Clay	Micas	Ch	Hb	Ep	Mag	Mf	F-py	Qz	Ch-II	Carb	Wa	Ep	Sn	Py	Po	Cp
16R-1, 53–55	Silty claystone	725.03	xxxx	xxxx	xxxx	xx	x						xxx	xxx	xx						
17R-1, 34–36	Sandstone	734.24	xxxx	xxxx	xxxx	xx	xx						xxx	xxx	xx						
17R-1, 146–148	Silty claystone	735.36	xxxx	xxxx	xxxx	xx	x						xxx	xxx	x	x					
17R-2, 10–13	Siltstone	735.50	xxxx	xxxx	xxxx	xx	x						v	v-xxx	xx	v					
17R-2, 53–55	Sandstone	735.93	xxxx	xxxx	xxxx	xx	x						v	v	xx	xx					
17R-3, 23–25	Sandstone	737.07	xxxxx	xx									xxx	xxx	xx	xx					
21R-1, 140–143	Silty claystone	773.60	xxxx	xxxx	xxxx	x	xx						xx	xx	xx	xx					
21R-2, 14–16	Sandy siltstone	773.84	xxxx	xxxx	xxxx	xx	x						xxx	xxx	x						
28R-1, 67–69	Sandstone	839.57	xxxx	xxxx	xxxx	x							xxxx	xxxx	x						
34R-1, 23–25	Silty claystone to siltstone	859.13	xxxx	xxxx	xxxx	x	x						xx	xx	x	x					
34R-1, 87–89	Sandstone	898.37	xxxxx	xxx									v-xxxx	v-xxxx	x	x					
37R-1, 38–40	Siltstone + sandstone	926.88	xxxx	xxx	xxxx	xx	xx						xxx	xxx	xx	xx					

Notes: xxxx = dominant (50%); xxxx = major (11–50%); xxxx = minor (3–10%); xx = trace (1–2%); x = rare (%); v = vein; F-py = pyrite; F-s = feldspar; Hb = hornblende; Ch = chlorite; Carb = carbonate; Wa = wairakite; Ep = epidote; Sn = sphene; Mag = magnetite; Mf = microfossils; F-py = frambooidal pyrite; Py = pyrrhotite; Po = pyrite; Cp = chalcopyrite.

The pattern of mineral zonation outward from the core of the upflow system is reflected in sediment compositions (Goodfellow and Peter, this volume) and Sr isotope compositions (Goodfellow et al., in press).

The Mg content of chlorite generally increases with depth through Zones IVb to IIb in Holes 858A and 858C, indicating higher fluid/rock ratios near the highly permeable, fractured, and higher-temperature core of the upflow zone. The removal of Mg from seawater increases from 200°C to 300°C, at which temperature it is virtually completely removed (Seewald et al., 1990). The alteration of illite and micas by chlorite is reflected by low K₂O contents of bulk sediment (Goodfellow and Peter, this volume), in contrast to the BH upflow zone, where reaction with hydrothermal fluid has produced a chlorite-illite/muscovite assemblage.

Hydrothermal minerals near the core of the AAV upflow zone formed from 270° to 300°C fluids with high Ca-activity. These fluids are similar in temperature and composition to vent fluids from AAV (Lydon et al., 1992). The low MgO content of Zone Ib indicates reaction of sediment with a “zero-Mg” end-member hydrothermal fluid (Seewald et al., 1990; Goodfellow and Peter, this volume). The high Ca activity of hydrothermal fluids accounts for the occurrence of wairakite and anorthitic plagioclase in the high-temperature core of the conduit. Seyfried et al. (1991) showed that the anorthite content of feldspar in equilibrium with hydrothermal fluids increases with increasing temperature.

Wirsching (1981) studied the experimental formation of calcium zeolites using different initial rock compositions and fluids with variable Na and Ca activities. This experimental work suggests that wairakite forms at high temperature either directly from a fluid with high Ca activity or by the transformation of analcime at low Ca activity. The high Ca activity of the hydrothermal fluid is supported by high Ca/Na in both vent fluids (Lydon et al., 1992) and fluid inclusions (Peter et al., this volume) and by the absence of Na-phases such as analcime or albite. The high anorthite content of the plagioclase is consistent with low bulk-rock Na₂O contents (0.60 wt%; Goodfellow and Peter, this volume).

Zone IVb at Site 858 is characterized by extensive hydrothermal precipitation of Mg-smectite (bulk sediments have 17.9–34.2 wt% MgO; Goodfellow and Peter, this volume). Based on mineralogical data from shallow piston cores near vent sites at the AAV, it is most likely that these Mg-smectites are saponite (Turner et al., 1991; Goodfellow et al., in press). The formation of saponite is consistent with the massive dumping of Mg from seawater entrained locally into the zone of fluid upflow (Goodfellow et al., in press). Oxygen isotope data indicates that this saponite formed between 119° and 134°C (Goodfellow et al., in press).

Reaction Zone (Site 857)

Site 857 consists of a thick sequence of interbedded hemipelagic and turbiditic sediments, and intercalated mafic sills. This site was drilled to test the hypothesis that the base of the sedimentary sequence represented a hydrothermal reservoir that supplied hydrothermal fluid to Site 858 (Davis, Mottl, Fisher, et al., 1992). The mineralogy, bulk chemical compositions (Goodfellow and Peter, this volume), and fluid inclusions all suggest that the reaction zone at Site 857 interacted with fluids similar to those venting at AAV. For example, fluid-inclusion temperatures measured in quartz and wairakite (250°–300°C) from Hole 857D are similar to those in wairakite from Hole 858F (Peter et al., this volume) and to vent fluid temperatures at Site 858 (Goodfellow and Franklin, in press). The mineral assemblage of the highest temperature zone at Site 857 (Zone Ic; wairakite-quartz-epidote-pyrite) is the same as the assemblage in the core of the upflow zone at Site 858. Zone IIc at Site 857 and IIb at Site 858 likewise consist of quartz-chlorite-epidote-pyrite-spheine. The bulk sediment chemistry from the high temperature zones at both sites is also similar (Goodfellow and Peter, this volume).

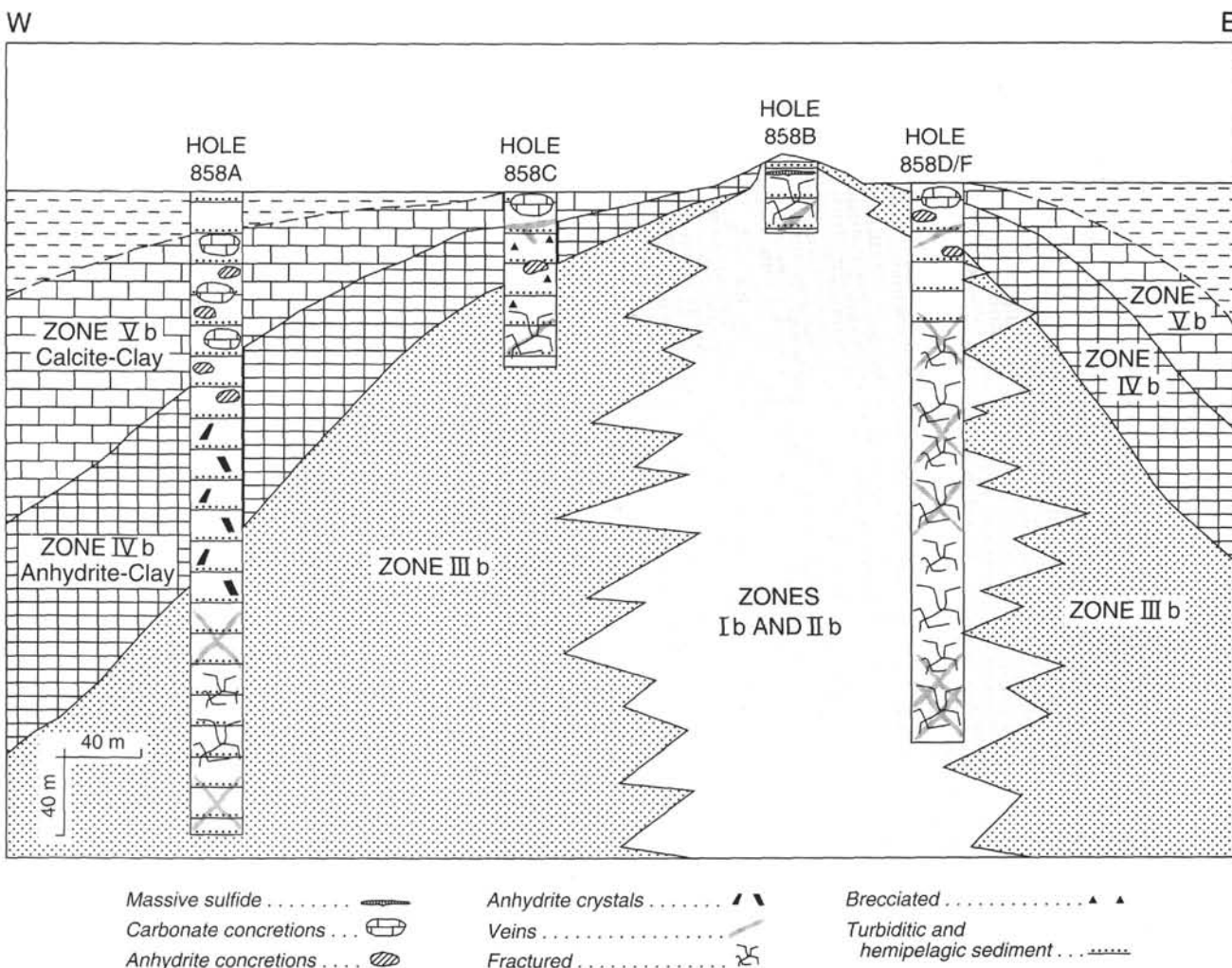


Figure 18. Profile across Site 858 (AAV) showing the distribution of alteration zones. Zone characteristics are given in the text and in Table 5.

Wairakite compositions also indicate a genetic link between the two sites. Wairakite from Hole 857D is more Ca-rich ($\text{Ca}/(\text{Ca} + \text{Na}) = 0.941\text{--}0.996$) than wairakite from Hole 858F ($\text{Ca}/(\text{Ca} + \text{Na}) = 0.871\text{--}0.967$). This difference in Na contents of wairakite is consistent with the mixing of Ca-rich fluids generated at Site 857 with Na-bearing pore water or seawater in the upflow zone at Site 858, and slightly higher fluid-inclusion temperatures in wairakite from Site 857 (Peter et al., this volume).

It is difficult to constrain the origin of the hydrothermal fluids, but it seems likely that the intrusions of sills into the sedimentary sequence has created a shallow hydrothermal circulation system that is feeding the nonmetalliferous vents at Site 858 and perhaps those presently venting at Site 856. The sills are also highly altered (Davis and Fisher, this volume), and high-temperature (Zone Ic) veins cross-cut both sills and sediment, indicating that alteration by hydrothermal fluids postdates the intrusions of the sills. There is no evidence for involvement of a high-temperature metalliferous fluid such as that which formed the Bent Hill massive sulfide deposit.

CONCLUSIONS

1. Site 856 represents a hydrothermally inactive upflow zone that is associated with the BH massive sulfide deposit. Hydrothermal alteration minerals at BH are zoned laterally from a high-temperature inner core assemblage to an outer low-temperature assemblage. Zone Ia is lithified and brecciated, and consists of quartz-(Fe)chlorite-muscovite-rutile-chalcopyrite-pyrrhotite. Zone IIa surrounds Zone Ia, is

less altered and indurated, and consists of albite-chlorite-pyrite alteration. Zones IIIa and IVa are less intensely indurated than sediments from the higher-temperature inner zones and are characterized by anhydrite and calcite, respectively, in addition to illite and pyrite.

2. Site 858 (AAV) is a hydrothermal fluid discharge conduit that is venting fluids up to 276°C . The core of this upflow zone consists of a wairakite-quartz-epidote-sphene-pyrite \pm plagioclase assemblage that formed at temperatures between 270° and 290°C (Peter et al., this volume). Zone Ib is surrounded by hemipelagic and turbiditic sediment that becomes progressively less indurated and hydrothermally altered with distance from the center of fluid upflow. Zone IIb, which surrounds Zone Ib, consists of quartz-epidote-pyrite. This zone is surrounded by Zone IIIb, which consists of albite-chlorite-pyrite. Outermost zones IVb and Vb are characterized by anhydrite and calcite, respectively.

3. Highly altered sediments in the core of the AAV upflow zone are characterized by the same mineral assemblage as that characterizing intensely altered sediment below 460 mbsf at the postulated reaction zone (Site 857). Furthermore, the formation temperatures, mineral chemistry, and bulk sediment compositions are similar for the two alteration zones. The mineralogical, geochemical, and thermal similarities between the zones are consistent with the generation of AAV (Site 858) vent fluids from a hydrothermal reaction zone near the base of the Middle Valley sedimentary pile, probably related to sill intrusion.

4. The mineral assemblages at the core of the BH and AAV upflow zones are mineralogically distinct and have clearly formed

from fluids of different temperature and composition. The alteration assemblage at BH was produced by an Fe-K-rich, high-temperature (300°–400°C) fluid with low Ca activity, whereas the core assemblage at AAV is the product of lower-temperature (270°–290°C) hydrothermal fluids with high Ca activity. In both upflow zones, mineral zonation and temperature gradients are controlled by the mixing of entrained seawater with upwelling and outwelling hydrothermal fluid.

ACKNOWLEDGMENTS

Bob Delabio is thanked for performing the XRD analyses, Laura Radburn for assistance with the SEM analyses, and Don Harris for help with the electron microprobe. We thank Martina Wecke for some of the drafting and Nancy McQuistion for editorial comments. We thank Jan Peter and Barry Cameron for discussions and for reviewing an earlier version of the manuscript. Reviews by J. Bruce Gemmell, Craig Leitch, and Michael Mottl improved earlier versions of the manuscript. This paper is Geological Survey of Canada Contribution No. 19293.

REFERENCES*

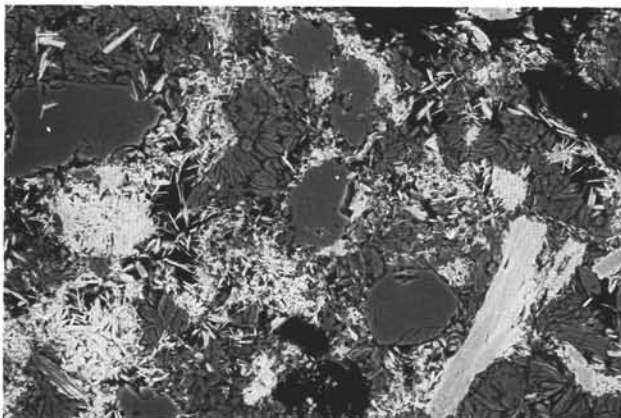
- Adshead, J.D., Bornhold, B.D., and Davis, E.E., 1986. Indurated deposits and possible plume bands in a hydrothermal mound, northeast Pacific. *Geol. Surv. Can. Curr. Res.*, 86-1A:737–748.
- Al-Aasm, I.S., and Blaise, B., 1991. Interaction between hemipelagic sediment and a hydrothermal system: Middle Valley, northern Juan de Fuca Ridge, subarctic northeast Pacific. *Mar. Geol.*, 98:25–40.
- Cathelineau, M., 1988. Cation site occupancy in chlorites and illites as a function of temperature. *Clay Mineral.*, 23:471–485.
- Davis, E.E., Currie, R.G., and Sawyer, B.S., 1987. Marine geophysical maps of western Canada: regional SeaMARC II acoustic image mosaics and Sea Beam bathymetry. *Geol. Surv. Can. Maps* 2-1987 to 17-1987.
- Davis, E.E., Goodfellow, W.D., Bornhold, B.D., Adshead, J., Blaise, B., Villinger, H., and Le Cheminant, G.M., 1987. Massive sulfides in a sedimented rift valley, northern Juan de Fuca Ridge. *Earth Planet. Sci. Lett.*, 82:49–61.
- Davis, E.E., and Lister, C.R.B., 1977. Heat flow measured over the Juan de Fuca Ridge: evidence for widespread hydrothermal circulation in a highly heat transportive crust. *J. Geophys. Res.*, 82:4845–4860.
- Davis, E.E., Mottl, M.J., Fisher, A.T., et al., 1992. *Proc. ODP, Init. Repts.*, 139: College Station, TX (Ocean Drilling Program).
- Davis, E.E., and Villinger, H., 1992. Tectonic and thermal structure of the Middle Valley sedimented rift, northern Juan de Fuca Ridge. In Davis, E.E., Mottl, M.J., Fisher, A.T., et al., *Proc. ODP, Init. Repts.*, 139: College Station, TX (Ocean Drilling Program), 9–41.
- Goodfellow, W.D., and Blaise, B., 1988. Sulfide formation and hydrothermal alteration of hemipelagic sediment in Middle Valley, northern Juan de Fuca Ridge. *Can. Mineral.*, 26:675–696.
- Goodfellow, W.D., and Franklin, J.M., in press. Geology, mineralogy and geochemistry of massive sulfides in shallow cores, Middle Valley, Northern Juan de Fuca Ridge. *Econ. Geol.*
- Goodfellow, W.D., Grapes, K., Cameron, B., and Franklin, J.M., in press. Hydrothermal alteration associated with massive sulfide deposits, Middle Valley, Northern Juan de Fuca Ridge. *Can. Mineral.*
- Lydon, J.W., Goodfellow, W.D., and Franklin, J.M., 1990. Chemistry of sediment pore waters around active hydrothermal vents, Middle Valley. *Am. Geophys. Union, S. F. Progr. Abstr.*, 71:1569.
- Lydon, J.W., Goodfellow, W.D., and Gregoire, D.C., 1992. Chemical composition of vent and pore fluids in an active hydrothermal discharge zone, Middle Valley. *Geol. Surv. Can. Minerals Colloq., Progr. Abstr.*, Ottawa, 24.
- Mottl, M.J., Holland, H.D., and Corr, R.F., 1979. Chemical exchange during hydrothermal alteration of basalt by seawater. II. Experimental results for Fe, Mn and sulfur species. *Geochim. Cosmochim. Acta*, 43:869–884.
- Rosenberg, P.E., 1967. Subsolidus relations in the system $\text{CaCO}_3\text{-MgCO}_3\text{-FeCO}_3$ between 350° and 550°C. *Am. Mineral.*, 52:787–798.
- Schiffman, P., Bird, D.K., and Elders, W.A., 1985. Hydrothermal mineralogy of calcareous sandstones from the Colorado River delta in the Cerro Prieto geothermal system, Baja California, Mexico. *Mineral. Mag.*, 49:435–449.
- Seewald, J.S., Seyfried, W.E., and Thornton, E.C., 1990. Organic-rich sediment alteration: an experimental and theoretical study at elevated temperatures and pressures. *Appl. Geochem.*, 5:193–209.
- Seyfried, W.E., Jr., Ding, K., and Berndt, M.E., 1991. Phase equilibria constraints on the chemistry of hot spring fluids at mid-ocean ridges. *Geochim. Cosmochim. Acta*, 55:3559–3580.
- Turner, R.J.W., Ames, D.E., Goodfellow, W.D., Leitch, C.H.B., Franklin, J.M., and Hoy, T., in press. Character of active hydrothermal mounds and nearby altered hemipelagic sediments in the hydrothermal areas of Middle Valley, northern Juan de Fuca Ridge: shallow core data. *Can. J. Earth Sci.*
- Turner, R.J.W., Leitch, C.H.B., Ames, D.E., Hoy, T., Franklin, J.M., and Goodfellow, W.D., 1991. Character of hydrothermal mounds and adjacent sediments, active hydrothermal areas, Middle Valley sedimented rift, northern Juan de Fuca Ridge, northeast Pacific: evidence from ALVIN push cores. *Geol. Surv. Can. Curr. Res., Pt. E.*, 99–108.
- Von Damm, K.L., 1990. Seafloor hydrothermal activity: black smoker chemistry and chimneys. *Annu. Rev. Earth Planet. Sci.*, 18:173–204.
- Wirsching, U., 1981. Experiments on the hydrothermal formation of calcium zeolites. *Clays Clay Miner.*, 29:171–183.

* Abbreviations for names of organizations and publications in ODP reference lists follow the style given in *Chemical Abstracts Service Source Index* (published by American Chemical Society).

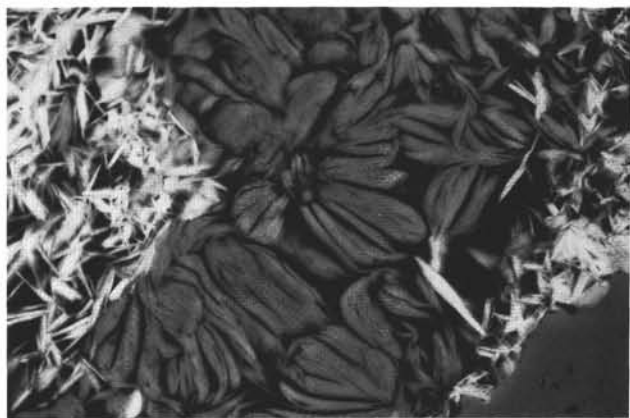
Date of initial receipt: 2 March 1993

Date of acceptance: 3 August 1993

Ms 139SR-220



1



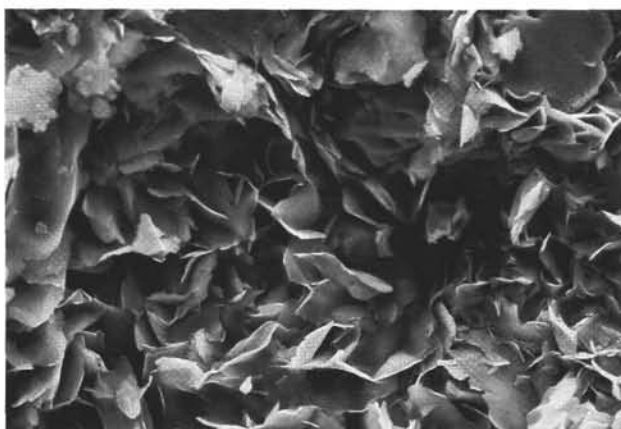
2



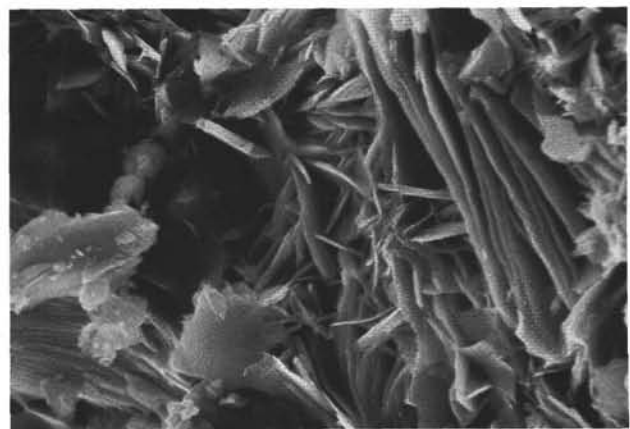
3



4

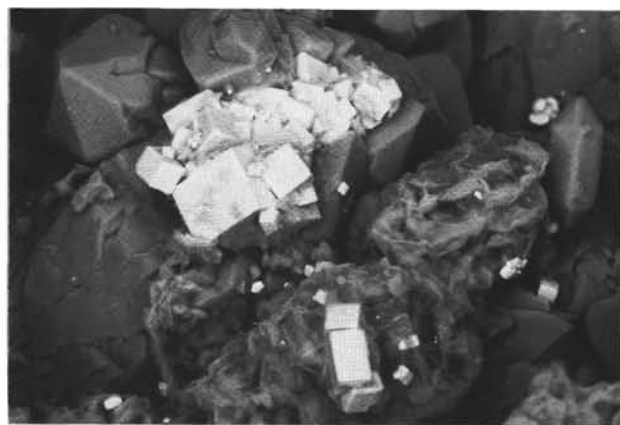


5

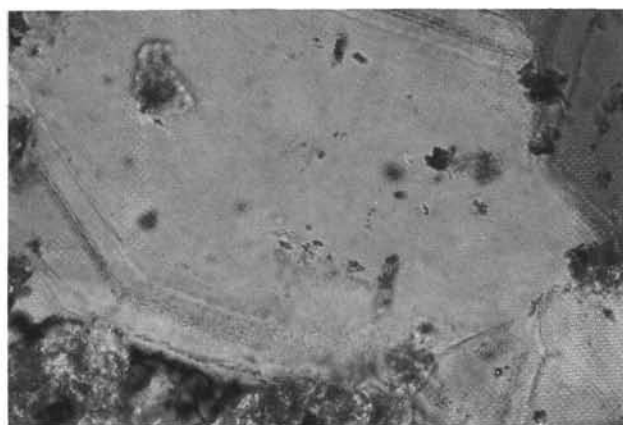


6

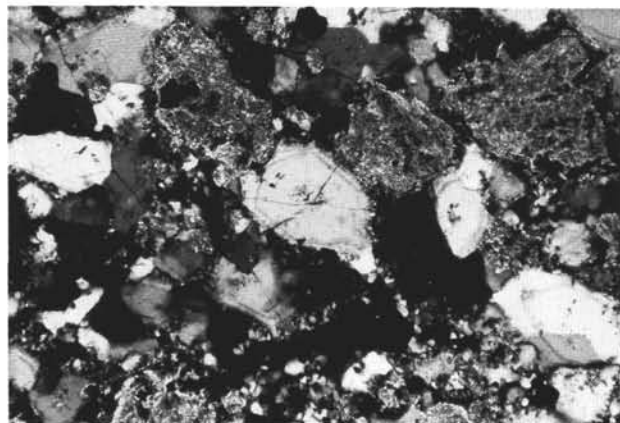
Plate 1. 1. Backscatter SEM image of authigenic Fe-chlorite (bright) and muscovite (dark, feathery texture) with authigenic quartz (dark). A large chlorite crystal at bottom right with darker Mg-rich core, rimmed by brighter Fe-rich chlorite. Sample 139-856B-15X-1, 124–126 cm. Field of view (fov) = 0.26 mm. 2. Backscatter SEM image of authigenic Fe-chlorite (bright) and muscovite (dark) with authigenic quartz (lower right). Sample 139-856B-15X-1, 124–126 cm; fov = 0.06 mm. 3. Backscatter SEM image of authigenic Fe-chlorite (bright) and muscovite (dark). Sample 139-856B-15X-1, 124–126 cm; fov = 0.053 mm. 4. Secondary SEM image of illite/muscovite. Sample 139-856B-14X-4, 50–53 cm; fov = 0.072 mm. 5. Secondary SEM image of muscovite with small chalcopyrite crystal in upper right corner. Sample 139-856B-15X-3, 8–10 cm; fov = 0.078 mm. 6. Secondary SEM image of muscovite crystals (right side) and chlorite crystals (bottom left). Sample 139-856B-15X-5, 106–108 cm; fov = 0.045 mm.



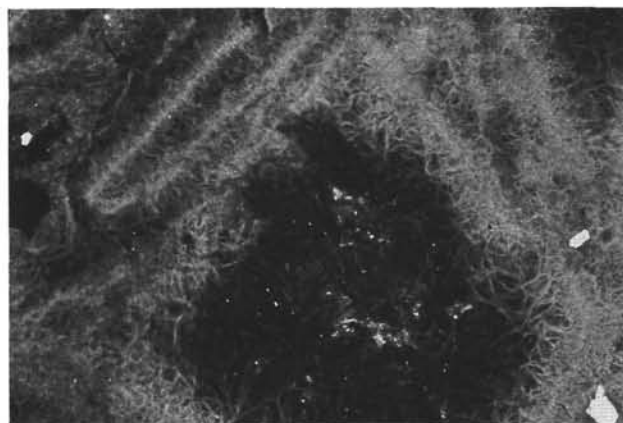
1



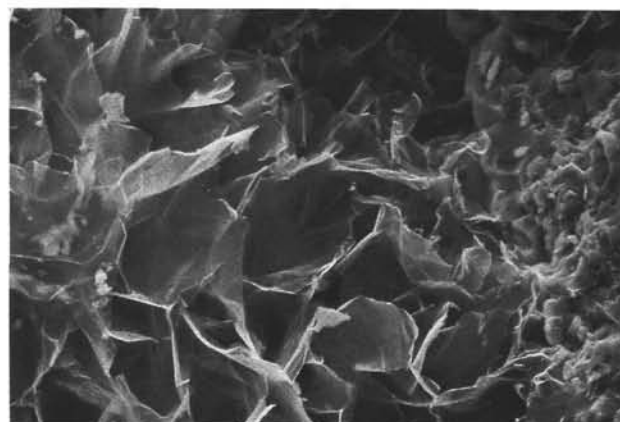
2



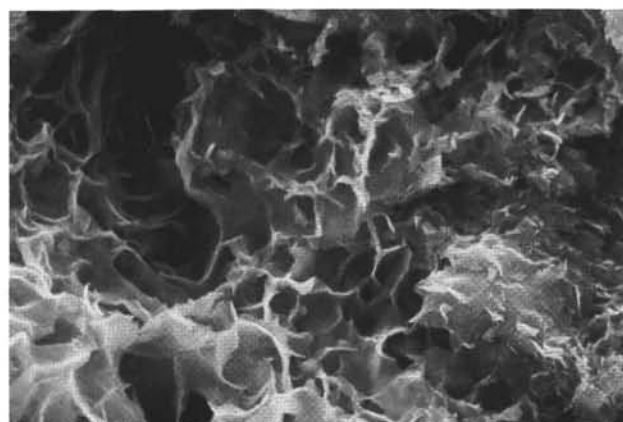
3



4

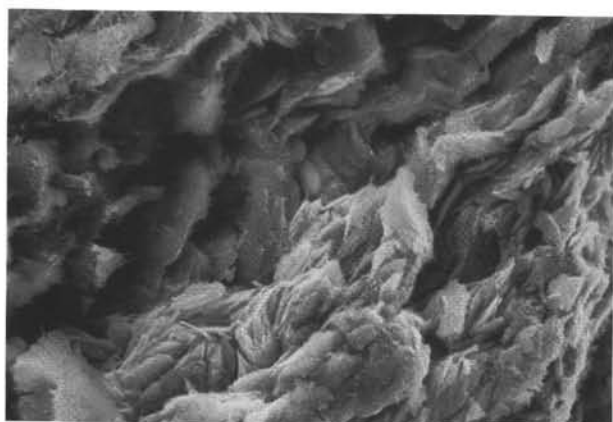


5

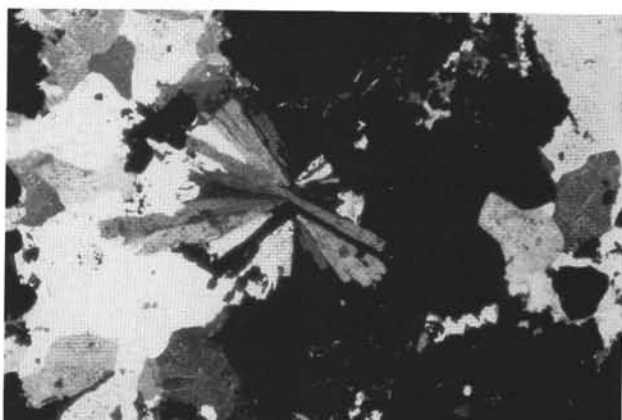


6

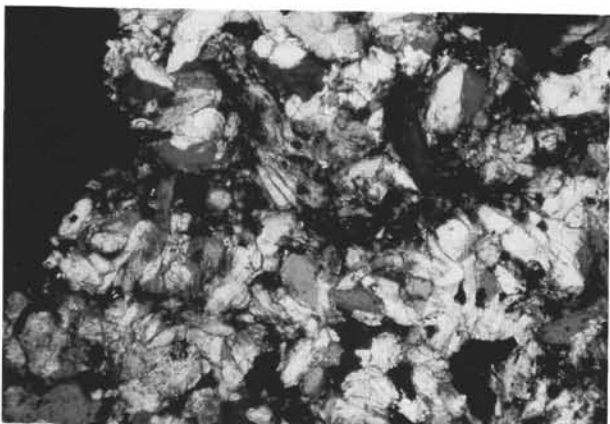
Plate 2. **1.** Backscatter SEM image of hexagonal quartz, euhedral pyrite, and talc. Sample 139-856D-1H-2, 43–46 cm; fov = 0.150 mm. **2.** Photomicrograph of zoned hydrothermal quartz with talc. Sample 139-856G-2R-2, 84–86 cm. Polarized transmitted light; fov = 0.23 mm. **3.** Photomicrograph of zoned hydrothermal quartz and clasts of talc with pyrite (black). Sample 139-856G-2R-2, 84–86 cm. Polarized transmitted light; fov = 0.92 mm. **4.** Backscatter SEM image of finely intergrown talc interstitial to collomorphic pyrite. Sample 139-856B-3H-5, 110–113 cm; fov = 0.264 mm. **5.** Secondary SEM image of talc interstitial to collomorphic pyrite. Sample 139-856B-3H-5, 110–113 cm; fov = 0.068 mm. **6.** Secondary SEM image of talc interstitial to quartz and pyrite. Sample 139-856G-2R-2, 54–56 cm; fov = 0.034 mm.



1



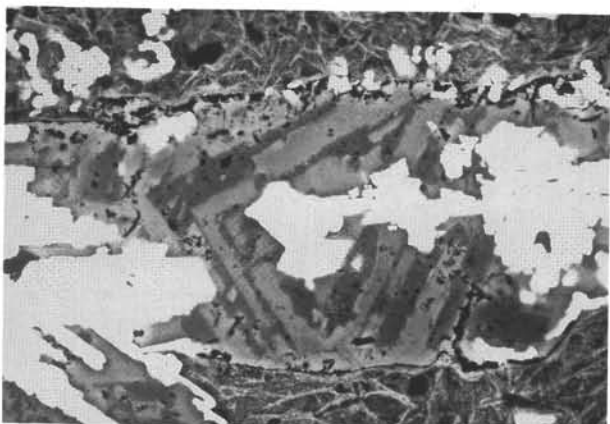
2



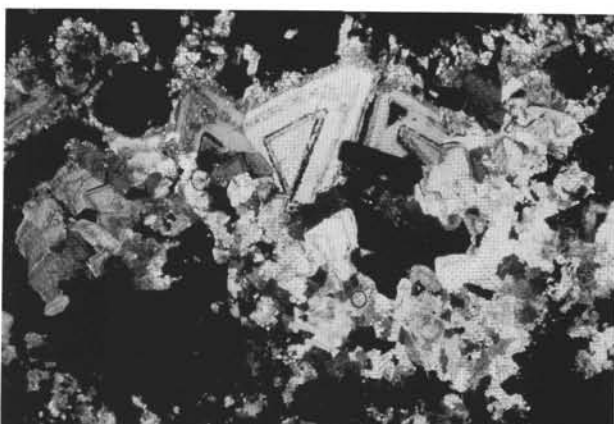
3



4



5

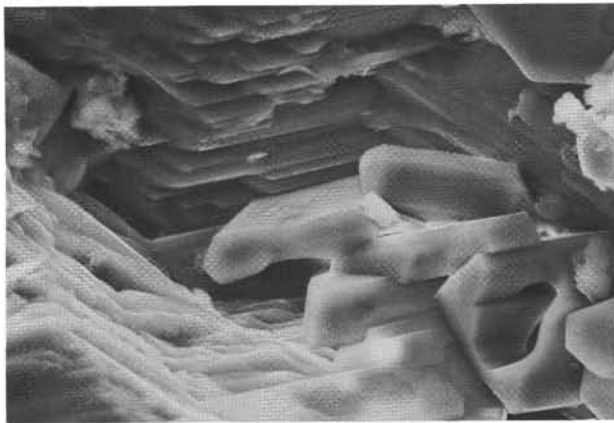


6

Plate 3. 1. Secondary SEM image of platy Mg-chlorite. Sample 139-856H-3R-3, 72–74 cm; fov = 0.052 mm. 2. Photomicrograph of barite rosette in massive sulfide and carbonate. Sample 139-856H-3R-1, 28–30 cm. Polarized transmitted light; fov = 0.92 mm. 3. Photomicrograph of magnesite interstitial to pyrite. Sample 139-856G-6R-3, 132–134 cm. Polarized transmitted light; fov = 0.92 mm. 4. Secondary SEM image of calcite cluster on talc. Sample 139-856H-4R-1, 88–90 cm; fov = 0.055 mm. 5. Backscatter SEM image of zoned dolomite in vein crosscutting talc and overgrown by magnetite. Sample 139-856H-3R-3, 17–19 cm; fov = 1.85 mm. 6. Photomicrograph of zoned dolomite in vein crosscutting massive sulfide. Sample 139-856H-3R-3, 72–74 cm. Polarized transmitted light; fov = 0.095 mm.



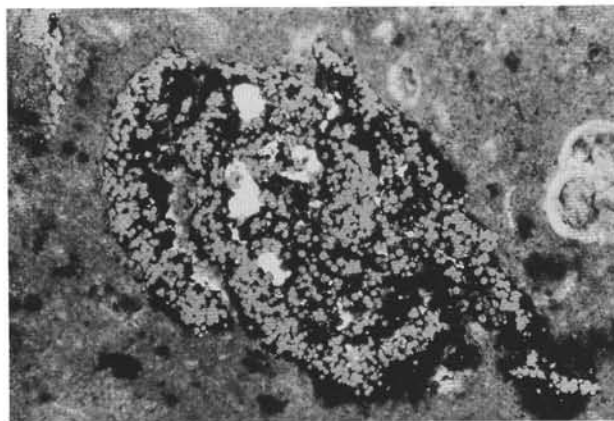
1



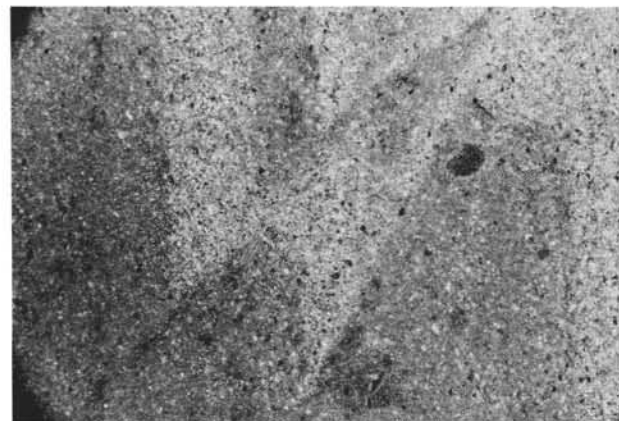
2



3



4

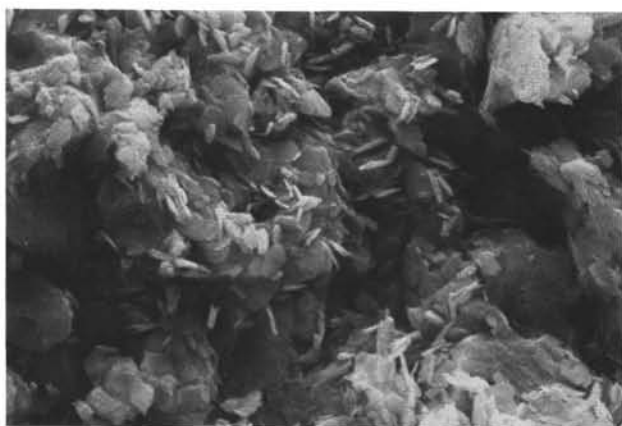


5

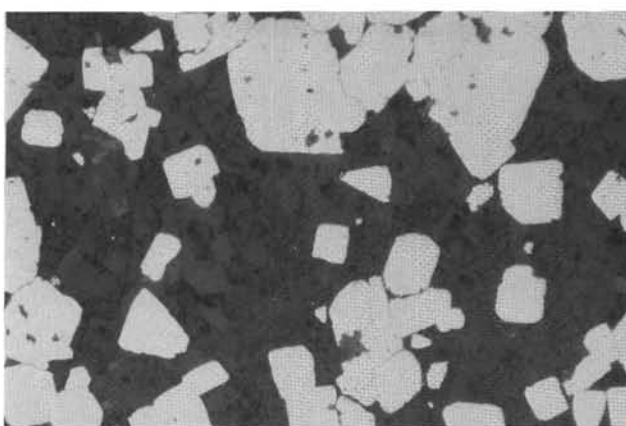


6

Plate 4. 1. Photomicrograph of anhydrite cluster in fine-grained sediment. Sample 139-858A-21X-2, 31–34 cm. Polarized transmitted light; fov = 0.92 mm. 2. Secondary SEM image of stacked and cubic anhydrite. Sample 139-858A-24X-1, 33–35 cm; fov = 0.075 mm. 3. Photomicrograph of authigenic anorthite (twinned crystal), wairakite (dark), and quartz (bright). Sample 139-858F-9R-CC, 9–11 cm. Polarized transmitted light; fov = 0.46 mm. 4. Photomicrograph of frambooidal pyrite. Sample 139-857A-2H-3, 125–127 cm. Plain transmitted and reflected light; fov = 0.92 mm. 5. Photomicrograph of offset of laminations in carbonate concretion by small microfault. Sample 139-857C-6R-1, 1–2 cm. Polarized transmitted light; fov = 1.85 mm. 6. Photomicrograph of hydrothermally altered sandstone with twinned albite, quartz, epidote and sphene. Sample 139-857D-17R-1, 34–36 cm. Polarized transmitted light; fov = 0.46 mm.



1



2



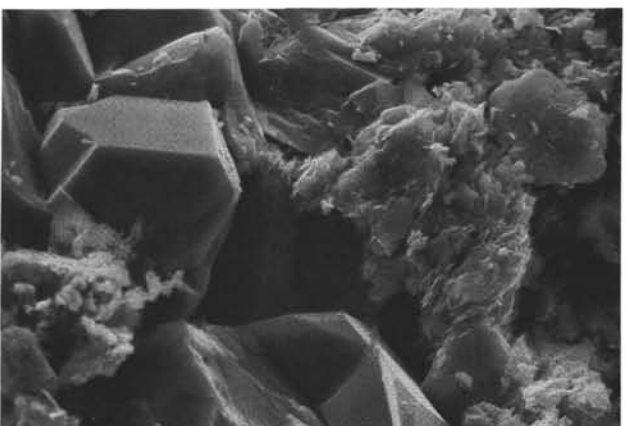
3



4



5



6

Plate 5. 1. Secondary SEM image of small chlorite plates on quartz. Sample 139-857D-5R-1, 26–28 cm; fov = 0.026 mm. 2. Photomicrograph of authigenic pyrite in altered sediment. Sample 139-857C-61R-1, 129–131 cm. Reflected light; fov = 0.92 mm. 3. Photomicrograph of corroded pyrite in altered sediment. Sample 139-857D-16R-1, 53–55 cm. Reflected light; fov = 0.92 mm. 4. Photomicrograph of twinned wairakite in vein. Sample 139-857D-6R-1, 20–22 cm. Polarized transmitted light; fov = 1.85 mm. 5. Photomicrograph of euhedral epidote with quartz in vein in altered sediment. Sample 139-857D-5R-1, 26–28 cm. Polarized transmitted light; fov = 0.46 mm. 6. Secondary SEM image of hexagonal-shaped epidote in quartz vein crosscutting chlorite and quartz. Sample 139-857D-5R-1, 26–28 cm; fov = 0.050 mm.